NORTHWESTERN UNIVERSITY

Functional Architecture and Visual Response Properties in the Mouse Superior Colliculus

A DISSERTATION

SUBMITTED TO THE GRADUATE SCHOOL
IN PARTIAL FULFILLMENT OF THE REQUIREMENTS

For the degree

DOCTOR OF PHILOSOPHY

Field of Neuroscience

By

Jad Barchini

EVANSTON, ILLINOIS

September 2017

Abstract

Functional Architecture and Visual Response Properties in the Mouse Superior Colliculus

Jad Barchini

The mouse visual system has recently been shown to possess many of the properties observed in the visual systems of the classically studied carnivores and primates. An ever-expanding genetic toolkit has given researchers who study vision in mice many advantages unavailable in other species.

In this thesis I study the mouse superior colliculus (SC), a midbrain structure involved in sensory-motor integration. The SC is central to the mouse's vision, and visually-guided behaviors; a function that is gradually deferred to the visual cortex in carnivores and primates. The centrality of the SC in mice in fact gives us some advantages. It represents a compact and simplified visual system, receiving direct input from the sensory periphery (the retina), with nonetheless great influence on behavior.

Here, and with invaluable help from many collaborators, I specifically explore three central questions about the organization and function of the most superficial lamina of the mouse SC, the *stratum griseum superficiale* (SGS), where neurons are responsive to visual stimuli. First, I demonstrate a functional organization of neurons in the SGS following the degree of their direction selectivity (DS). Specifically, I show that neurons that are selective for motion direction tend to be

concentrated in the topmost lamina of the SGS, and become gradually scarcer in the deeper laminae. Second, in a knockout mouse line where the DS of direction selective ganglion cells (DSGCs) is reduced, I show a complimentary reduction in the DS of SGS neurons. This is the first direct demonstration that retinal DSGCs are the source of the DS observed in the SGS. Third, I provide a first description of visual saliency responses in the mouse SGS, showing a fundamental difference in the response of excitatory and inhibitory neurons. This sets the stage for a better understanding of the contribution of different functional cell types in the SGS to visual signal processing at the microcircuit level.

Acknowledgements

To Jianhua ‘JC’ Cang. Many times I entered your office frustrated with my progress and apologetic; felling like I owed the “boss” something. As many times I came out encouraged, commended on my work, and made to feel like a mentor owed me a successful career. I thank you for being the patient and caring mentor that you are, and for the constructive criticism and stern advice when necessary. Although I still have long way to go, you’ve been instrumental in putting me on the right path. I’ve learned so much from your example.

To Daniel Dombeck, Gregory Schwartz, and Mark Segraves. Having you serve on my thesis committee has been a great privilege and a blessing. I benefited just as much from the example you set as dedicated and passionate scientists as I have from your insightful guidance and advice throughout the years. I thank you for your time and expertise.

I am extremely fortunate to have had labmates for mentors, whom I look up to and admire. Samsoon Inayat, by closely working with you, I learned the true meaning of perseverance and of a positive outlook, even if (especially when) it seemed that there was no silver lining. Xuefeng Shi, your tireless hard work and sense of urgency shall always be an example for me to strive after. Hui Chen, I am thankful for all I’ve learned from you and for your technical expertise, but I am even more thankful for your selflessness and kindness, and your willingness to step in and help whenever I needed it.

To Indira Raman and Catherine Woolley. Through your interactions with your colleagues and students you set an admirable example of what a scientist ought to be. I regard you as exemplar scientists, but also as wholesome human beings. Matching your passion towards science and your gift of communicating it to others will always be an aspiration of mine.

To Andrew Kuang, Jared Levine, Samsoon Inayat, Yin Peng Chen, Mingna Liu, Hui Chen, Elise Savier, Xuefeng Shi, Liang Feng, Xiaorong Liu, Genn Suyeoka, Yeechan Wu, Elif Tunc-Ozcan, and Ranit Sengupta. I thank you all deeply for your friendship and support throughout the years. You made this experience, through its ups and downs, a memorable and enjoyable one. I also thank you for all the discussions and input that pushed me to refine and improve my work. I wish you all the best in what's to come!

To JC's former graduate students: Krsna Rangarajan, Rashmi Sarnaik, Bor-Shuen Wang, Lupeng Wang, and Xinyu Zhao. Even though there wasn't much overlap between our stays in the lab, when I first joined you each took the time to make sure I felt welcome and at home. Your hard work and enthusiasm towards science have been nothing short of inspirational, and so was the impressive and elegant body of work you left behind. Every time we've met since you moved on you've been supportive and encouraging, and genuinely caring about my work. I will always look up to you as my academic big brothers and sister.

To Wei Wei and her lab members at the University of Chicago. I thank you for your valuable collaboration, and for sharing your mice with us. It's been a pleasure working with you, and a great lesson in the collaborative nature of science.

To Corey. You've been beyond patient and understanding through all this; I thank you for all the sacrifices you've made. You've kept me anchored and sane throughout the years, and have played an instrumental part in any success I may have had.

To Martha, Joseph, and Dana. I miss you more than you can imagine, and I know you miss me too. I thank you for all your sacrifices and encouragement, and for understanding that this was something I had to pursue. I hope one day I'm able to repay you all that you've given me, but know now that I'll always be grateful for it.

A special thank you to *Mus*;
Without whom our knowledge of ourselves would be wanting.

Table of Contents

List of Figures

CHAPTER 1

Introduction

Organization and Connectivity of the Visual System

The visual system detects, transmits, and hierarchically transforms light information into behaviors, ranging from the reflexive to the highly complex. This process starts in the retina and continues in many downstream brain centers, such as the lateral geniculate nucleus of the thalamus and the superior colliculus; the major retinal targets. Many more brain regions receive direct retinal inputs and subserve a vast array of functions, highlighting the breadth and intricacy of the visual system.

Retina

The retina is a layered light-sensitive sensory epithelium lining the back of the eye. It follows two major functional organizational principles: feedforward and lateral interactions (Demb and Singer, 2015; Masland, 2012). In the feedforward pathway, light information is relayed between three major cell-types in a serial fashion and with different levels of convergence. Photons first comes

in contact with the photoreceptors in the outer retina, after traveling through the inner layers. Photoreceptors serve to transduce the light signal into changes in electrical activity that can be processed by the rest of the visual system. This is achieved by a light-dependent conformational change of photopigment molecules present in the photoreceptor outer segments, knows as opsins. This conformational change leads to a transduction cascade that controls the electrical excitability of photoreceptors, and ultimately regulates their neurotransmitter release. Two types of photoreceptor cells exist in the mammalian retina, the rods and the cones. The rods are highly sensitive to light and are important for vision in dim light conditions. While cones are less sensitive, they are important for color vision and resolving fine details in the visual scene. Some of the differences between these two photoreceptor types are dictated by their location, density, and connectivity to downstream cells in the retina. Certain mammalian species, such as primates, possess a specialization in their retina, called the fovea. The fovea is a small region of high visual acuity that is tightly packed with cone photoreceptors, while the rest of the retina is dominated by rods. The high resolving power of the cone system is mainly the result of low convergence in connectivity between cones and their postsynaptic partners, the bipolar cells. A much higher convergence takes place in the rod system.

Photoreceptor cells are depolarized in dark conditions and constantly release glutamate onto bipolar cells in the outer plexiform layer (OPL) of the retina, where these two cell types synapse. Bipolar cells can be classified as Off and On cells depending on the type of glutamate receptors that they express. Off-bipolar cells express ionotropic glutamate receptors whose activation leads to the depolarization of the cell. These cells are therefore sensitive to light decrements. On-bipolar cells, on the other hand, express the metabotropic glutamate receptor

mGluR6. The activation of mGluR6 receptors by glutamate results in hyperpolarization. These cells are therefore inhibited in darkness. Under light conditions, a decreased rate of glutamate release leads to the depolarization of On-bipolar cells, which then report light increments (Demb and Singer, 2015). This early segregation of the On and Off pathways sets up the visual system for a wealth of information that can potentially be extracted from this differential signal. On and Off bipolar cells can further be subdivided into more specialized channels of information. Close to 12 different types of bipolar cells have been described to date, based on their morphology, the stratification of their processes in the retina, specific genetic identifiers, and particular visual response characteristics (Masland, 2012).

Bipolar cells connect to the third and final cell type in the feedforward retinal pathway, the retinal ganglion cells (RGCs), in the inner plexiform layer (IPL) of the retina. RGCs are the output neurons of the retina, bundling their axons into the optic nerve which relays the retinal output to several visual centers in the brain (Dhande et al., 2015). Many more RGC cell types have been identified than bipolar cell types, following similar classification principles. Each type tiles the retina, and so different RGCs extract different features from the same region of space. Bipolar-cell properties are conserved and reflected in the activity of RGCs, with can be divided into On, Off, or On-Off cells, responding to increments or decrements in light, or both.

In addition to the feedforward pathway, there's a lateral transmission of information in the retina. This is mediated by horizontal cells at the synapse between photoreceptors and bipolar cells, in the OPL. These cells are inhibitory, and can play an important role in mediating surround-suppression in the retina (Thoreson and Mangel, 2012). At the level of the IPL, where bipolar cells synapse with RGCs, another cell type mediates the lateral transfer of information and surround

suppression, the amacrine cell. The many identified amacrine cell types can be broadly classified according to the size of their dendritic fields. These cells are inhibitory (releasing either GABA or glycine), but can also co-release excitatory neurotransmitters such as dopamine and acetylcholine. A particular type of amacrine cell, the starburst amacrine cell (SAC), is involved in the extraction of complex visual features such as motion direction (Wei and Feller, 2011).

The majority of RGCs are either simple spot detectors of the On or Off type, or possess the classically described center-surround receptive field, which detects luminance contrast (Dhande et al., 2015; Kuffler, 1953). These cells are collectively referred to as alfa RGCs. In addition to the alfa RGCs, several RGC types have been described in the mouse and rabbit retinas that respond to more complex visual features, such as stimulus orientation, object motion, or particular directions of motion. Neurons in this latter group are the direction selective ganglion cells (DSGCs), which acquire their selective responses by virtue of their asymmetric connectivity to SACs. Whether such response property exists in the primate retina is still shrouded in doubt.

DSGCs can be further subdivided into three categories and many subtypes based on their On and Off response properties, speed tuning, and preferred direction of motion. These are namely the On, Off, and On-Off DSGCs. On-DSGCs have been described that prefer thee distinct motion directions on the retina; ventral, dorsal, and temporal; but not nasal. These cells are tuned to slow speeds. A single type of Off DSGC is known so far; the Jam-B cells, which possess an asymmetric dendritic morphology, and prefer ventral motion. There exist four types of On-Off DSGCs, each preferring one of the four cardinal directions of motion. These cells are generally tuned to fast speeds, with a few exceptions (Dhande et al., 2013; Dhande et al., 2015; Kay et al., 2011).

Another important and distinct type of ganglion cell is the intrinsically photosensitive RGCs (ipRGCs). These cells express the photopigment melanopsin making them effective light detectors themselves, although they also integrate into the canonical retinal feedforward circuit and can respond to light through the classical activation of photoreceptors cells. These cells have also been shown to exist in primates, and can regulate circadian rhythms (Berson et al., 2002; Dhande et al., 2015).

Retinofugal pathway: Geniculo-cortical pathway

The major projection target of RGCs in the brain is the lateral geniculate nucleus (LGN) of the thalamus. This is particularly true in cats and primates where this pathway was classically studied. Neurons in the LGN subsequently project to primary visual cortex (V1, or area 17) in a retinotopic fashion that preserves the spatial relationship of objects in space.

The LGN is a layered structure where retinal inputs remain segregated in an eye-specific manner, before finally being integrated in V1. In mice, however, the LGN loses its laminar organization, but can still be segregated into a more superficial thin "shell" region, and a deeper "core" (Fig. 1.1). A fair segregation of inputs from each eye is also maintained in the mouse LGN. This structure receives inputs mainly from the contralateral eye, with a small region in the core being dedicated to ipsilateral eye inputs. The LGN has long been regarded as a relay station between the retina and V1, where the center-surround receptive field properties of RGCs are largely conserved (Hubel and Wiesel, 1961; Kuffler, 1953). Subsequent findings in cats and primates, and more recent studies in mice, have however challenged this concept by identifying LGN neurons that respond to more complex features, such as object orientation (Daniels et al.,

1977; Marshel et al., 2012; Piscopo et al., 2013; Smith et al., 1990; Zhao et al., 2013). These features, might however still be inherited from the retina, where orientation and direction selective responses have been reported in mice and rabbits (Barlow and Hill, 1963; Nath and Schwartz, 2016; Weng et al., 2005; Zhao et al., 2013).

In cat and primate V1 more complex visual response features become the rule rather than the exception. Binocularity is a property that emerges in V1 where individual neurons are found to be responsive to inputs from both eyes. Orientation selectivity is another feature that emerges in V1 after integration of spatially aligned center-surround LGN inputs (Hubel and Wiesel, 1962; Reid and Alonso, 1995). Direction selectivity has also been shown to emerge in V1 neurons where spiking is more favorable in particular directions of motion but not others due to spatio-temporal delays in the integration of untued LGN inputs (Priebe and Ferster, 2005).

V1 itself is a layered structure that follows general and widespread cortical organizational principles (Fig. 1.1). Layer 4 is the input layer, containing neurons that receives LGN input, and relay it to layer 2/3. Layer 2/3 neurons can form local connections with each other or project to other cortical areas, such as higher visual areas. Layer 5 neurons are output cells that project to subcortical structures like the superior colliculus (SC), while layer 6 neurons send cortical feedback signals to the thalamus (Douglas and Martin, 2004). Layer 1 neurons might be part of a specialized feature-selective visual pathway, and receive direct LGN inputs, bypassing layer 4 (Cruz-Martin et al., 2014). In mice, it is estimated that more than 85% of V1 neurons are excitatory, while less than 15% are inhibitory (Meyer et al., 2011). With the current availability of genetic and imaging tools in this species, different functional subtypes of excitatory and inhibitory neurons

have been described in V1, and their specific contributions to local microcircuit computations and feature selectivity are now being elucidated (Kim et al., 2015; Pfeffer et al., 2013).

Retinofugal pathway: Superior colliculus

Outside of the few mammalian species with a highly evolved cortex, the superior colliculus (SC) remains the major retinorecipient target in the visual system. In mice, it's estimated that close to 90% of RGCs (and all known major functional types) project to the SC, while only a fraction of them send additional collaterals to the LGN (Dhande et al., 2015; Ellis et al., 2016). In non-mammalian species, such as birds and lower vertebrates, which have not evolved a cortex, the optic tectum (the SC homologue) is the primary visual structure.

The SC is a layered midbrain structure, important for sensory-motor transformation (Gandhi and Katnani, 2011). Its most superficial layers are visually responsive, and receive direct retinal inputs (Fig. 1.1). The deeper layers are multimodal and premotor, leading to orienting behaviors (eye, head, and body movements) towards relevant sensory stimuli. Just like in LGN and V1, the visual layers of the SC maintain a retinotopic representation of visual space. The SC is predominantly innervated by the contralateral eye, but receives some ipsilateral input as well. In addition to retinal input, the SC is known to receive cortical input from layer 5, as well as from subcortical sources. The visual layers of the SC project to several targets in the brain, including the deep SC layers, the visual thalamic nuclei, and the parabigeminal nucleus, where they influence visually-guided premotor activities.

Studies in several mammalian species more or less agree on a morphological classification of cell types in the SC. However, genetic approaches have yet to isolate molecular markers that

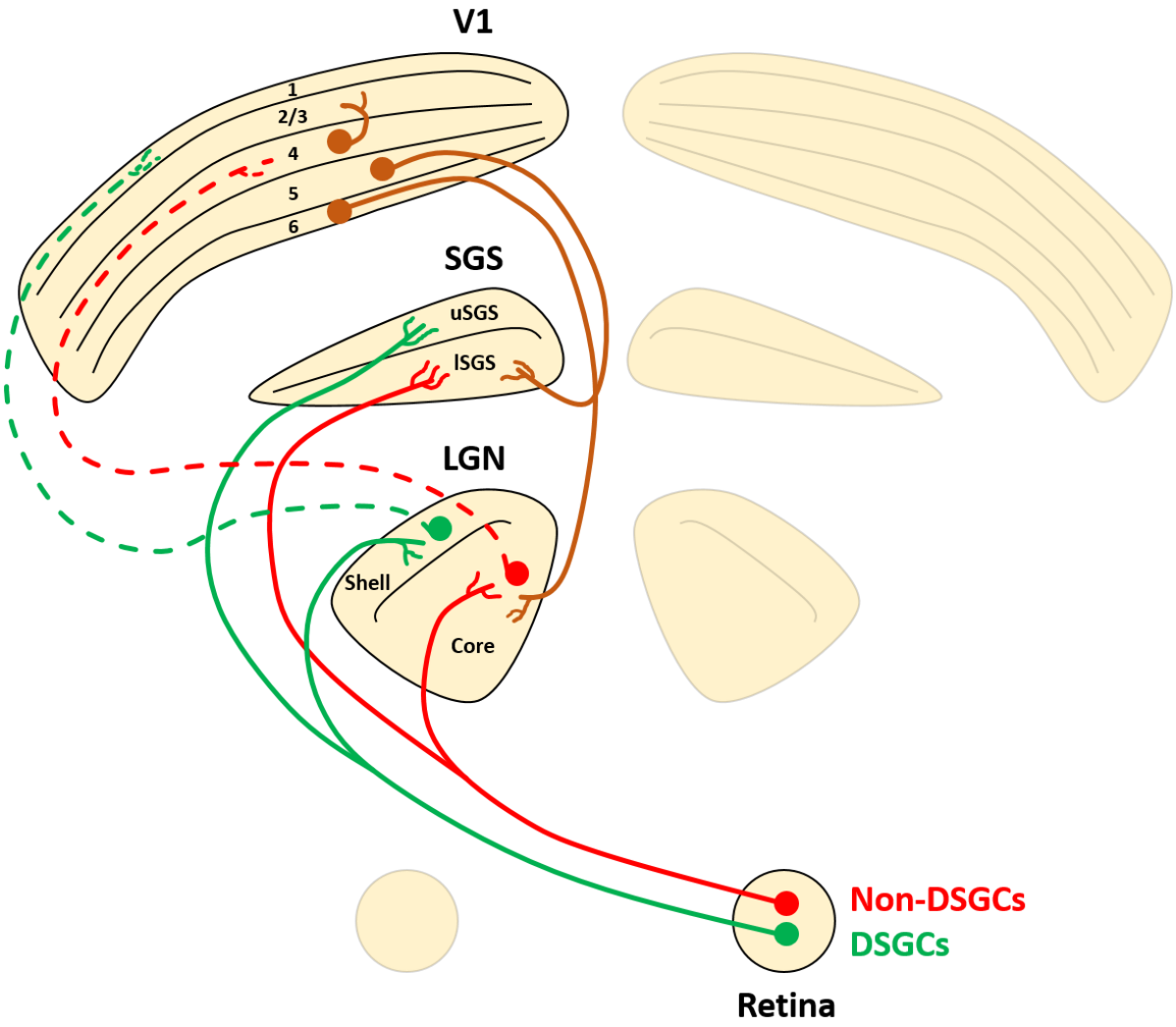

Figure 1.1. Major retinal targets and downstream connectivity in the retinofugal pathway. Illustration of the projection targets of DSGCs and non-DSGCs in the LGN and the *stratum griseum superficiale* (SGS) of the SC, as well as the connectivity between the different laminar structures of the LGN, V1, and the SGS. Retinal projections are mainly contralateral; cortical projections to subcortical structures are ipsilateral. DSGCs, direction selective ganglion cells; LGN, lateral geniculate nucleus of the thalamus; uSGS, upper SGS; lSGS, lower SGS; V1, primary visual cortex. The cortical layers in V1 are numbered 1 through 6. This diagram is a simplified synthesis of results from several studies (Cruz-Martin et al., 2014; Dhande and Huberman, 2014; Douglas and Martin, 2004; Wang and Burkhalter, 2013).

are specific to particular morphological and functional types, as has been achieved in the mouse cortex; although some progress has been made on that front (Byun et al., 2016; Gale and Murphy,

2014). This will open up the door for a better description of the microcircuit-level organization in the SC. Additionally, through targeted manipulations, the contribution of each identified neuronal element to the function of the microcircuit can finally become apparent. The retino-tectal pathway will be described in more detail later on in this chapter.

Other retinorecipient structures in the brain

The retina transmits the wealth of its information to numerous targets in the brain (Dhande et al., 2015). In mice, while the SC has been shown to receive information from all output channels of the retina, other retinal targets only receive a subset of this information. In addition to the SC and thalamus, the better studied retinorecipient brain targets are the suprachiasmatic nucleus (SCN), the olivary pretectal nucleus (OPT), and the nuclei of the accessory optic system (AOS).

ipRGCs integrate light over large regions of space and over long periods of time. They project to the SCN and OPT, which are part of the non-image forming visual system. The SCN plays an important role in entraining circadian rhythms, whereas the OPT mediates the pupillary light reflex.

The AOS is important for image stabilization on the retina. It engages the optokinetic reflex (OKR), which allows the eyes to track slow-moving objects. On-DSGCs have been known to project to the nuclei of the AOS, although some On-Off DSGCs which are tuned to slow speeds have recently been shown to project there as well (Dhande et al., 2013). The projection targets of these DSGCs in the AOS depend mainly on the preferred direction of the input. Specifically, forward motion preferring DSGCs project to a nuclear complex composed of the nucleus of the optic tract (NOT) and the dorsal terminal nucleus (DTN), which drive horizontal eye movements.

DSGCs preferring upward and downward motion, on the other hand, project to the dorsal and ventral factions of the medial terminal nucleus (MTN), respectively. The MTN drives vertical eye movements. Interestingly, the directions of motion encoded by the AOS correspond to those detected by the semicircular canals of the vestibular system. This system drives compensatory eye movements in response to fast head movements by engaging the vestibule-ocular reflex (VOR). These two systems, therefore, work together to generate a stable image on the retina.

The Mouse Superior Colliculus

Why study the mouse superior colliculus?

Classical studies in primates and carnivores have greatly advanced our understanding of visual system architecture, function, and development (Hubel and Wiesel, 1962, 1968; Wiesel and Hubel, 1963). In recent years, the mouse visual system has been shown to possess many of the properties observed in the more traditional animal models; making it an attractive model to study (Huberman and Niell, 2011; Niell and Stryker, 2008).

Modern advances in genetics, coupled with advances in functional microscopy, gave researchers a toolkit of unprecedented precision, discriminability, and throughput, when exploring this new system. Gene knockouts and knockins helped answer many longstanding questions about the development and function of the visual system, implicating specific molecular substrates. The ability to visualize genetically identifiable neuronal types, and correlate their morphology, connectivity, and response properties with each other, rejuvenated the field of neuronal taxonomy and allowed for a more meaningful exploration of the visual system at the microcircuit level. Bulk-loaded and genetically encoded activity reporters allowed the simultaneous monitoring of the

activity of many more neurons than was possible with traditional electrophysiology. Until this toolkit becomes available in species with more complex visual systems, mice will remain an invaluable model system for understanding vision.

The SC is vital to the mouse's vision and visually-guided behaviors, a function that is gradually deferred to the visual cortex in carnivores and primates. The centrality of the SC in mice in fact gives us some advantages. It represents a compact and simplified mammalian visual system, monosynaptically connected to the sensory periphery (the retina), with nonetheless great influence on behavior. It can be studied to gain a better understanding of fundamental principles of sensory input processing, like the emergence of different feature selectivities. It can also give us some insight into how those visual feature are further processed to generate appropriate behavioral responses.

Morphological organization

From a morphological point of view the SC can be described at three different levels of organization: Its overall laminar structure, the different cell types that populate it, and its interconnectivity with the rest of the brain (inputs and outputs).

Laminar structure

The SC is a multilayered midbrain structure, important for sensory-motor integration (Gandhi and Katnani, 2011). Its laminar structure is fairly conserved in mammals, and can be subdivided into two major parts; the superficial SC (sSC) and the deep SC (dSC).

The sSC consists of two layers. The more superficial layer is the *stratum griseum superficiale* (SGS), or the superficial gray layer, which contains the cell bodies of visually responsive neurons. These neurons receive direct retinal input from RGC axons that course in the deeper *stratum opticum* (SO), or the optic layer. While the SO consists mostly of white matter, it contains some cell bodies as well. The SGS can be further subdivided into an upper and lower SGS (uSGS and lSGS, respectively), based on histological properties and termination zones of different types of RGCs (Fig. 1.1) (Dhande and Huberman, 2014; May, 2006).

The dSC is subdivided into intermediate and deep layers that follow a similar organizational pattern as the SGS, with an alternation of cell body and fiber layers. Collectively the dSC contains neurons that receive multisensory inputs, predominantly from the auditory and somatosensory system. Oftentimes these neurons exhibit saccade-related responses as well. Neurons in the dSC are regarded as sensory-motor integrators, and the sensory and motor maps in these layers are in spatial register with each other and with the visual map in the sSC (Cang and Feldheim, 2013; du Lac and Knudsen, 1990; Schiller and Stryker, 1972).

Cell types

Studies in numerous species, including rats and mice, agree on the broad strokes of a morphological classification of neurons in the SC. Several cell types have been identified, and some associated functional properties and projection patterns have even been proposed (Gale and Murphy, 2014; Langer and Lund, 1974; May, 2006; Mize, 1992). Much, however, remains to be done for a comprehensive functional classification of neurons in the SC. For the purpose of this

work, I will only focus on the neurons in the sSC. These fall under the following morphological categories:

- Narrow-field (NF) cells: The cell bodies of these neurons fall in the lSGS. They extend their dendritic fields in a narrow column around the soma, in both upward and downward directions. Narrow-field cells (in addition to Wide-field cells) form one of the two major excitatory (glutamatergic) outputs of the SGS.
- Wide-field (WF) cells: These are the other major excitatory output neurons of the sSC. Their cell bodies have been observed in the lSGS or even the SO. Their obliquely-extending dendrites towards the SC surface cover a very large area in comparison to their NF counterparts. However, the width of the WF dendritic tree can vary between species, and is narrower in animals with higher visual acuity.
- Horizontal cells: These are perhaps the only unambiguously inhibitory (GABAergic) neurons in the SGS. They possess an oblong cell body ending in polarly-opposed dendrites, giving them a bipolar morphology. These dendrites can extend for large distances and are capable of dendro-dendritic interactions. Horizontal cells are predominantly found in the uSGS (Langer and Lund, 1974).
- Stellate cells: Although stellate cells can be immunoreactive to GABA antibodies, they are usually classified as excitatory neurons. They have smaller dendritic fields and are considered to be locally projecting neurons; although a mouse study has shown them to project outside the SGS as well (Gale and Murphy, 2014).

- Pyriform cells: Possibly GABAergic neurons with a pear-shaped soma and ascending dendrites (Mize, 1992). They are found at the separation between the horizontal and vertical (NF/WF) cell layers in rats (Langer and Lund, 1974).
- Marginal cells: The cell bodies of these neurons are located on the dorsal surface of the SGS and extend their processes downward. Functionally-speaking, in mice, neurons with marginal-cell morphologies were found to be indistinguishable from stellate cells (Gale and Murphy, 2014). There is, however, a possibility that these cells might be local inhibitory neurons.

In the visual cortex, GABAergic neurons can be further subdivided into functional categories based on their expression of certain molecular markers, such as parvalbumin (PV), somatostatin (Som), and vasoactive intestinal peptide (VIP). These different cell types are largely non-overlapping, and each has been shown to play a different role in the local cortical microcircuit (Atallah et al., 2012; Lee et al., 2012; Pfeffer et al., 2013; Wilson et al., 2012). In the SC, however, no such molecular stamp has been found that differentiates between GABAergic morphological cell types, or that separates similar morphological types into distinct functional types. The molecular markers expressed by cortical interneurons have been shown to not be specific to GABAergic neurons in the SC. For example, PV, which defines the largest interneuron group in cortex, does not co-localize well with GABA in the SC (Behan et al., 2002).

At least two types of SGS neurons, the stellate, and marginal cells, have been difficult to classify. They might constitute a single functional type that nonetheless presents with different morphological characteristics, simply based on the constraints that their mere location in the SGS

imposes (Gale and Murphy, 2014). Better genetic tools that improve discriminability, such as the use of intersectional approaches, hold the key for a more thorough classification of cell types in the mouse SGS. Once genetic identifiers are found that cluster with the morphological and functional properties of SGS neurons, a circuit-level connectome can be pursued akin to what has been achieved in mouse V1 (Bock et al., 2011; Pfeffer et al., 2013).

Inputs and outputs

The different divisions of the SC are interconnected with each other, as well as with many other brain centers. This allows the transformation of sensory and modulatory inputs into premotor outputs.

SGS neurons receive their main input from the retina, coursing through the SO. Depending on the species, different proportions of RGCs project to the SGS. In mice, all known major RGC types have been shown to project to the SGS (Dhande et al., 2015). Different RGC types have also been shown to project to different depths in that species (Fig. 1.1), with possible functional implications (Huberman et al., 2008; Huberman et al., 2009). Specifically, DSGCs, like the posterior-motion preferring DRD4 RGCs, have been show to preferentially target the uSGS. Whereas, non-selective RGCs, like the alfa-RGCs, project to the lSGS. This suggested a possible depth-specific functional organization of SGS neurons according to their direction selectivity.

lSGS neurons also receive excitatory inputs from layer 5 of V1 (Fig. 1.1) (Wang and Burkhalter, 2013). These inputs are retinotopically organized, and could at least play the role of a gain modulator of local SGS activity in mice (Zhao et al., 2014). They have also been shown to play a role in driving innate defensive behaviors in those animals through their connection to the

SGS (Liang et al., 2015). In primates and cats, V1 inputs, in addition to inputs from extrastriate areas like MT, also provide SGS neurons with visual information for further processing (Joly and Bender, 1997; May, 2006). Retinal and cortical inputs can converge on individual SGS neurons, but target different compartments of their dendritic trees (May, 2006; Phillips et al., 2011).

Additionally, the SGS sends topographic projections to several nuclei of the visual thalamus. WF neurons are the main source of projections to the dorsal LGN (dLGN) in many species (May, 2006). In mice, however, the dLGN receives most of its SGS inputs from horizontal and stellate cells (Gale and Murphy, 2014). The ventral LGN (vLGN) also receives SGS inputs, but the neuronal types responsible for these projections vary depending on the species. In the mouse SGS, horizontal cells are a prominent source of vLGN projecting fibers (Gale and Murphy, 2014). The SGS, in return, receives feedback projections from the vLGN, but the overall function of this SGS-vLGN interconnection is not well understood (May, 2006). A third prominent thalamic nucleus that receives SGS inputs is the pulvinar (or lateral posterior (LP) nucleus). While most tectogeniculate neurons lie in the uSGS, tectopulvinar cells are located deeper, in the lSGS or SO. In mice, as well as in many other species, WF neurons have been shown to be the main source of pulvinar projections in the SGS (Gale and Murphy, 2014; May, 2006).

In the midbrain, two major centers interconnect with the SGS in a topographic manner as well; the parabigeminal (PBg nucleus), and the pretectal nuclei (or pretectum, (May, 2006)). The PBg receives substance P releasing ipsilateral excitatory inputs from neurons in the SGS and SO, and sends back bilateral cholinergic projections to local inhibitory neurons in the SGS. In mice, horizontal, stellate, and NF cells of the SGS project to the PBg (Gale and Murphy, 2014). However, feedback projections from the PBg, in addition to cholinergic projections from the brain stem,

predominantly target the intermediate layers of the SC in those animals (Mufson et al., 1986; Stubblefield et al., 2015). The pretectum also receives inputs from the SGS, but sends back inhibitory GABAergic inputs onto excitatory projection neurons (Born and Schmidt, 2004, 2007; May, 2006).

Excitatory projection neurons in the sSC project to the dSC to combine their output with multimodal and premotor information. This output to the dSC is relayed by NF cells in mice (Gale and Murphy, 2014). Neurons of the dSC in turn project, contralaterally, to eye and head movement centers in the brain stem the spinal cord (May, 2006).

Functional organization

Given what we know about the morphological organization of the SC and its connectivity to the rest of the nervous system, we can now ask questions about its functional organization. Understanding how neurons in the SC represent sensory and motor activity, and how these neurons are arranged according to their functional properties (functional architecture), is an important and insightful step to understanding the function of the SC and its importance for behavior. In this section, I will focus predominantly on the functional organization of the visually responsive layers of the SC, the SGS and SO.

Development of retinotopic organization

Topography is a hallmark of sensory system organization in the brain, where adjacent regions (or similar properties) in sensory space are systematically represented by adjacent neuronal populations. The visual system is a prime example of topographic representations, the simplest of

which is retinotopy, where adjacent points in the visual scene fall onto adjacent receptors in the retina to preserve the spatial relationship between objects. This map is relayed, in a conserved manner, to downstream retinorecipient targets in the brain. Some distortions of the map can occur to assign larger regions of the brain to specific parts of the retina that have evolved specialized functions, such as the high-acuity fovea in higher mammals. Motor maps follow similar organizational principles, and are heavily influenced by sensory maps (Cang and Feldheim, 2013).

The developmental processes that lead to topographic map formation have been of great interest. Studies in mice have uncovered molecular, as well as activity dependent mechanisms that lead to the establishment and further refinement of retinotopic maps in the SGS (Cang and Feldheim, 2013).

A particular class of receptor tyrosine kinases (RTKs) and its ligand, the Eph and ephrin respectively, have been shown to play an important role in map development. Both molecules are membrane bound, and their interaction leads to bidirectional signaling cascades that result in repulsion between the neuronal processes they're embedded in. The EphA/ephrin-A system, specifically, has been shown to be important in mapping the naso-temporal dimension of the retina onto the anteroposterior axis of the SGS. Complementary gradients of EphA and ephrin-A are expressed in RGCs, as well as in the SGS, in such a way as to direct, through repulsion, nasal RGC axons to the posterior part of the SGS, and temporal RGC axons anteriorly. A triple KO of Ephrin-A subtypes can thus lead to deficits in the formation of the collicular map, creating a patchy organization with nonetheless normal receptive field properties of individual neurons (Liu et al., 2014). This suggests the importance of the EphA/ephrin-A system in setting up the coarse and systematic retinotopic profile of the map (Cang et al., 2008). Although the mechanisms of targeting

the dorso-ventral retinal axis onto the medio-lateral SGS are not well understood, the EphB/ephrin-B system is thought to at least play a partial role in the process (Cang and Feldheim, 2013).

Before eye opening and the onset of visual experience, spontaneous acetylcholine-mediated waves are prevalent in the retina, and serve to generate locally correlated activity. A KO of the beta-2 subunit of the nicotinic acetylcholine receptor disrupts the normal structured pattern of these waves, and leads to abnormal visual response properties downstream in SGS neurons (Wang et al., 2009).

Experiments in triple ephrin-A KO animals with an additional beta-2 KO to disrupt retinal waves have therefore suggested that molecular gradients are important for the initial establishment of a coarse topographic map in the SGS, which is further refined in an activity dependent manner (Cang et al., 2008; Wang et al., 2009).

Response properties

The response properties of SGS neurons were studied in may animal species, including primates, cats, and mice. In higher mammals, no simple feature selectivity could be observed in sSC neurons. These cells are mostly thought of as feature-independent saliency detectors, which instruct saccade-related activity in the dSC (Veale et al., 2017; White et al., 2017). In mice, however, a substantial proportion of SGS neurons were shown to be either orientation of direction selective; although many neurons are still not well tuned to these particular features (Drager and Hubel, 1975; Wang et al., 2010). Mouse SGS neurons are also tuned to a wide range of spatial and temporal frequencies, albeit with certain biases (Wang et al., 2010). The receptive field (RF) size of these cells can vary with depth; the more superficial cells possessing smaller RFs (Drager and

Hubel, 1975). The On and Off RF subunits of SGS neurons are poorly segregated, presenting a large proportion of overlap. This is in contrast with neurons in V1 with fairly segregated On and Off regions (Bonin et al., 2011). SGS neurons are also tuned to different speeds of a looming stimulus (Zhao et al., 2014), a behaviorally relevant visual stimulus that can elicit freezing or escape behaviors in mice (Yilmaz and Meister, 2013). This response property has been particularly observed in PV+ (excitatory) neurons in the SGS (Shang et al., 2015).

Many morphological cell types in the mouse SGS have also been associated with particular RF and tuning properties (Gale and Murphy, 2014). NF cells have small RFs and are direction selective to small moving objects; Stellate cells have similar response properties to NF cells, but are rarely direction selective; WF cells respond to the non-specific motion of small objects within their large RF; horizontal cells have large RFs as well, but respond to either stationary objects or faster moving objects than is detected by their counterparts in the SGS. In addition to possessing these distinct response properties, the projection targets of these neurons (discussed earlier) will ultimately be important for understanding the functional contribution of the SGS to visual signal processing and visually guided behaviors.

Higher-order functional organization

On top of a retinotopic organization, neurons of the visual system can be arranged in higher-order topographies based on their functional response properties (Hubel and Wiesel, 1962). This can facilitate local computations (Chklovskii and Koulakov, 2004), but can also lead to the emergence of distinct functional pathways that deal with different properties of the visual scene.

Indeed, neurons in cat V1 have been shown to be arranged in functional columns along the depths of the cortex. In addition to a shared RF location, neurons in each column share the same preferred stimulus orientation; whereas neurons in neighboring columns preferred slightly different orientations (Hubel and Wiesel, 1962). Later on, these columns were shown to be arranged in a pinwheel structure that systematically represents the full range of orientations for a particular region of visual space (Bonhoeffer and Grinvald, 1991; Hubel and Wiesel, 1974). In fact, several orthogonal functional maps, representing different response properties, can be overlaid onto the same retinotopic landscape (Swindale et al., 2000). This cortical cytoarchitecture has been demonstrated in many other species, such as monkeys (Nauhaus et al., 2012), ferrets (Yu et al., 2005), and tree shrews (Bosking et al., 2002). A columnar organization was not, however, observed in mouse V1 (Bonin et al., 2011), despite the high degree of selectivity of their V1 neurons to several features (Niell and Stryker, 2008). This raises some questions about the function of these columns, and whether they might not simply be an emergent architecture of a wiring optimization scheme for large neuronal populations (Chklovskii and Koulakov, 2004); an optimization that might not be necessary for structures as small as, say, mouse V1. In gray squirrels, however, which are highly visual animals with a larger V1, no columnar organization could be observed either (Van Hooser et al., 2005). The function of this types of organization thus remains an open question. Further functional segregations of neurons takes place in cortical areas downstream of mammalian V1, leading to several specialized regions along two major extrastriate visual streams; a ventral stream, which deals with object recognition (The “what” pathway), and a dorsal stream (the “where” pathway), dealing with object location and motion (Goodale and Milner, 1992). While a clear functional clustering is not observed in mouse V1 (but see (Ringach

et al., 2016)), different spatial and temporal frequency preferences can be observed in downstream extrastriate areas. This supports the existence of segregated visual streams in mice that could potentially perform different functions, akin to the dorsal and ventral streams in higher mammals (Andermann et al., 2011; Marshel et al., 2011).

In the SC, beyond retinotopy and RF size (Drager and Hubel, 1975), a functional organization of neurons had been rather elusive. Two recent studies, however, using 2-photon calcium imaging and multi-unit electrode recordings (Ahmadlou and Heimel, 2015; Feinberg and Meister, 2015), have demonstrated the existence of orientation columns in the mouse SC. These columns, in contrast to those seen in higher mammalian V1, are much coarser than the retinotopic representation. This means that all neurons representing a particular region of space will respond preferentially to certain stimulus orientations, but not others, within that region. This stark contrast with cortical cytoarchitecture shifts the emphasis in signal processing from a fine discrimination and representation of objects in V1 to a global computation in the SC, fitted with a biased filter towards the detection of particular stimulus properties in particular regions of space. These findings may have future implications for understanding the behavioral and ethological functions of the SC.

A columnar organization has also been described in the SC of the ground squirrel (Michael, 1972). In contrast to the orientation-specific organization described in the mouse SC, neurons in the same column of the ground squirrel SC prefer the same direction of motion. While this study showed that DS neurons are predominantly clustered in the SGS, a finer-scale organization of neurons in that lamina was not provided.

As discussed previously, anatomical studies have shown that different functional subtypes of RGCs, specifically DSGCs and non-DSGCs, tend to project to different sublaminae in the SGS (Dhande and Huberman, 2014; Huberman et al., 2008; Huberman et al., 2009). Whether or not this particular projection pattern correlates with the cytoarchitecture of neurons in the SGS was not known. The description of such correlation in the mouse SGS constitutes a first step towards proposing a mechanism for the emergence of DS in a central brain structure.

In chapter 2 of this thesis, we set out to describe a depth specific cytoarchitecture of neurons in the mouse SGS according to the degree of their DS. First, we used two-photon calcium imaging to describe, for the first time in mice, the response properties of a very superficial and histologically distinct lamina in the SGS; the superficial SGS (sSGS). We showed that the vast majority of both excitatory and inhibitory neurons in that lamina are highly DS. We next performed single unit recordings using tungsten electrodes, and showed that the degree of DS declined with depth in the SGS. This study is the first demonstration of a lamina-specific cytoarchitecture in the mouse SGS, and is largely consistent with anatomical descriptions of DSGC projection patterns (Dhande and Huberman, 2014).

Our findings in chapter 2 paved the way for questions about the origins of DS in the SGS. I present and address this particular problem in the following section of the introduction and in chapter 3 of this thesis.

Origins of visual response properties

The same visual response properties can arise at different stages of visual signal processing in different species. A reductionist approach to studying those properties, in any given brain structure

of any given species, presumes (rather justifiably) the existence of evolutionarily conserved computational principles that lead to their emergence. Even partially conserved or homologous mechanisms may still provide a fairly generalizable understanding of the visual system. That said, caution is advisable as it is conceivable that the same properties might also arise through different mechanisms, or a combination thereof, even in the same animal. In this section, I introduce two fundamental visual response properties, namely orientation and direction selectivity, and discuss what is known about their emergence in the visual system, with a special emphasis on direction selectivity.

Orientation selectivity

Orientation selectivity is perhaps the most prominently studied response property in the visual system. It was first described in cat V1 by Hubel and Wiesel in the early 1960s. They described its columnar organization in the cortex, whereby neurons preferring similar orientations tend to cluster together along the cortical depth. They also proposed a model that can potentially explain its emergence from a specific alignment of untuned receptive fields (RFs) from the LGN. It has been referred to as the feedforward model given its exclusive reliance on converging excitatory inputs with spatially offset RFs (Hubel and Wiesel, 1962). This model has been the subject of intense investigation ever since, and the importance of local cortical inhibition in setting up, or at least influencing, orientation selectivity remains an open question. That being said, there is compelling evidence that supports the feedforward model in both cats (Reid and Alonso, 1995) and mice (Lien and Scanziani, 2013), demonstrating the sufficiency of untuned individual thalamic inputs in at least setting up cortical orientation selectivity. This is particularly interesting in mice,

given the recent discovery of orientation selective responses in the retina and LGN of these animals (Marshel et al., 2012; Piscopo et al., 2013; Zhao et al., 2013), and the projection of tuned LGN inputs into layer 4 of V1 (Sun et al., 2016).

These findings raise questions about the origin of orientation selectivity in the SC, and whether orientation selective retinal inputs (Nath and Schwartz, 2016; Zhao et al., 2013) might play a more important role in the emergence of tuned responses in that structure than they do in V1.

Direction selectivity

Two theoretical models were proposed in the 1950s and 60s describing possible mechanisms for the emergence of direction selectivity (DS) in the visual system. These were the Hassenstein-Reichardt model (Reichardt, 1961), introduced in the experimental context of insect vision, and the Barlow-Levick model (Barlow and Levick, 1965), in the mammalian retina. The Hassenstein-Reichardt model proposed that direction selectivity can arise in a postsynaptic cell that integrates untuned excitatory inputs as a coincidence detector. This can be achieved when these inputs are spatially and temporally offset. Those that are activated first by a stimulus moving in the preferred direction are delayed so that they arrive at the same time postsynaptically as the subsequently activated inputs. They would then integrate and drive the postsynaptic membrane potential past the firing threshold. Conversely, when the stimulus is moving in the null direction, this delay line arrangement leads to a more diffuse and less effective postsynaptic integration. The Barlow-Levick model, on the other hand, proposes a delayed inhibitory input on the null side. This input will

hence only be effective when a stimulus is moving in the null direction, leading to postsynaptic direction selectivity (Fig. 1.2B-C).

Direction selectivity has long been studied in the optic tectum (OT) of lower vertebrates, such as the goldfish (Wartzok and Marks, 1973). More recently, the zebrafish has emerged as a prominent model for the study of tectal DS (Gabriel et al., 2012). It has been shown that subtypes of zebrafish RGCs that prefer particular motion directions project to segregated layers in the tectum, and that tectal neurons with matching preferred directions arborize their dendrites in the corresponding layers (Gabriel et al., 2012; Lowe et al., 2013; Nikolaou and Meyer, 2012; Robles et al., 2013). In other words, the DS retinal inputs could largely determine the direction preference in at least some neuronal populations in the OT (Gabriel et al., 2012). While excitation onto some of these cells is tuned, it is not clear whether it's inherited directly and exclusively from DSGCs. Indeed, new preferred directions emerge in the OT that are different from the preferred directions described in DSGCs (Hunter et al., 2013), indicating either the convergence of DSGC inputs with different preferred directions, or the involvement of local inhibition is the emergence of DS. In fact, some DS tectal neurons have been shown to receive inhibitory input tuned to the null direction that acts on untuned excitation (Grama and Engert, 2012), indicating the involvement of local computations in this emergence of DS. Several mechanisms might therefore be at play in the emergence of DS in the zebrafish OT.

In zebrafish, DS in the OT is a largely genetically determined process. DS emerges in an activity and experience independent manner (Niell and Smith, 2005; Ramdya and Engert, 2008). The same was shown for the emergence of DS in the mouse retina. Spontaneous retinal activity preceding eye opening is not required for the normal functional development of this particular

property (Elstrott et al., 2008; Wei et al., 2011). After eye opening, and as the mouse transitions into adulthood, a slight sharpening of direction tuning is observed in DSGCs. In addition, a more uniform distribution of DSGC preferred directions, compared to a more biased one in P14 animals, starts to emerge in adults. However, this distribution remains restricted to the cardinal directions of motion (Elstrott et al., 2008).

Mechanistically, starburst amacrine cells (SACs) in the mouse retina have been implicated in generating DS in ganglion cells. Individual SAC processes are themselves DS to a stimulus moving centrifugally from the soma outwards, along their axis. Ganglion cells receive inhibitory GABAergic inputs from neighboring SACs that connect to them asymmetrically, providing stronger inhibition from what will therefore become the "null" side. This circuit contains many elements of the Barlow-Levick model for the emergence of DS.

Conversely, the emergence of direction selectivity in cat V1 has been shown to follow the Hassenstein-Reichardt model (Priebe and Ferster, 2005), akin to the emergence of orientation selectivity in V1, through integration of feedforward excitatory inputs. How direction selectivity emerges in the SC, however, was not understood. We decided to address this question by using the SGS of the mouse SC as our model system. As discussed earlier, direction selective responses can be observed in the mouse SGS, and prominently so in the sSGS, making it an ideal system to study this property. Additionally, the discovery of DSGCs in the mouse retina, and showing that they tend to project into the SGS in a manner that matches the distribution of DS neurons, provided enticing anatomical evidence that the DSGCs are the direct source of DS in the SGS. This foregoes the need for a sophisticated computation at this particular synapse (Fig. 1.2A). Although this hypothesis was the more parsimonious and least metabolically and computationally costly for the

organism, it remained to be experimentally demonstrated. This was important in light of the recent discovery that orientation selectivity arises in mouse V1 through the integration of untuned thalamic input (Lien and Scanziani, 2013), despite the identification of orientation selective cells in the retina and the LGN of those animals. The emergence of direction selectivity in mouse V1 remains the subject of ongoing investigations.

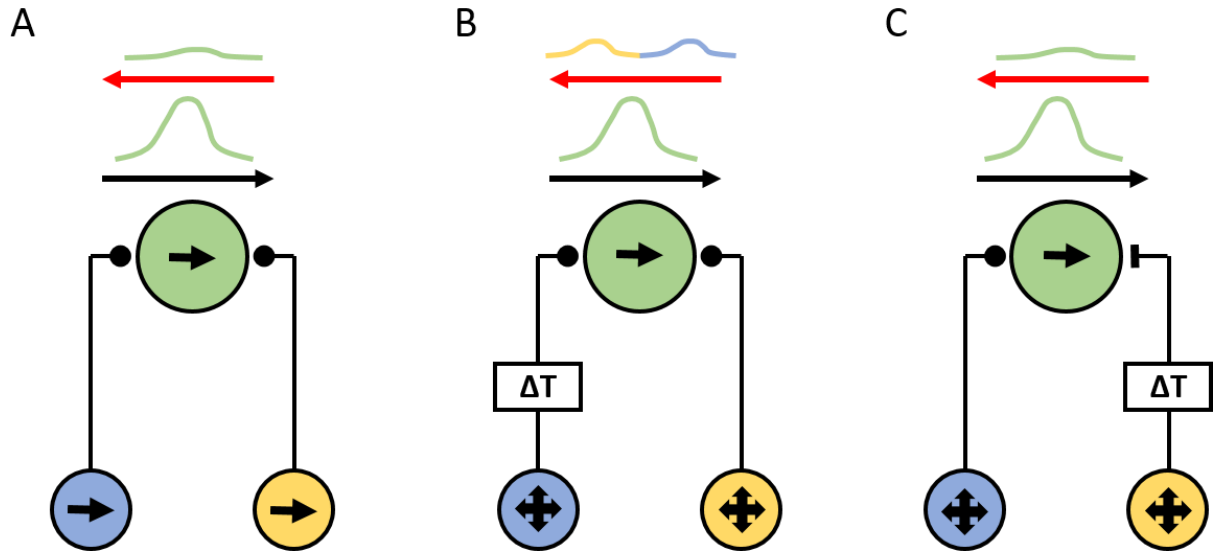

Figure 1.2. Models for the emergence of direction selectivity in a postsynaptic neuron. (**A**) Direction selectivity (DS) can simply be the result of convergent inputs from presynaptic DS cells (directional short black arrows) that prefer similar directions of motion. DSGCs are found in the retina of certain animal species and the mechanisms that result in their selectivity are well described, borrowing principles from **B** and **C**. Alternatively, DS can emerge through special integration of untuned inputs (Quad arrows in **B**-**C**). (**B**) The Hassenstein-Reichardt model, where a delayed arrival (ΔT) of a portion of the excitatory input (black circle synapse) can lead to a better integration under a particular sequence of presynaptic activity (long black arrow; preferred direction) and a temporally diffuse and ineffective integration under another sequence (long red arrow; null direction). (**C**) The Barlow-Levick model, where a delayed inhibitory input (ΔT, black bar synapse) coincides with untuned excitation during null-direction motion, but not for motion in the preferred direction.

In chapter 3 of this thesis I discuss how we confirmed the hypothesis that DSGCs are the direct source of selectivity in the SGS, by selectively reducing the DS of these cells and demonstrating a subsequent reduction of DS in SGS neurons. In that same study (not included in chapter 3), we also performed whole cell voltage clamp recordings in DS neurons of the SGS while optogenetically silencing local excitation, in order to isolate retinal inputs. We showed that retinal EPSCs are already tuned in the postsynaptic cell, and that they're the result of individually tuned DSGC inputs (Shi et al., 2017).

Local computations in the stratum griseum superficiale

To date, little is known about the role of local circuits in the SGS in transforming the wealth of inputs they receive. We've ruled out the role of local SGS circuits in setting up direction selective responses, but have also shown that local excitation is important for amplifying the retinal input without affecting its tuning (Shi et al., 2017). Our data suggests that inhibition is not necessary for the emergence of DS, and so its role remains rather poorly understood. There is, however, some evidence for its role in mediating surround suppression.

Surround suppression

When a visual stimulus exceeds the RF of a neuron in size, a decrease is this neuron's activity is usually observed. This phenomenon is termed "surround suppression", and is ubiquitously observed at all stages of the visual system, and in many animal species (Fig. 1.3A). Despite its manifestation in the responses of RGCs, several visual structures downstream of the retina have been implicated in at least partially mediating the effects of surround suppression, and contributing

to its local emergence (or re-emergence). Surround suppression is thought to be useful for efficient coding, through response sparsification and the elimination of responses to redundant stimuli in the visual scene (Sachdev et al., 2012).

While lateral inhibition is implicated in mediating surround suppression in the retina (Demb and Singer, 2015), the downstream mechanisms of this phenomenon remain debatable. Surround suppression can be mediated simply by a withdrawal of excitation, as has been shown in cat V1 (Priebe and Ferster, 2006). In that case, a large visual stimulus leads to a withdrawal of feedforward thalamic input to V1, resulting in a balanced withdrawal of excitation and inhibition. However, such mechanism does not exclude the influence of lateral inhibition somewhere upstream of V1. An alternative phenomenon, implicating local inhibition by somatostatin positive (Som^+) neurons, has been proposed to mediate surround suppression in mouse V1. Som^+ neurons have poor size tuning, as their response increases monotonically with stimulus size. These cells were shown to be actively involved in suppressing local excitatory neurons by pooling excitatory input from the stimulated surround (Adesnik et al., 2012).

Surround suppression is also observed in the SC of many species (Binns and Salt, 1997; Goldberg and Wurtz, 1972; Sterling and Wickelgren, 1969; Wang et al., 2010; Zahar et al., 2012). Pharmacological manipulations, slice recordings, and in vivo calcium imaging in rats and mice have allowed a more detailed exploration of its possible mechanisms in the SGS. Slice recordings and pharmacological studies in rodents suggest a Mexican-hat-type interaction between center and surround in the SGS (Phongphanphanee et al., 2014), and the involvement of $GABA_A$ receptors in mediating surround suppression (Binns and Salt, 1997). A more recent two-photon imaging study in the mouse SGS using a two-point visual stimulus to probe surround-suppression showed that

the activity of local inhibitory and excitatory neurons is equally suppressed by the surround (Kasai and Isa, 2016). All these studies point to long range inhibitory input from horizontal cells in the SGS as the mediator of this phenomenon. The role of these neurons, however, is yet to be directly demonstrated. Achieving this is limited by a lack of genetic discriminability between long range and local GABAergic cell types in the SGS, which prevents the manipulation of specific circuit components.

Modulating effects of the surround

Non-specific surround suppression represents only a subset of the effects the surrounding areas of a RF can exert on the activity within it. Depending on the types of stimuli presented in the center and surround, and their relationship to each other, differential levels of suppression have been observed in many brain structures of different species. Facilitatory effects by the surround have even been observed under certain conditions (Jones et al., 2001; Jones et al., 2002; Kastner et al., 1999; Knierim and van Essen, 1992; Nothdurft et al., 1999; Sengpiel et al., 1997; Sillito et al., 1995).

In primate and cat V1, where neurons are orientation selective, differential levels of surround suppression can be observed. Neurons experience stronger suppression when the orientation of the surround stimulus matches that at the center. Conversely, an attenuation in suppression, or even response facilitation, can be achieved by an orthogonally oriented surround. Such differential effect can play an important role in the discrimination between particular properties of the visual scene at the level of individual neurons, providing them with feature-contrast sensitivity, and the capacity to represent objects contextually. A similar phenomenon was

described in mouse V1, involving differential levels of suppression, but with no evidence of response facilitation (Self et al., 2014).

In the optic tectum of birds and fish, where neurons are direction selective to a stimulus within their RF, motion-contrast sensitivity has been observed (Ben-Tov et al., 2015; Frost et al., 1981; Sun et al., 2002; Zahar et al., 2012). Neurons in the tectum can modulate their response to a moving stimulus depending on how much it contrasts with motion direction (or other motion properties) in the surround (Fig. 1.3B).

Conversely, in the primate SC, neurons are not highly feature selective, and so are thought to receive feature-specific inputs from cortical areas, and generate a feature-agnostic saliency map that instructs orienting motor responses downstream in the circuit (Veale et al., 2017). This suggests a gradual evolutionary migration of saliency computation from a single locus in the OT/SC of lower vertebrates/mammals to a multi-structural process that involves cortical inputs in higher mammals (Zhaoping, 2016).

The mouse SC is well situated on the evolutionary scale to study feature-specific center-surround interactions. As is the case in the tectum of birds and lower vertebrates, neurons in the mouse SGS exhibit direction selective responses. Should these neurons also exhibit feature-contrast sensitivity, the mouse SGS would become a rare mammalian model to study the emergence of saliency representation, and its transformation from a feature-specific to a feature-agnostic one, within the same brain structure. Whether or not the activity of mouse SGS neurons can be differentially modulated by the surround had not been explored.

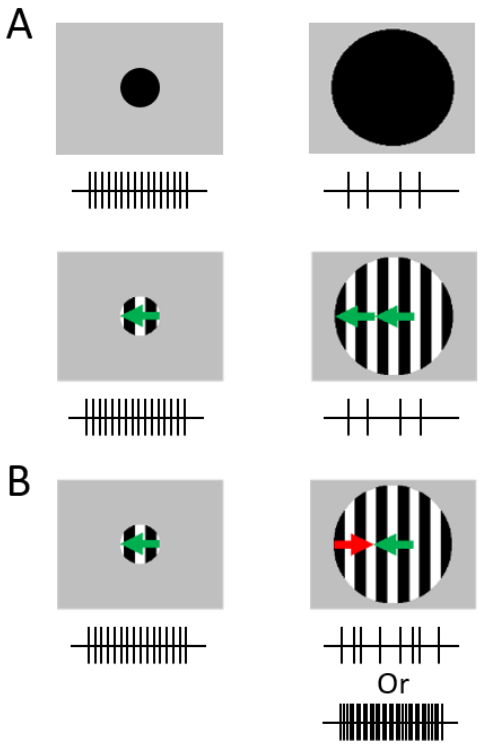

Figure 1.3. Surround modulation of neuronal activity. (**A**) Classical surround suppression whereby, all other properties alike, a larger visual stimulus leads to a suppression of a neuron's activity. The decreased spiking activity is depicted under the larger stimuli (**right**), compared to the smaller ones with the same properties (**left**). (**B**) A surround possessing contrasting properties to those of the smaller center stimulus, such as an opposite direction of motion in this example, can lead to either an attenuated suppression (compare to **B, right)**, or even to a potentiated activity. In chapter 4, we show that neurons with this type of feature-contrast sensitivity exist in the mouse SGS.

In chapter 4 of this thesis, we show that neurons in the mouse SGS encode motion contrast between their RF center and surround. The responses of superficial excitatory neurons are bidirectionally modulated, increasing monotonically as a function of the direction difference between the center and surround, from suppression by the same-direction surround to maximal potentiation by an oppositely-moving surround. The degree of potentiation declined with depth in the SGS, along with direction selectivity, suggesting a potential specialization of the most superficial lamina of the SGS in motion processing. Inhibitory neurons, on the other hand, are always suppressed by the surround stimuli; though different levels of suppression were observed. These cell type- and depth-specific response profiles update our view of the functional architecture

of the mouse SGS, and are likely important for the animal to detect object motion in the environment and distinguish it from self-induced full-field motion in the background.

Behavioral importance (saliency)

As discussed in the previous section, the organization of a neuron's effective RF in a way that takes into account feature-opponency can help to not only situate a particular set of features in space, but also discriminate multi-dimensional feature clusters as a separate object within a contrasting background.

Having demonstrated the existence of motion-contrast responses in the mouse SGS (chapter 4), neurons in that region of the mouse SC could be playing an important role in the detection of salient objects in the environment. This will instruct downstream premotor actions, ultimately leading to orienting behaviors. An eye movement map was recently described in the mouse dSC that supports this proposed function (Wang et al., 2015). Even though the mouse retina does not have a fovea, it nonetheless possesses some specializations that might require eye movements (Demb and Singer, 2015). While visual saliency and eye movements have been classically studied in the primate SC, these recent findings establish the mouse SC as a valid model system to study saliency and orienting behaviors.

Having the ability to record from and manipulate specific neuronal populations in the mouse SC, especially when the mouse is awake and behaving, will give us a better understanding of how visual signals are represented in the SC under those conditions, and to what extent and in what way they influences downstream activity and behavior.

CHAPTER 2

Neurons in the Most Superficial Lamina of the Mouse Superior Colliculus Are Highly Selective for Stimulus Direction

Summary

The superior colliculus (SC) is a layered midbrain structure important for multimodal integration and sensorimotor transformation. Its superficial layers are purely visual and receive depth-specific projections from distinct subtypes of retinal ganglion cells. Here we use 2-photon calcium imaging to characterize the response properties of neurons in the most superficial lamina of the mouse SC, an undersampled population with electrophysiology. We find that these neurons have compact receptive fields with largely overlapping ON and OFF subregions, and are highly direction selective. The high selectivity is observed in both excitatory and inhibitory neurons. These neurons do not cluster according to their direction preference and lack orientation selectivity. In addition, we perform single unit recordings and show that direction selectivity declines with depth in the SC. Together, our experiments reveal for the first time a highly specialized lamina in the most superficial SC for movement direction, a finding that has important implications for understanding signal transformation in the early visual system.

Introduction

The superior colliculus (SC) in mammals (or optic tectum, OT, in lower vertebrates) is a midbrain structure involved in multimodal sensorimotor integration, saccade generation, and orientating head and body movements (Gandhi and Katnani, 2011; May, 2006). The superficial layers of the SC, including the *stratum griseum superficiale* (SGS) and *stratum opticum*, are purely visual and receive direct retinotopic inputs from the retina. The intermediate and deep layers of the SC are multimodal and premotor, containing auditory, somatosensory, and eye movement maps that are aligned with the retinotopic maps in the SGS. Such a layered organization facilitates the integration of visual, auditory, and tactile information and the initiation of orienting movements to redirect attention toward a stimulus (Cang and Feldheim, 2013).

Studies in a number of species, including goldfish, zebrafish, mice, rats and tree shrews, indicate that visual layers in the SC/OT can be further divided into sub-laminae (Albano et al., 1978; Gabriel et al., 2012; Girman and Lund, 2007; Huberman et al., 2008; Schmidt, 1979). For example, in mice, a subtype of ON-OFF direction-selective (DS) retinal ganglion cells (the DRD4 RGCs) was found to project exclusively into the upper SGS (Huberman et al., 2009). In contrast, the transient OFF α-RGCs project into the lower SGS (Huberman et al., 2008). These studies thus suggest that the visual layers of the SC may receive a stack of superimposed retinotopic inputs that each encodes a different feature of the visual world (Dhande and Huberman, 2014). However, the functional properties of SGS neurons cannot be easily inferred from anatomical projection patterns, in part because different RGC subtypes often project to the same SGS sub-laminae. For example, the upper SGS, in addition to receiving DS input from DRD4 and other types of RGCs (Kay et al., 2011), is also the primary, if not exclusive, target of the W3-RGCs which are motion

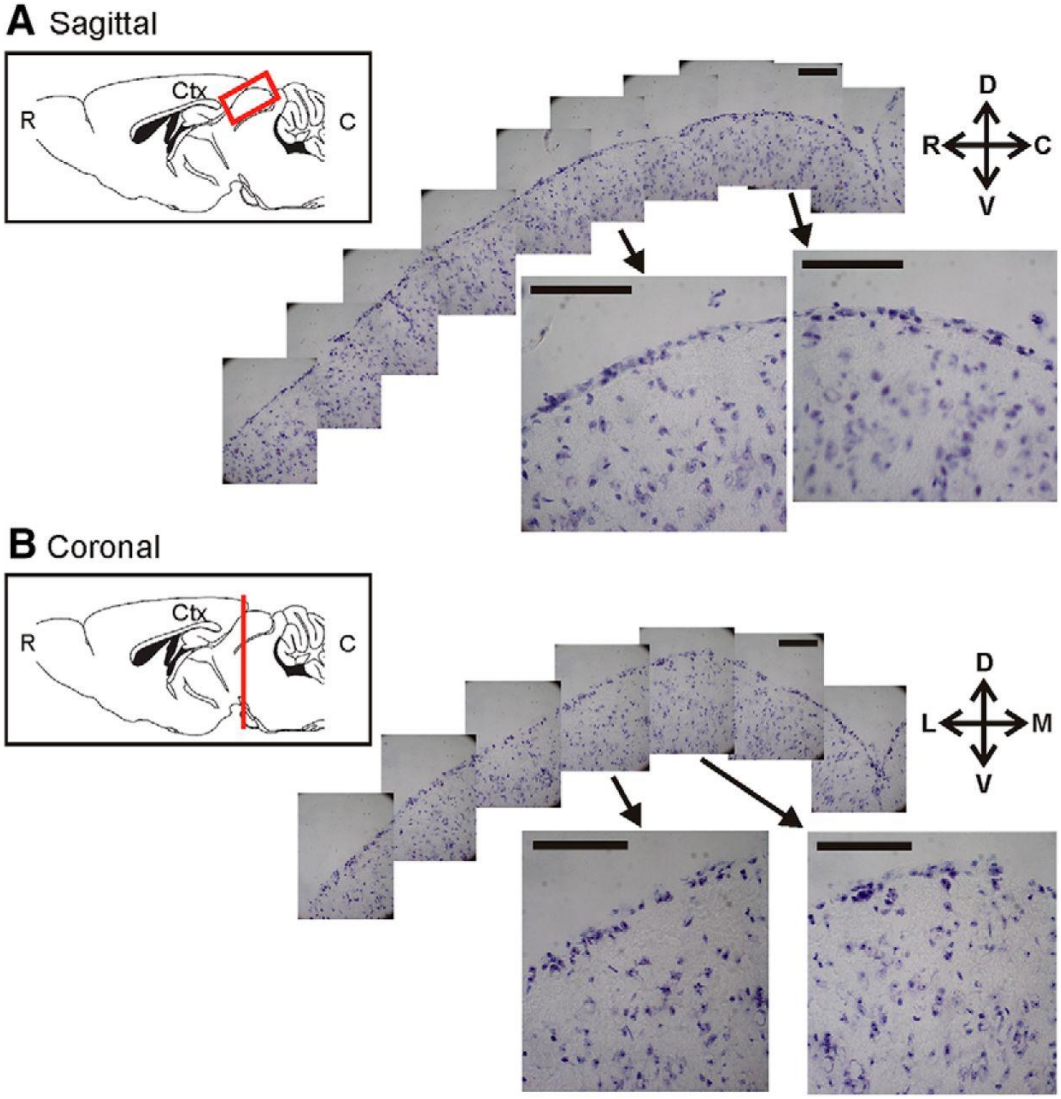

Figure 2.1. The most superficial lamina of the mouse SC is densely packed with cells.
A, A series of Nissl staining images of a sagittal section of the SC in an adult mouse. Two of these images are shown at higher magnification. This section was ~500 μm from the midline. In the inset is a schematic of the mouse brain along the rostral (R)–caudal (C) axis, with the red box marking approximately the region shown in the images. ***B***, Images of a coronal section of the SC from a different mouse. This section was ~1500 μm from the caudal end of the SC, as diagrammed by the red line in the inset. The cortex (Ctx) was removed in both sections. D, Dorsal; V, ventral; L, lateral; M, medial. Scale bars, 100 μm.

sensitive but not direction selective (Kim et al., 2010; Zhang et al., 2012). In addition, the information carried by RGC axons is likely further transformed by local circuits in the SC through

dynamic interactions between excitatory and inhibitory inputs, thereby endowing individual SGS neurons with particular functional properties.

Several electrophysiology studies have described the receptive field properties of visual collicular neurons in mice (Drager and Hubel, 1975; Gale and Murphy, 2014; Wang et al., 2010). However, despite thorough characterizations in these investigations, no studies have examined the response properties of SGS neurons by sub-laminae or depth. In fact, the topmost lamina of the SGS is often under-sampled, if not entirely missed, by conventional electrophysiology. This is because the electrode tip is usually tens of microns below this level before it finally breaks through the collicular membrane and is able to pick up single units. As a result, the receptive field properties of the neurons in the most superficial lamina of SGS (Fig. 2.1) remain largely a mystery. To address this issue, we have therefore performed 2-photon calcium imaging in this study to characterize the response properties of neurons in the most superficial lamina of the mouse SGS.

Materials and Methods

Animal preparation

Adult C57BL/6 mice of both genders were used in this study (postnatal day 53-123), including 16 wild type (WT) and 7 transgenic mice that express the red fluorescent protein tdTomato in GAD2+ (GABAergic) neurons. These transgenic mice were generated by crossing homozygous Gad2-IRES-Cre knock-in mice (Jackson Lab stock #010802**,** (Taniguchi et al., 2011)) with homozygous Ai9 Cre reporter mice that have a *loxP*-flanked STOP cassette preventing transcription of tdTomato (Jackson Lab stock #007909, (Madisen et al., 2010)). Both lines of mice were on a C57BL/6 background. The mice were housed under a 12h light/dark cycle and provided with food and water ad libitum. All animals were used in accordance with protocols approved by Northwestern University Institutional Animal Care and Use Committee.

In both imaging and physiology experiments, the mice were first anesthetized with Urethane (1.3 g/kg in sterile saline solution, i.p.), and then sedated with chlorprothixene (10 mg/kg in water, i.m.). Subcutaneous Atropine (0.3 mg/kg) and Dexamethasone (2 mg/kg) were also administered before the surgery, to avoid respiratory secretions and brain edema, respectively. The animals' core temperature was maintained at 37 °C via a rectal probe and a feedback heater (Frederick Haer Company). A thin layer of silicone oil was applied to the eyes to prevent drying.

After the mice were anesthetized, the scalp was shaved and cleaned with betadine and isopropanol. The skin was then removed to expose the skull. After the connective tissue was removed and the area washed with ACSF, a craniotomy was performed on the left hemisphere, starting at the lambda point and extending ~5 mm both laterally and rostrally. An 18 gauge needle

with a beveled tip was linked to a suction line, and used to remove the overlying cortical tissue above the SC.

Dye preparation, loading, and imaging

For every experiment, a fresh solution of the fluorogenic calcium-sensitive dye Cal-520 AM (AAT Bioquest) was prepared. A solution of 20% Pluronic F-127 in DMSO was freshly prepared, and sonicated for 10 min. 4 µl of this solution were used to reconstitute 50 µg of powdered Cal-520. The resulting solution was sonicated for another 12-15 min, and then brought to a total volume of 40 µl by adding 35.2 µl of a calcium-free solution (150 mM NaCl, 2.5 mM KCl, 10 mM HEPES, pH 7.4) and 0.8 ul of 5 mM Sulforhodamine (SR) 101, to reach a final concentration of 1.13 mM Cal-520 and 100 µM SR101. After 5 more min of sonication, the solution was ready to be bolus loaded. To load the dye solution into the SC, we used a Nanoject II (Drummond) fitted with a glass pipette with a beveled tip at 45° and with an inner diameter of 10-20 µm.

Once the SC was exposed, the pipette containing the dye was lowered into the tissue using a fine hydraulic manipulator. Twenty pulses of 2.3 nl each (46 nl total volume), at 30 s interval, were delivered to inject the Cal-520 solution at a depth of 500 µm below the surface. The same procedure was repeated after retracting the pipette to a depth of 250 µm. The pipette was left in the tissue for 1-2 min before being slowly retracted. The SC was then covered by ACSF. Imaging was performed 1-2h after loading.

Once the injection procedure was complete, a small metal plate was mounted on the mouse's head with MetaBond (Parkell), which, when clamped under the microscope, resulted in the imaged SC surface being largely flat and perpendicular to the objective. A light-shielding cloth

was then placed around the craniotomy to block light from the visual stimulus during imaging. The SC was covered by 2.5% agarose in ACSF for stability. Imaging was performed with a 2-photon microscope (2P-SGS, Prairie technologies) at an excitation wavelength of 800 nm, and with a 40X/0.8NA objective (Leica). Data were acquired using PrairieView software with a spiral scan at 2X optical zoom, resulting in a circular field of view with a diameter of 138 μm. Image resolution was 256x256 pixels and the acquisition rate 8.079 Hz. We also took red-channel images of each field of view at excitation wavelength of 800nm for SR101 (to identify glial cells) and 720nm for tdTomato (to identify GAD2+ cells).

Visual stimuli

Visual Stimuli were generated with Matlab Psychophysics toolbox (Brainard, 1997; Niell and Stryker, 2008) on a 37.5 x 30 cm LCD monitor (60Hz refresh rate, ~50 cd/m^2 luminance). The monitor was placed 25 cm away from the eye contralateral to the imaging site (the right eye). The screen was also tilted at an angle matching that of the mouse's head, given that the mouse's nose was slightly elevated to correct for the curvature of SC and allow imaging from a relatively flat surface.

To map the RFs of imaged cells, a 5°x5° white (to map ON) or black (to map OFF) square was flashed on a grey background, in a 6x6 grid in a pseudorandom order. The flash duration was 1 s and repeated (at a different location) after a wait period of 3 s to allow for the calcium signal to decay substantially between flashes. The RFs of the imaged areas, which were always rostral to the lambda suture, were roughly between contralateral 20° and 120° horizontally from the vertical meridian, and 40° and -45° vertically (with 0° corresponding to the eye level, negative values for

lower visual space; and the majority of RFs fell between 10° and -45°). To determine direction/orientation selectivity, drifting sinusoidal gratings of 12 directions (0°-330°, with 30° increments) were presented in a pseudorandom order either within a circular window (30° in diameter and surrounded by a grey background) near the center of the imaged cells' RFs or full screen of the stimulus monitor. For imaging, the gratings were displayed for 3 s, and a grey background was shown for 5 s between presentations. The spatial and temporal frequencies of the drifting gratings were 0.08 cycles/degree (cpd) and 2 Hz, respectively, chosen according to our previous electrophysiology study of SC neurons (Wang et al., 2010). In addition, we also used full screen gratings of the same parameters and moving bright bars (5° in width and 30 deg/sec speed) in some of the experiments. For all types of stimuli, 5-7 trials of all conditions were presented to the animal. For single unit recording, the small gratings were presented at 4 spatial frequencies (0.02, 0.04, 0.08, and 0.16 cpd), for a duration of 1.5 s followed by 0.5 s of grey screen.

Analysis of imaging data

Custom Matlab scripts were used to analyze the 2-photon imaging data. After the end of recording sessions, all collected frames of individual time-series were averaged, and regions of interest (ROIs) were selected on the average images where cell bodies were clearly identifiable. A few recordings with drifts and large tissue motion where cell bodies were blurred in the average images were excluded from further analyses. The ROIs were either polygons or rectangles drawn manually inside cell bodies to measure the intracellular Ca^{2+} signal with minimal neuropil activity contamination. The intensity values for all pixels in each ROI were averaged for each frame to obtain the raw temporal Ca^{2+} signal of the respective cell. From the raw signal, for each stimulus

presentation, the relative change in the fluorescence signal from the baseline, i.e., $\Delta F/F_0 = (F-F_0)/F_0$, was calculated as follows. F_0 was the mean of the baseline signal over a fixed interval before stimulus onset. The fixed interval was the last 25% of the duration between stimuli offset and next onset, which was chosen to allow the fluorescence signal from the previous stimulus presentation to decay sufficiently to baseline. F was the fluorescence signal from 250 ms after stimulus onset to 500 ms (for gratings and 100ms for spots) after stimulus offset (Scott et al., 2013) and was chosen to improve signal to noise ratio.

A cell was considered responsive to flashing spots or drifting gratings if its mean fluorescence during the visual stimulus period (as defined by F above) was more than two standard deviations above the mean baseline fluorescence (F_0) for at least one of the stimulus conditions (out of the 36 positions for spots or 12 directions for gratings). For bars, because the cell's fluorescent signal rose only when the stimulus entered its RFs, it was considered responsive if the peak of the averaged F over all trials was more than three standard deviations above F_0 for at least one of the 12 directions. The mean value of $\Delta F/F_0$ for each of the stimulus conditions of flashes and gratings, or peak value for bars, was then used to determine the RF or direction tuning curves for every responsive cell.

The RF area was determined by two methods. First, the ON- and OFF-evoked $\Delta F/F_0$ on the grid were each fitted with a two-dimensional Gaussian distribution with independent standard deviations, a and b, in the coordinate system defined by the axes of the response field, as shown in the following equation: $G(x,y) = \frac{A}{2\pi ab} exp(\frac{x'^2}{2a^2} + \frac{y'^2}{2b^2})$, where x' and y' are the polar transformations of space coordinates x and y at an angle θ, along which the Gaussian distribution is oriented (Wang et al., 2010). The area enclosed by the fitted ellipse (with a and b as its semi-

major and semi-minor axes) was used to quantify the area covered by each subregion ($Area_{on}$ and $Area_{off}$). Second, the area of each subfield was calculated by counting the area of squares in the grid where the cell was responsive as determined by the criterion described above (Liu et al., 2014).

The RF center was also determined using two methods. First, the RF center was the location of the maximum response in the fitted Gaussian. Second, the RF center was determined by the following "center of mass" equation, $RF\ Center, [x, y] = \frac{\sum R_i r_i}{\sum R_i}$, where i represents the places in the grid where the cell was responsive. R and r represent the response magnitude ($\Delta F/F_0$) and position vector at the ith location respectively. The relative spatial relationship of the ON and OFF subregions were quantified by an area ratio: $\frac{Area_{on} - Area_{off}}{Area_{on} + Area_{off}}$, where the areas were determined in the two ways described above. The values of the area ratio range between -1 and 1 with positive values indicating a larger ON subregion and negative values indicating a larger OFF subregion. In order to determine the degree of overlap between ON and OFF subregions, an overlap index (OI) was determined using the following equation, $OI = \frac{S_{ON-OFF}}{S_{ON} + S_{OFF} - S_{ON-OFF}}$, where S_{ON} and S_{OFF} are the number of squares of the 6x6 grid where the cell responded to ON and OFF stimuli respectively, and $S_{ON\text{-}OFF}$ is the number of squares where the cell responded to both ON and OFF stimuli. The values of OI range between 0 and 1 with larger values indicating a larger degree of overlap.

For direction selectivity, a DSI was calculated: $DSI = \frac{R_{pref} - R_{opp}}{R_{pref} + R_{opp}}$, where R_{pref} is the cell's mean $\Delta F/F_0$ value at the preferred direction (i.e., maximal response), and R_{opp} is the cell's response to the direction opposite to the preferred one. In addition, we also calculated a global DSI as the vector sum of responses normalized by the scalar sum of responses (Gale and Murphy, 2014):

$gDSI = \frac{\sum R_\theta e^{i\theta}}{\sum R_\theta}$, where R_θ is the response magnitude ($\Delta F/F_0$) at θ direction of gratings. Similarly, an orientation selectivity index (OSI) and global OSI were calculated, $OSI = \frac{R'_{pref} - R_{orth}}{R'_{pref} + R_{orth}}$, where R'_{pref} was the mean response of R_{pref} and R_{opp}, and R_{orth} was the mean response to the two directions orthogonal to θ_{pref}; and $gOSI = \frac{\sum R_\theta e^{i2\theta}}{\sum R_\theta}$.

Tuning widths were calculated as full-width at half-height (fwhh) by fitting the raw tuning curves with Von Mises function (Elstrott et al., 2008; Oesch et al., 2005): $R = \frac{R_{max} e^{k\cos(\theta-\mu)}}{e^k}$, where R is the response at the θ direction (in radians), μ is the preferred direction determined by angle of sum vector ($\sum R_\theta e^{i\theta}$), R_{max} is the maximum response and k is the concentration parameter accounting for the tuning width. The fwhh was then calculated as follows, $fwhh = 2 * acos\left[\frac{ln\left(\frac{1}{2}e^k + \frac{1}{2}e^{-k}\right)}{k}\right]$.

Two-photon imaging guided cell-attached recording

In a few imaging experiments, we performed simultaneous 2-photon imaging and cell-attached recording. We used glass electrodes (1B150F-4 from WPI, tip opening ~1-2 μm). The electrodes were filled with ACSF (125 mM NaCl, 5 mM KCl, 10 mM glucose, 10 mM HEPES, 2 mM $CaCl_2$, pH 7.4) containing 20 μM Alexa 594 for visualization under the microscope. Once a neuron of interest was located, the electrode was advanced to its vicinity with a positive pressure of 60-100 mbars. The pressure was then reduced to 20-40 mbars and the pipette was slowly approached to a position a few microns on top of the target cell. The pipette was further lowered down until it was in contact with the cell. An increase in resistance was observed upon contact, and the pressure was

released. A little bit of suction was occasionally applied to get a good seal that varied anywhere from 30 MΩ to 1 GΩ, and to observe spiking activity with a detectable amplitude above the background. A MultiClamp 700B amplifier (Molecular Devices) in current-clamp mode and a System 3 workstation (Tucker-Davis Technologies) were used to record extracellular spiking. The spiking data was then compared with the imaging data for the same cell. In particular, we compared the number of spikes in a given cluster (a 1 s period preceded by 1 s of quiescence) and the amplitude of the corresponding $\Delta F/F_0$, and saw a linear relationship between the two (Fig. 2A-D, n = 3 neurons from 3 WT mice).

Single unit recording

Mice were anesthetized as previously described for imaging, and mounted on a stereotaxic frame with ear bars. The same surgical procedure was performed as for imaging to expose the SC. Tungsten microelectrodes (5-10 MΩ, FHC) were used for single unit recordings. The surface was estimated as the point where the electrode touches the SC surface and forms a closed circuit. This was further confirmed visually under the microscope. Agarose was then added onto the recording site to stabilize the brain, and kept moist with ACSF throughout the recording session. The electrode was then slowly lowered, perpendicular to the surface, into the SC and the depth of every recorded unit was noted. Two to 3 electrode penetrations were performed per animal, yielding 1 to 5 units in total. Spikes and field potentials were acquired using a System 3 workstation (Tucker-Davis Technologies) following our published procedures (Liu et al., 2014; Sarnaik et al., 2014; Wang et al., 2010; Zhao et al., 2014).

For each electrode penetration, the RF center was located based on the local field

potential's response to moving bars. Drifting gratings were then presented at that location within a circular window, 30° in diameter, as described above. The direction selectivity of the recorded single unit was quantified using the same DSI as described for imaging.

Nissl staining

Mouse brains were dissected after perfusion with 4% paraformaldehyde (PFA) fixative, cryo-protected in 30% sucrose, and embedded in OCT (Tissue-Tek, Elkhart, IN), following our published procedures (Chen et al., 2015). Serial sections of the brains were cut at 14 µm either coronally or sagittally. Sections were then nissl-stained (Cresyl Violet Acetate, Sigma C5042, 0.5%) and cover-slipped with Permount (SP15-500, Thermo Fisher Scientific, Waltham, MA). Images were captured using the Leica DMRB Widefield Fluorescence System (Leica, Germany), and assembled in Adobe Photoshop.

Statistics

Statistical analyses and graph plotting were done in Matlab (Mathworks), and values were presented as mean ± SEM. T-tests, and ranksum test were performed as mentioned in the text.

Results

Two-photon calcium imaging of the superficial SGS in mouse Superior Colliculus

The most superficial lamina of the SGS, which we refer to as "sSGS", appears to be more densely packed with cells than deeper laminae (Fig. 2.1). In order to characterize the functional properties of these neurons, we performed *in vivo* 2-photon calcium imaging in urethane-anesthetized adult mice. The SC was exposed after removing overlaying cortical tissues, and sSGS neurons (within the top 50 μm, and the mean depth of the imaged planes was 31.0 ± 2.2 μm, n = 22 recordings) were then loaded with a recently characterized synthetic Ca^{2+} indicator, Cal-520 (Tada et al., 2014). We first characterized the calcium response of the indicator by performing simultaneous 2-photon imaging and cell-attached recordings (Fig. 2.2A-C). We compared the number of spikes and the corresponding fluorescent signal changes ($\Delta F/F_0$, see Methods for details) and observed a linear correlation between the two (Fig. 2.2D). Consistently, the receptive fields (RFs) mapped by cell-attached recording and calcium signals displayed a close match in their size and shape (Fig. 2.2E, see below for details of mapping RFs), indicating the reliability of Cal-520 over the physiological range of sSGS neurons and its efficacy in measuring their visual response properties.

We thus used the Cal-520 indicator to perform 2-photon calcium imaging of sSGS neurons in response to primarily two different visual stimuli, flashing spots and drifting gratings, in order to determine their RF structures and selectivity for stimulus direction and orientation. These experiments were conducted in both wild type (WT) C57BL/6 and transgenic mice where GAD2 positive neurons were fluorescently labeled with tdTomato (GAD2-cre X floxed tdTomato, (Madisen et al., 2010; Taniguchi et al., 2011). Imaging these transgenic mice allowed us to compare the response properties of inhibitory GABAergic neurons (GAD2+) and putative

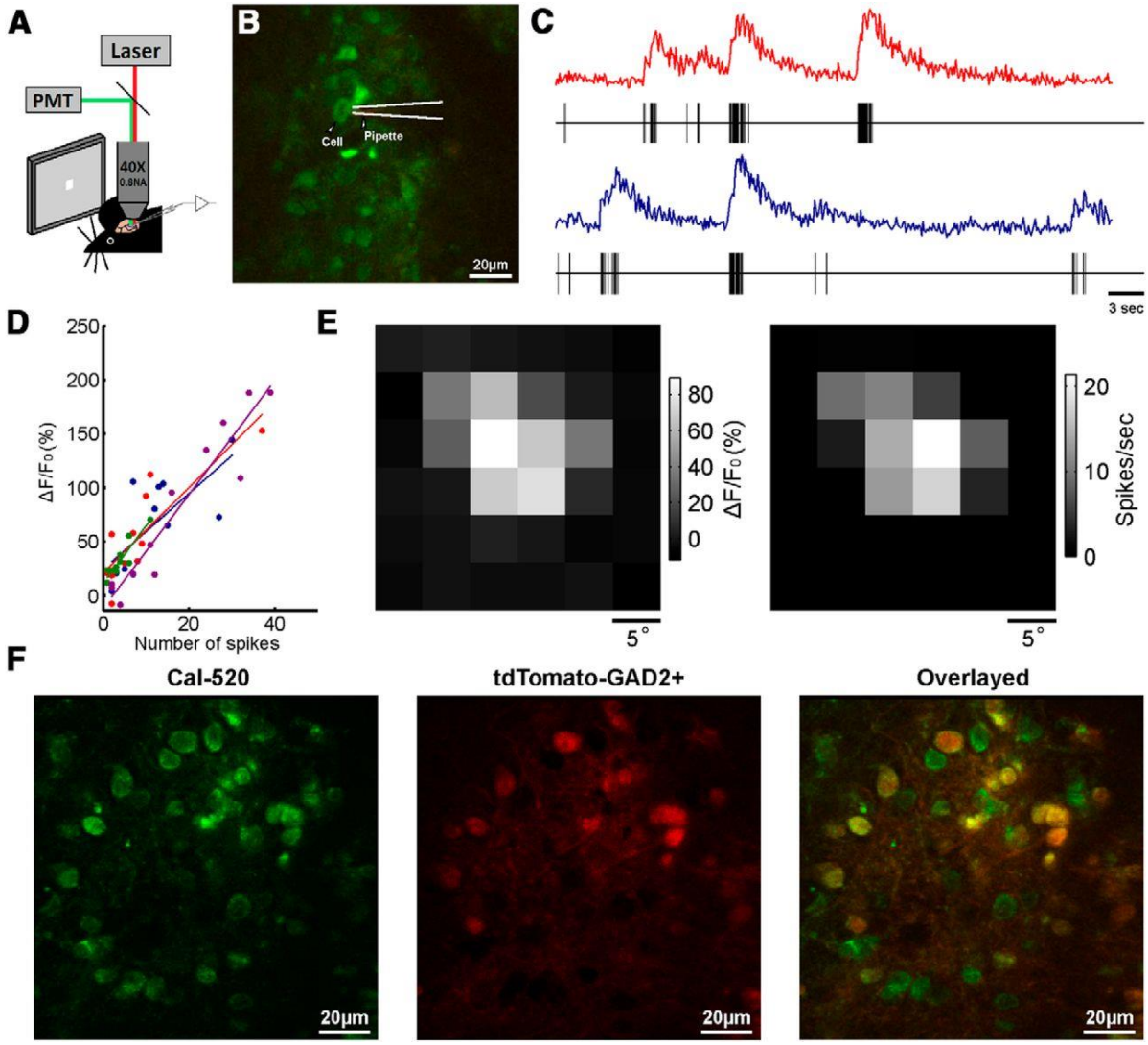

Figure 2.2. Two-photon calcium imaging of the sSGS in mouse SC.
A, Schematic of the experimental setup with simultaneous imaging and cell-attached recording. ***B***, An image of sSGS neurons loaded with the calcium indicator Cal-520 and a pipette filled with 20 μm Alexa Fluor 594. ***C***, Two example traces of fluorescent signal and simultaneous spiking activity (below each calcium trace) during flashing spot stimulus. ***D***, Relationship between the amplitude of fluorescent signal changes and the number of visually evoked spikes. Each data point was one cluster of spikes within a 1 s period and the corresponding $\Delta F/F_0$. Points of the same color were from individual repetitions of the flashing spot stimulus that covered all possible positions on a 6 × 6 grid in a pseudorandom sequence, and the line of the same color was the corresponding linear fit. ***E***, RFs determined from the calcium signal (left) and spikes (right) for the neuron shown in ***B***. The brightness of each square represents the evoked $\Delta F/F_0$ (left) or spike rate (right) by flashing spots at that location. ***F***, Two-photon images showing Cal-520-loaded neurons in the green channel (left), tdTomato-labeled GAD2$^+$ neurons in red (center), and a merged image of both (right).

excitatory neurons (GAD2-) (Fig. 2.2F). In total, we imaged the activity of 913 sSGS neurons (388 GAD2+ and 472 GAD2- cells from 7 GAD2-tdTomato mice; and 53 cells from a WT mouse). The response properties of these neurons are described below.

Receptive field properties of excitatory and inhibitory sSGS neurons

We displayed small bright and dark squares (5°x5°, on a 6x6 grid) on a grey background in a pseudorandom order to separately map the ON and OFF subregions of sSGS neurons' RFs (Fig. 2.2A). For individual recordings, the stimulus screen was placed in front of the contralateral eye such that the RFs of the majority of neurons in the field of view were covered by the 6x6 grid. Out of the 741 cells we imaged with the "flashing spot" stimuli, ~64% (n=477/741) and ~67% (499/741) responded to ON and OFF spot stimuli respectively with various response magnitudes at different spot locations (Fig. 2.3A-B, see Methods for details of determining responsive cells). The vast majority of the responsive cells responded to both ON and OFF squares (n = 440/536), although some responded only to ON (n = 37) or to OFF stimuli (n = 59).

We next quantified the RF size of the sSGS neurons using two different methods following our previous physiological studies. First, the RF areas were estimated after fitting them with 2D Gaussians (Wang et al., 2010). The majority of RFs were well-fitted (88% cells had $R^2 \geq 0.7$ for ON subregions; and 89% for OFF) and displayed compact ON and OFF subregions (ON area: 66.7 ± 3 deg^2 with a median of 55.3, n = 421; OFF area: 71.7 ± 2.9 deg^2 with a median of 56.8, n = 443). Second, we simply counted the number of grid positions where significant visual responses were evoked by the flashing spots (Liu et al., 2014) and determined the subregion areas (ON: 154 ± 5 deg^2 with a median of 150, n = 477; OFF: 173 ± 6 deg^2 with a median of 150, n = 499). With

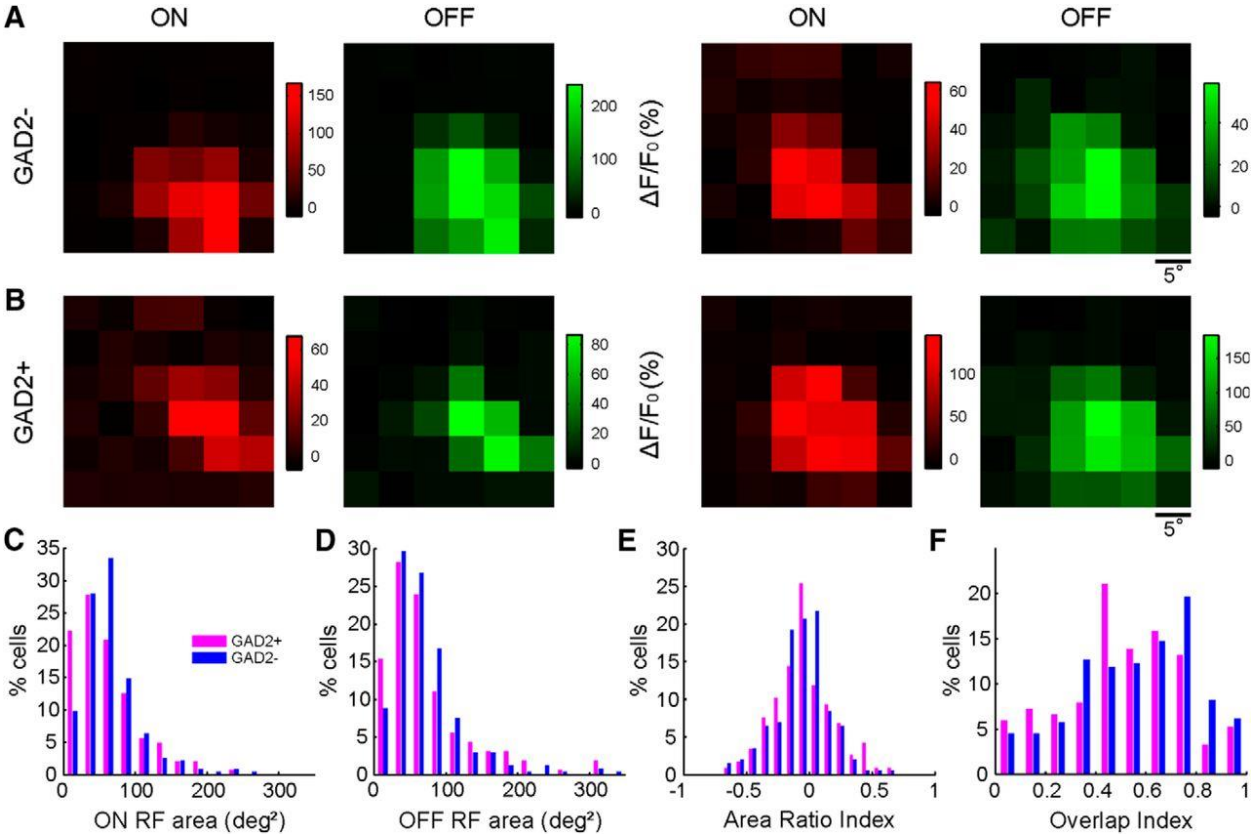

Figure 2.3. RF properties of excitatory and inhibitory sSGS neurons.
A, ON (red) and OFF (green) RF subregions of two GAD2$^-$ neurons determined by two-photon imaging. The brightness of each square represents the evoked $\Delta F/F_0$ by flashing spots at that location according to the scale on the right of each panel. ***B***, ON and OFF RF subregions of two GAD2$^+$ neurons. ***C***, ***D***, Distribution histograms of ON (***C***) and OFF (***D***) subregion areas of GAD2$^+$ (magenta) and GAD2$^-$ (blue) neurons, calculated by 2D Gaussian fitting. ***E***, Distribution of the area ratio index between ON and OFF subregions showing a small bias toward negative values, for both GAD2$^+$ and GAD2$^-$ neurons. ***F***, Distribution of the OI between ON and OFF subregions is biased toward larger values for both groups of neurons.

both measures, the RFs of the most superficial SGS neurons appeared to be smaller than what was previously reported for the whole population of SGS neurons (Liu et al., 2014; Wang et al., 2010). But more importantly, with 2-photon calcium imaging, we were able to analyze separately the RFs of excitatory and inhibitory neurons (Fig. 2.3A-B). The distributions of RF areas for GAD2+ and GAD2- cells were similar to those for the whole population and to each other (Fig. 2.3C-D; p >

0.05 in all comparisons by ranksum test). This is in contrast to the primary visual cortex where layer 2/3 inhibitory neurons have larger RFs than excitatory neurons (Liu et al., 2009).

For cells which responded to both ON and OFF squares, we analyzed the relationships between ON and OFF subregions. We compared the ON and OFF subregions by calculating an area ratio index and found its distribution skewed towards negative values (mean ± SEM, -0.05 ± 0.01; and median -0.05, n = 359). This indicates that OFF subregions of the sSGS neurons were slightly larger than their ON subregions, consistent with our previous physiological studies of the entire SGS population (Wang et al., 2010). In addition, the ON and OFF subregions of these neurons were highly overlapping, with the distribution of the overlap index skewed towards 1 (mean ± SEM, 0.56 ± 0.01; and median 0.57, n = 440), again similar to what was observed in the previous study (Wang et al., 2010). The OFF subregions were similarly larger than ON subregions in both GAD2+ and GAD2- cells (Fig. 2.3E), and a trend of lower overlap was seen in GAD2+ cells (Fig. 2.3F; p = 0.02, ranksum test, but not significant by K-S test).

sSGS neurons are highly selective for stimulus direction

We next studied how the sSGS neurons responded to drifting sinusoidal gratings in order to determine their selectivity for stimulus direction and orientation. Because most SGS neurons display substantial surround suppression (Binns and Salt, 1997; Wang et al., 2010), we restricted the gratings (12 directions, 0.08 cpd, 2 Hz) to a small area covering the RFs of the imaged neurons (30° in diameter, Fig. 2.4A-B). sSGS neurons responded with significant and reliable calcium transients to the presentation of drifting gratings (Fig. 2.4C-D; n = 450/913). Remarkably, the vast majority of these responsive neurons had a high degree of direction selectivity, displaying strong

calcium transients to certain directions, but small or no responses to the opposite directions (Fig. 2.4D-E).

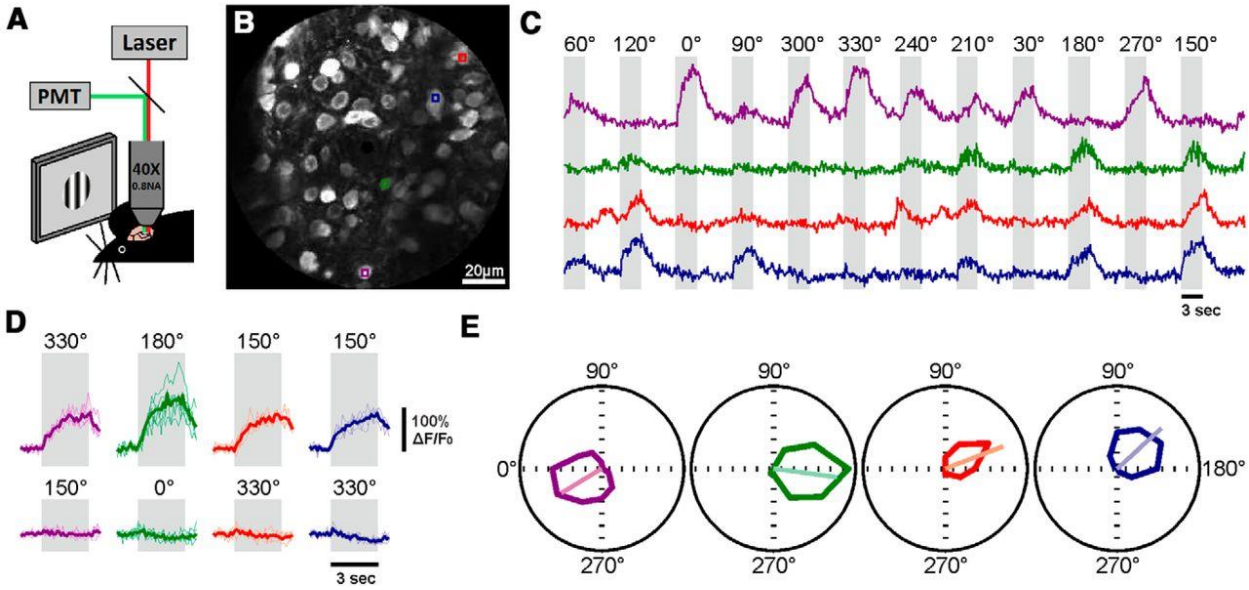

Figure 2.4. Determining direction selectivity in sSGS neurons.
A, Two-photon imaging of sSGS during the presentation of spatially restricted drifting gratings. ***B***, Average image of a full recording used to select ROIs, showing four selected neurons marked by colored boxes. ***C***, Traces of calcium signals of the four neurons in ***B*** to drifting gratings of different directions. Periods of stimulus presentation are marked by the shaded areas, and the values on top indicate stimulus direction. ***D***, Calcium signal from individual trials (thin lines) and the mean over five trials (thick lines) for preferred (top) and null (bottom) directions of the four neurons in ***B*** and ***C***). ***E***, Tuning curves of these neurons show high selectivity for stimulus direction. The color code in this figure follows the colors of the boxes within each selected neuron in ***B***.

We quantified the selectivity of the responsive cells by calculating two indices. In one, we calculated the direction selectivity index (DSI) by comparing the cell's response at the preferred and opposite directions (R_{pref} and R_{opp}, respectively): $DSI = \frac{R_{pref}-R_{opp}}{R_{pref}+R_{opp}}$, in order to compare with the results in our previous electrophysiology study where the same index was used (Wang et al., 2010). However, this index does not take into account the responses at all directions and may not

provide a robust measure of selectivity under certain conditions (Mazurek et al., 2014). We thus also calculated the normalized vector sum of the responses at all directions (Gale and Murphy, 2014) and referred to it as global DSI (gDSI). With both indices, the superficial SGS neurons were clearly highly selective. The mean DSI of the responsive cells was 0.71 ± 0.01, with a median of 0.83 (n = 450; Fig. 2.5A). In fact, ~74% of the sSGS neurons had DSI values greater than 0.5, a value that indicates that the response magnitude at the preferred direction is three times that at the opposite direction. This is in striking contrast to the DSI distribution from our previous studies of SGS neurons across all depths, where ~30% cells had DSI ≥ 0.5 (Wang et al., 2010). Similarly, the gDSI values of these neurons were also high (mean of 0.47 ± 0.01, with a median of 0.50, n = 450), with 78% cells showing gDSI ≥ 0.25 (Fig. 2.5B), a cutoff value for highly direction selective cells (Gale and Murphy, 2014). Again, this was a much greater percentage compared to the entire SGS population (Gale and Murphy, 2014).

On the other hand, these sSGS cells had low orientation selectivity, as determined by OSI and gOSI calculations (mean OSI, 0.30; mean gOSI, 0.18, n = 450). Only ~20% of OSI values were greater than 0.5, and ~22% of gOSI values were greater than 0.25 (Fig. 2.5C-D). In fact, most of these "high OSI" cells had even higher DSI (Fig. 2.5E), indicating that they were not truly orientation selective, but direction selective. This is because the OSI was calculated by comparing the average response at the preferred and opposite directions with that at the "orthogonal" directions (inset of Fig. 2.5F). Consequently, a direction selective cell could have a high OSI value if it has weak responses at the "orthogonal" directions. For this reason, the observation that most sSGS neurons have high DSI yet low OSI suggests that these cells still showed substantial responses at the "orthogonal" directions. This was indeed the case as the vast majority of the sSGS

cells showed larger responses at the "orthogonal" directions than at the non-preferred (or "null") direction (Fig. 2.5F). This further suggests that the tuning widths of these sSGS neurons should be quite broad. Indeed, for cells whose tuning widths could be estimated by fitting with the Von Mises function (~76% of the 450 cells with $R^2 \geq 0.7$, see Methods for details), the vast majority had broad tuning (mean ± SEM of full width at half height, 118.4° ± 1.2°, and median of 119.1°, n = 342; Fig. 2.5G).

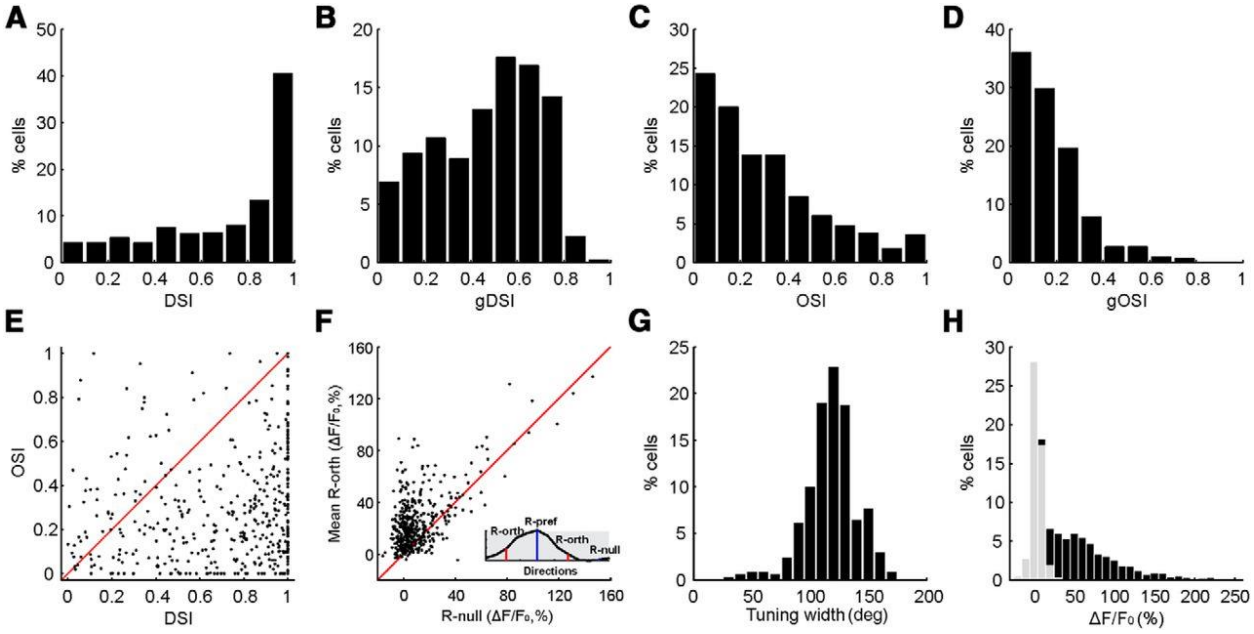

Figure 2.5. sSGS neurons are highly selective for stimulus direction.
A, ***B***, DSI and gDSI distributions for all cells that responded to drifting gratings. ***C***, ***D***, OSI and gOSI distribution for the same cells. ***E***, Scatter plot for OSI versus DSI of individual neurons, with the unity line in red for comparison. ***F***, Scatter plot showing that most neurons had larger responses at the orthogonal directions (*R*-orth in inset) than at the null direction (*R*-null in inset). ***G***, Tuning width distribution for neurons whose tuning curves can be well fitted by the Von Mises function ($R^2 \geq 0.7$, fwhh). ***H***, Distribution of the mean $\Delta F/F_0$ values at the preferred directions for individual cells, with responsive cells shown in black and nonresponsive ones in gray. Note that a number of cells displayed negative values of $\Delta F/F_0$, i.e., some of them were possibly suppressed by the gratings. These cells were not included in the analysis.

To determine whether the high direction selectivity we just revealed in sSGS neurons depended on the type of visual stimulus, we also used full screen drifting gratings (n = 6 mice) and moving bars (n = 2 mice). The sSGS neurons indeed displayed very high values of DSI and gDSI to both stimuli. To moving bars, the mean DSI of the responsive cells was 0.70 ± 0.03 (n = 86 cells responsive, out of 172), median of 0.71, and ~71% of them ≥ 0.5 (n = 61/86); and the mean gDSI was 0.44 ± 0.02, median of 0.45, ~74% of them ≥ 0.25 (n = 64/86; Fig. 2.6A-B). Importantly, the gDSI values and preferred directions of individual sSGS neurons in response to bars matched closely with those to small patches of drifting gratings (Fig. 2.6C-D). Furthermore, in response to full screen gratings, the DSI (0.70 ± 0.02, n = 301 responsive out of 652) and gDSI (0.47 ± 0.01) of the sSGS neurons were similarly high to those evoked by the small gratings. These results thus indicate that high direction selectivity is a robust feature of sSGS neurons.

We next compared the direction selectivity between GAD2+ and GAD2- neurons. A recent electrophysiology study showed that the GAD2+ neurons in the mouse SGS (presumably most of them, if not all, were from deeper laminae than where we imaged), were "rarely" DS (Gale and Murphy, 2014). In contrast, we found that in the most superficial SGS, the GAD2+ neurons were also highly selective, with 68% cells having DSI ≥ 0.5 (n = 131/192; Fig. 2.7A). On the other hand, an even larger proportion of GAD2- cells had high DSI (80% DSI ≥ 0.5; n = 183/230; Fig. 2.7A), indicating a slightly better selectivity in the putative excitatory neurons. The opposite trend was seen for the OSI distributions, where a larger proportion of GAD2+ cells had OSI ≥ 0.5 (Fig. 2.7B). But most importantly, very few cells had high OSI values in both cell types (24% GAD2+ and 12% GAD2- cells with OSI ≥ 0.5), indicating that most sSGS neurons were not orientation selective regardless of the cell type. A small but significant difference was observed for the

direction tuning width: the GAD2- cells had broader tuning width (mean ± SEM, 121.4° ± 1.5° and median, 122°; n = 180) than the inhibitory GAD2+ cells (mean ± SEM, 117.9° ± 1.9° and median, 114°; n = 140; Fig. 2.7C, p = 0.002, ranksum test).

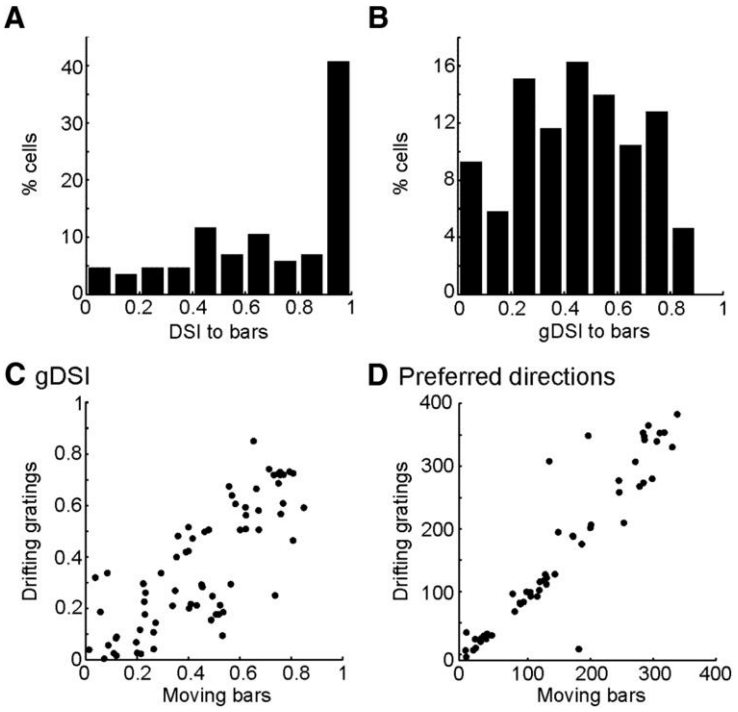

Figure 2.6. High direction selectivity of sSGS neurons in response to moving bars.
A, ***B***, Distributions of DSI (***A***) and gDSI (***B***) values of sSGS neurons in response to moving bars. ***C***, ***D***, The gDSI values (***C***) and preferred directions (***D***) of the sSGS neurons in response to moving bars match closely with those evoked by the small drifting gratings. Cells that responded to both stimuli were included in ***C*** (*n* = 73 of 172 cells tested), and the selective ones (gDSI > 0.15 to both) were included in ***D*** (*n* = 55).

We also observed that sSGS neurons displayed a full range of preferred directions (Fig. 2.7D), although proportionally more cells preferred 60°, an anterior and upward moving direction. We found that this peak in the distribution was more prominent in the putative excitatory (GAD2-) cells (Fig. 2.7D), but the source or significance of this bias is unknown. We next examined whether the preferred direction of the imaged neurons could be predicted by their RF structure, namely, the asymmetry between the ON and OFF subregions. For cells that responded to both the ON and OFF spots and drifting gratings (n = 317/741), we calculated the angle of the vector connecting the OFF to ON centers of each cell, and compared it with the cell's preferred direction.

However, no clear trend was observed between the two angles, whether the RF centers were determined by center of mass or after 2D Gaussian fitting (data not shown), suggesting that factors other than RF asymmetry must be involved in generating direction selectivity in sSGS neurons.

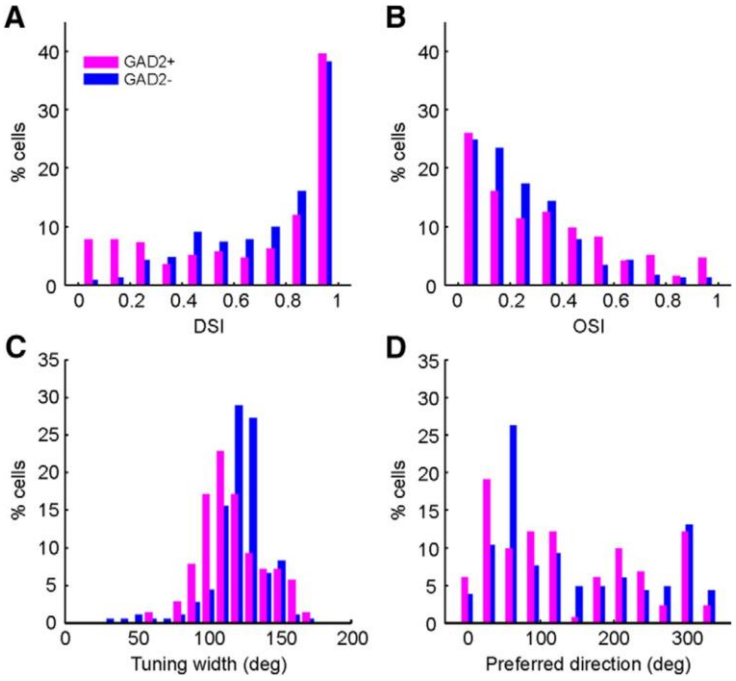

Figure 2.7. Comparing direction selectivity in excitatory and inhibitory sSGS neurons.
A, DSI distribution for $GAD2^+$ (magenta) and $GAD2^-$ (blue) neurons. ***B***, OSI distribution for these neurons. ***C***, Distribution of tuning widths for both populations. ***D***, Distribution of preferred directions for selective cells (DSI $\geq$ 0.5) in both populations.

Direction selectivity declines with depth in the SGS

The high degree of direction selectivity we revealed for the most superficial SGS neurons is in striking contrast to the results we obtained previously in the mouse SGS across all depths. This difference suggested that different sub-laminae of the SGS may contain cells with different degrees of selectivity. Unfortunately, we were not able to test this idea by directly imaging deeper cells, as there were large neuropil signals in deeper regions that severely contaminated the measurement of individual cells' selectivity (data not shown). We therefore performed single unit recordings under the same surgical condition as in the 2-photon imaging experiments (Fig. 2.8A), and kept track of

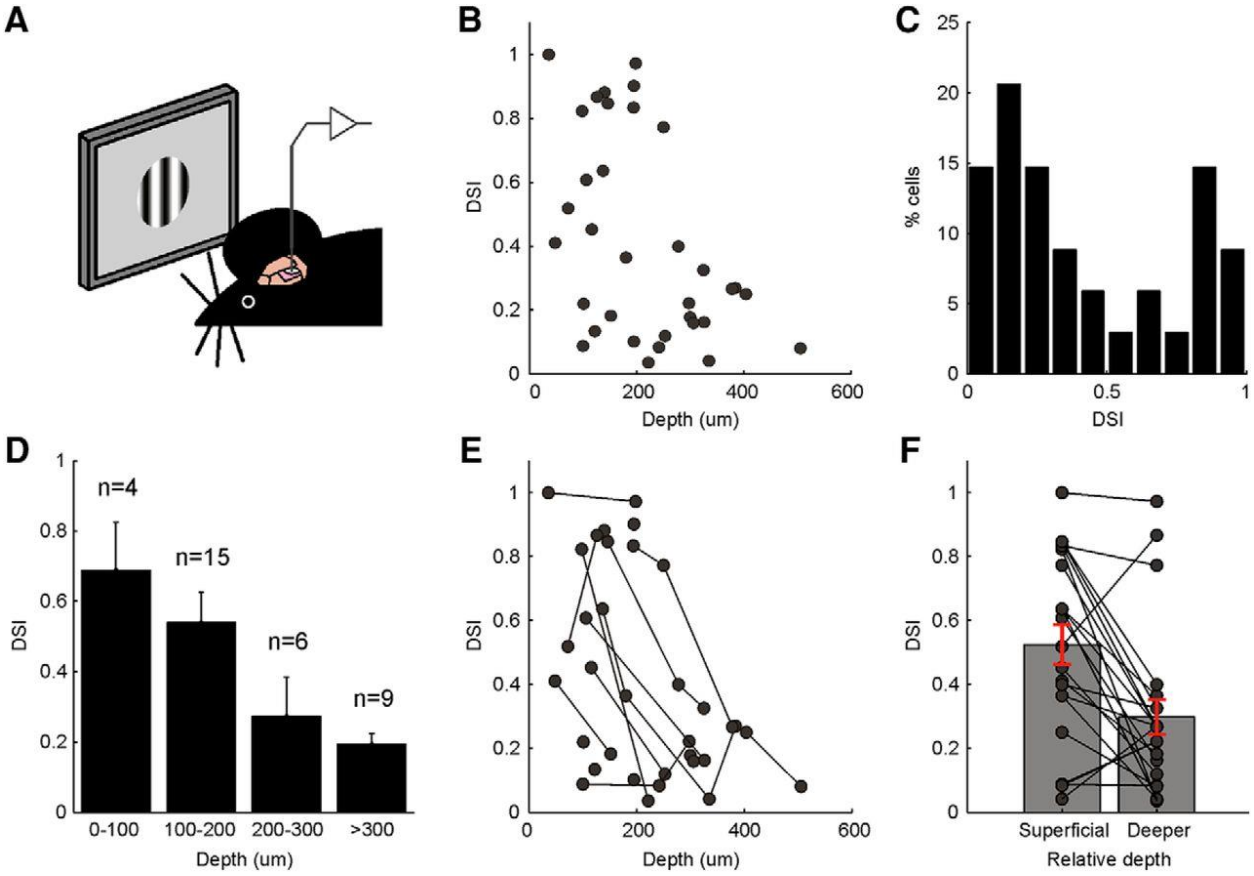

Figure 2.8. Direction selectivity declines with depth in the SGS.
A, Single-unit recordings from the SC of anesthetized WT mice during the presentation of spatially restricted drifting gratings. ***B***, Scatter plot showing DSI of the recorded units versus their depth (*n* = 34 units, 10 mice). ***C***, DSI distribution of the recorded units (mean ± SEM, 0.42 ± 0.06; median, 0.30). ***D***, DSI declines with depth (number of units is shown above each depth bin, values of each bar are means ± SEM). ***E***, Same data as in ***B*** but with units recorded sequentially in the same electrode penetration linked together. ***F***, Comparison between all possible pairs of neurons recorded in individual penetrations. The mean DSI decreases from 0.57 ± 0.06 for the more superficial units to 0.28 ± 0.06 for the deeper units ($p = 0.0003$, paired *t* test).

the depth of every recorded unit (n = 10 mice, 34 units). The same visual stimuli were used as in the imaging experiments (12 direction drifting gratings within a 30° circular window), except that they were presented at 4 spatial frequencies (0.02, 0.04, 0.08, and 0.16 cpd). Remarkably, the direction selectivity of SGS neurons indeed appeared to decrease with depth (Fig. 2.8B). The DSI distribution of the entire population of the recorded cells was comparable to what was previously

reported (Wang et al., 2010), as well as the mean (0.42 ± 0.06) and median (0.30) DSI (Fig. 2.8C). However, when separated by depth, cells in the top 100 μm had the highest DSI among the population (mean of 0.69; Fig. 2.8D). Note that few neurons were sampled at this depth, reflecting the under-sampling of superficial neurons in electrophysiology experiments. Cells between 100 and 200 μm had a slightly lower DSI (mean of 0.54), because a significant portion of them was not selective. In contrast, cells deeper than 200 μm had a substantially lower DSI (Fig. 2.8D). Because the above analysis is confounded by the fact that the depth estimates could vary between mice and/or different electrode penetrations, we further analyzed the data for individual penetrations. In Figure 2.8E, we connected the neurons that were recorded in the same electrode penetrations to better illustrate the change in DSI. Indeed, when comparing all possible pairs of neurons recorded for each penetration, we found that the mean DSI decreased from 0.57 ± 0.06 for the "more superficial" units to 0.28 ± 0.06 for the "deeper" units of the pairs (Fig. 2.8F; $p = 0.0003$, paired t-test). Together, our electrophysiology and imaging results demonstrate that highly DS cells are concentrated in the most superficial SGS of the SC, and the degree of selectivity declines with depth.

Spatial organization of receptive field properties of sSGS neurons

Finally, simultaneous imaging of dozens of sSGS neurons allowed us to examine their spatial organizations. We first analyzed retinotopic organization of RF positions, separately for ON and OFF subregions. We determined the center of mass of subregions and examined how they varied as a function of physical distance between pairs of cells. On average, cells close to each other had RF centers that were closer in visual space compared to cells farther away (Fig. 2.9A-D), revealing

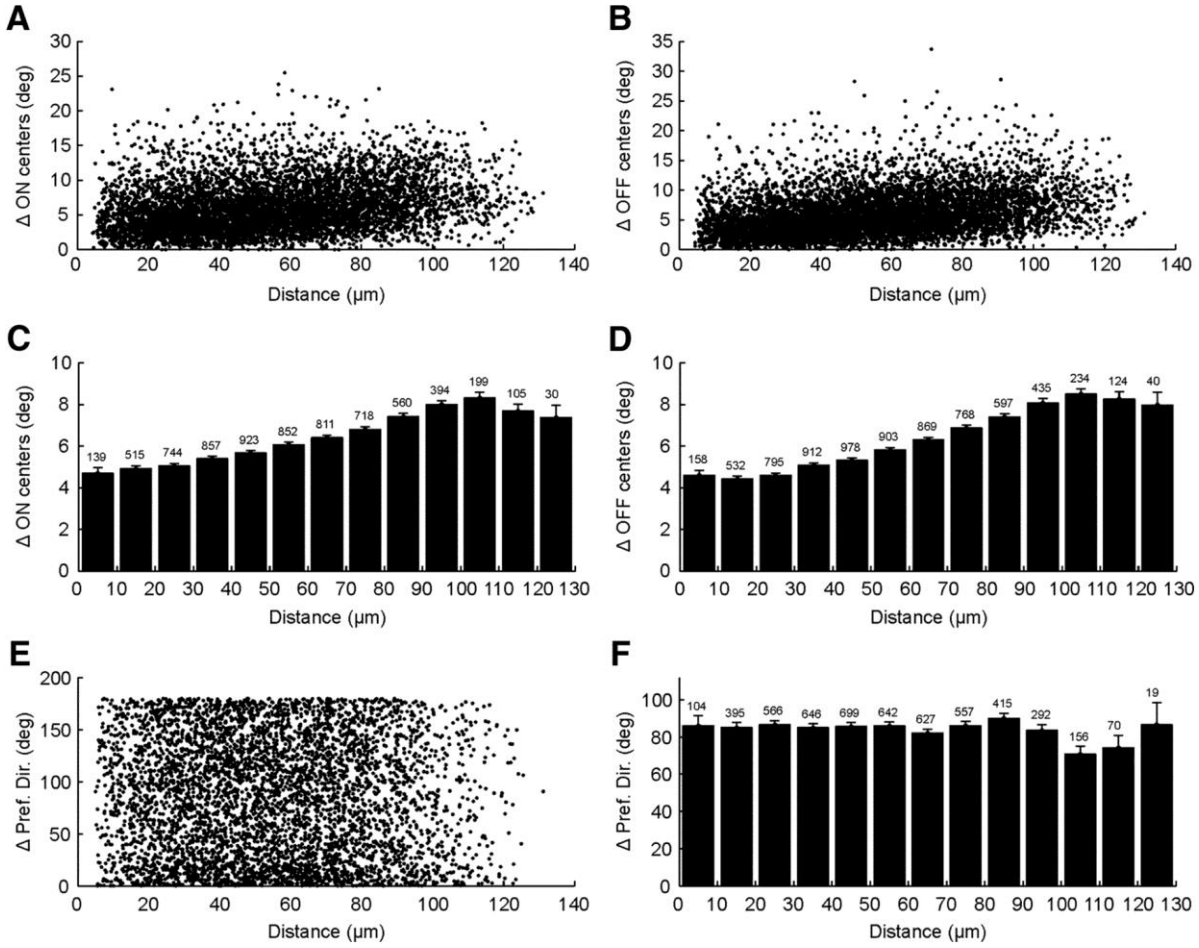

Figure 2.9. Spatial organization of RF properties of sSGS neurons.
A, Scatter plot showing the distance between the ON subregion centers of pairs of neurons versus the distance between their cell bodies in the SGS. ***B***, Same scatter plots for OFF subregions. ***C***, Bar graphs of the data in ***A***, with values representing means ± SEMs. The number of cell pairs is indicated above each bin. ***D***, Same bar graphs for the data in ***B***. ***E***, Scatter plot showing the difference in preferred directions (ΔPref. Dir.) between pairs of neurons versus the distance between their cell bodies. ***F***, Bar graphs of the data in ***E***. The number of cell pairs is indicated above each bin.

a retinotopic organization (Cang et al., 2008). However, there were tremendous scatters in this organization at finer scale. In fact, many cells that were next to each other (within 20 μm) had RFs as far apart as 10° (Fig. 2.9A-B). A similar result was obtained when RF centers were estimated by fitting 2D Gaussians (data not shown). Additionally, we analyzed retinotopic organization of

GAD2+ and GAD2- neurons separately (data not shown) and observed similar results as in the whole population.

We also examined whether sSGS cells that prefer similar directions are clustered spatially. The difference in preferred directions of pairs of cells was plotted against their physical distance, and no obvious trend was observed (Fig. 2.9E). In fact, when the data points were binned into increments of 10μm for the physical distance between cells, a flat distribution was seen for their difference in preferred directions (Fig. 2.9F). This was also the case when these analyses were separately performed for GAD2+ and GAD2- cells (data not shown). In other words, there is no map of directional preference in the most superficial lamina of the mouse superior colliculus.

Discussion

In this study we examined the functional properties of neurons in the most superficial layer of the mouse SC (sSGS). We found that the most salient property of the sSGS neurons is their direction selectivity, which is remarkably higher than that of deeper neurons. Interestingly, the high degree of selectivity is seen in both excitatory and inhibitory neurons in the sSGS, with the excitatory neurons tuned slightly more broadly than the inhibitory neurons. We also showed that these neurons have compact RFs that are mostly comprised of overlapping ON and OFF subregions, largely consistent with what is known about the RF organization of all SGS neurons. Our results thus provide critical information for understanding the organization and signal transformation in the early visual system.

Comparison with previous functional studies of the mouse SC

A handful of studies characterized visually-evoked response properties of SC neurons in mice (Drager and Hubel, 1975; Gale and Murphy, 2014; Wang et al., 2010). These studies determined RF organizations, discovered direction and orientation selective responses, and revealed cell-type specific properties in the mouse SC. However, because all of these studies used electrophysiology, with metal or glass electrodes, the most superficial layer of the SC was likely severely under-sampled. Consequently, only indirect comparisons can be made between the current and previous studies. For example, the much higher direction selectivity we observed in the superficial neurons suggested a laminar-specific organization of DS neurons, a hypothesis that was directly confirmed by single unit recordings in this study. Similarly, we also observed many fewer neurons with good orientation selectivity in the sSGS compared to what was reported previously for the entire SGS

(Wang et al., 2010). It is thus likely that orientation selective neurons are more concentrated in the deeper laminae. Furthermore, we found no striking differences between the response properties of GAD2+ and GAD2- neurons to flashing squares and drifting gratings. This is in contrast with a recent electrophysiology study showing that the GAD2+ neurons (corresponding to horizontal cells in that study) were rarely DS, while the excitatory narrow field vertical cells were often so (Gale and Murphy, 2014). This difference between these results is again likely due to the fact that the most superficial cells were severely under-sampled, if not entirely missed, in that study. On the other hand, many of the cells we imaged in this study could very possibly be marginal cells, simply by virtue of their superficial location in the SGS. Indeed, it has been suggested that marginal cells in the hamster SC could be highly direction selective (Mooney et al., 1985).

A very recent study also used 2-photon calcium imaging to examine response properties in the mouse SC, and revealed the existence of "orientation columns" (Feinberg and Meister, 2015). In contrast, we find that almost no cells in the superficial SC are truly orientation selective. Instead, these cells are highly direction selective, and importantly, they are not clustered according to their preferred directions. A number of technical differences exist between the two studies, including the imaged depth and region, calcium indicators, the anesthetized/awake state of the animal, and whether the cortex was intact. Among them, the difference in imaged depth and region is most intriguing. We imaged the most superficial lamina in the SC, whereas the other study imaged slightly deeper, and in more posterior and medial SC, which represents a more peripheral and dorsal visual field. Whether there is a depth and/or region specific organization of orientation columns in the mouse SC is an interesting possibility that should be answered in future studies.

Direction selectivity in the Superior Colliculus

What might be the source of the high direction selectivity seen in the sSGS? A substantial population of retinal ganglion cells are direction selective (Vaney et al., 2012; Wei and Feller, 2011), and most of them project to the SC (Dhande and Huberman, 2014; Huberman et al., 2010). It was shown in mice that the DRD4 RGCs, which are selective for posterior motion, project exclusively into the upper SGS, and in contrast, the non-DS transient OFF α-RGCs project into the lower SGS (Huberman et al., 2008; Huberman et al., 2009). These results thus raise an intriguing possibility that the high selectivity we observe in the most superficial SGS neurons could be inherited from the DS RGCs. However, this idea, at least in its simplest form, is not supported by the projection patterns of other subtypes of RGCs. For example, the most numerous type of mouse RGCs, the W3-RGCs, are motion sensitive but not DS (Zhang et al., 2012); and yet, they project to the most superficial lamina in the SC (Kim et al., 2010). Furthermore, individual SGS neurons are estimated to receive inputs from at least 4-5 RGCs (Chandrasekaran et al., 2007). Finally, the superficial SGS neurons exhibit a full range of preferred directions, unlike the RGCs, which are selective for cardinal directions. For these reasons, local collicular circuits must be involved in the emergence of the observed response properties in the sSGS. In particular, our finding of GAD2+ neurons' selectivity suggests precise and dynamic interactions between the excitatory and inhibitory circuits in transforming direction selectivity in the SGS. It is worth noting that inhibitory neurons in the primary visual cortex (V1) are less orientation/direction selective than excitatory neurons (Kerlin et al., 2010; Liu et al., 2009; Niell and Stryker, 2008), indicating that the synaptic mechanisms underlying stimulus selectivity are likely different between V1 and SC. Future studies are needed to determine the circuit mechanisms underlying this important

transformation in the SC.

Zebrafish is the other model system where signal transformation from the retina to the SC/OT is intensively studied. It has been shown that subtypes of zebrafish RGCs that prefer different directions project to segregated layers in the tectum, and that the tectal neurons with matching preferred directions arborize their dendrites in the corresponding layers (Gabriel et al., 2012; Lowe et al., 2013; Nikolaou and Meyer, 2012; Robles et al., 2013). In other words, the DS retinal inputs could largely determine the direction preference in at least some of the tectal cells ((Gabriel et al., 2012), but see (Grama and Engert, 2012)). On the other hand, new preferred directions emerge in the OT (Hunter et al., 2013), and DS tectal neurons receive inhibitory inputs that are tuned to the null directions (Grama and Engert, 2012), indicating the involvement of local computations in this process. Investigations of the similarities and differences between direction selectivity in mice, zebrafish and other species will help reach a more complete understanding of functional organization and signal transformation in the visual system.

Dedicated circuits for direction selectivity in the visual system

Many of the DS ganglion cells also project to the dorsal lateral geniculate nucleus (dLGN) in both mice (Dhande and Huberman, 2014) and cats (the “W cells”, (Chen et al., 1996). Consistently, a number of studies have reported direction and orientation selective responses in the dLGN of mice (Marshel et al., 2012; Piscopo et al., 2013; Scholl et al., 2013; Zhao et al., 2013), cats (Daniels et al., 1977; Soodak et al., 1987; Vidyasagar and Urbas, 1982), and monkeys (Cheong et al., 2013; Smith et al., 1990; White et al., 1998; Xu et al., 2002). In mice, DS cells appear to be more concentrated in the dorsal shell of the dLGN (Marshel et al., 2012; Piscopo et al., 2013), where

some of the DS-RGCs terminate (Huberman et al., 2008; Huberman et al., 2009). Even more interestingly, the geniculate neurons in the dorsal shell project to layer 1 of the primary visual cortex (V1), suggesting a dedicated circuit linking direction selective RGCs to the superficial V1 (Cruz-Martin et al., 2014). In the current study, we reveal for the first time a lamina in the superficial SC that is highly direction selective, mirroring the finding in the dLGN and V1. This remarkable similarity between the collicular and cortical pathways highlights the evolutionary and behavioral significance of direction selectivity in the visual system.

The dedicated DS circuits in the SC and dLGN-V1 could potentially interact with each other via two pathways: the cortico-collicular and colliculo-geniculate pathways. The cortico-collicular pathway, however, is an unlikely substrate because it originates from layer 5 in the cortex, where DS response is rarely seen (Niell and Stryker, 2008). On the other hand, many SC neurons, including those in the superficial SGS, project directly to the dLGN, as seen in mice (Gale and Murphy, 2014), rats (Lee et al., 2001), hamsters (Mooney et al., 1988), cats (Graham, 1977), tree shrew (Diamond et al., 1991), and monkeys (Harting et al., 1978). This pathway thus provides a likely link between the direction selective sSGS neurons and those in the dLGN.

In summary, we have examined visually-evoked responses of neurons in the most superficial lamina of the mouse SC. The high direction selectivity we have revealed in this lamina will guide future investigations to understand the functional organization and signal transformation in the visual system, and their underlying circuit mechanisms.

Notes on CHAPTER 2

This chapter consisted of a collaborative effort with Dr. Samsoon Inayat. Since we both contributed to nearly all aspects of the research, the unabridged published manuscript was featured. The manuscript was published as follows:

Inayat, S.*, Barchini, J.*, Chen, H., Feng, L., Liu, X., and Cang, J. (2015). Neurons in the most superficial lamina of the mouse superior colliculus are highly selective for stimulus direction. J Neurosci *35*, 7992-8003.

* These authors contributed equally to this work.

Author contributions: S.I., J.B., and J.C. designed research; S.I., J.B., L.F., and X.L. performed research; S.I. wrote the Matlab code to extract the $\Delta F/F_0$ signal from imaging time-series. S.I., J.B., H.C., X.L., and J.C. analyzed data; S.I., J.B., X.L., and J.C. wrote the paper.

Acknowledgements: We thank Dr. David Wokosin (who was supported by NIH P30NS054850) for his help in setting up our 2-photon microscope. We also thank Dan Dombeck, David Ferster, Sunil Gandhi, and Josh Trachtenberg for their help with 2-photon calcium imaging. This work was supported by US National Institutes of Health (NIH) grants (EY020950 and EY023060) to J.C.

CHAPTER 3

Retinal Origin of Direction Selectivity in the Superior Colliculus

Summary

Detecting visual features in the environment such as motion direction is crucial for survival. The circuit mechanisms that give rise to direction selectivity in a major visual center, the superior colliculus (SC), are entirely unknown. Using 2-photon calcium imaging, we show that SC direction selectivity is dramatically reduced in transgenic mice that have decreased retinal selectivity. This study demonstrates a retinal origin of direction selectivity in the SC, and reveals a central visual deficit as a consequence of altered feature selectivity in the retina.

Introduction

Neurons in the brain are specialized in detecting unique features in the environment. In the visual system, many neurons at various stages of processing respond selectively to stimuli moving along specific directions or having particular orientations (Priebe and Ferster, 2012; Vaney et al., 2012; Wei and Feller, 2011). Such direction and orientation selectivity are critical for motion sensing and image processing, leading to visually-guided behaviors that are important for survival. Not surprisingly, the circuit mechanisms of direction and orientation selectivity have been extensively studied. However, these studies have mostly focused on the retina and primary visual cortex (V1) (Priebe and Ferster, 2012; Vaney et al., 2012), while neglecting the superior colliculus (SC), a major retinal target and vision center.

The SC, or optic tectum, is an evolutionarily conserved structure that receives direct retinal input in all vertebrates (Cang and Feldheim, 2013; Gandhi and Katnani, 2011; May, 2006). It was the most sophisticated visual center until the neocortex recently evolved in mammals. Even in mice, a mammalian species that has become a useful model in vision research (Huberman and Niell, 2011), 85-90% of retinal ganglion cells (RGCs) project to the SC (Ellis et al., 2016), making it the most prominent visual structure in this species. Although the SC is mostly known for its functions in initiating rapid gaze shift towards salient stimuli, neurons in its superficial layers (i.e., the visual layers), including the *stratum griseum superficiale* (SGS) and *stratum opticum* (SO), display diverse visual response properties. In particular, selectivity for motion direction has been observed in the superficial SC of all mammalian species that have been studied, including tree shrews (Albano et al., 1978), cats (McIlwain and Buser, 1968), hamsters (Rhoades and Chalupa, 1976), ground squirrels (Michael, 1972), rabbits (Masland et al., 1971), rats (Fortin et al., 1999)

and mice (Drager and Hubel, 1975). Direction selectivity has also been observed in the primate SC, although it is much less prominent (Cynader and Berman, 1972; Marrocco and Li, 1977). However, despite that it has been almost half a century since direction selectivity was first described in the mammalian SC, its underlying circuit and synaptic mechanisms remain entirely unknown.

Several mechanisms could give rise to the direction selectivity seen in superficial SC neurons. First, they could inherit it directly from direction selective (DS) retinal inputs. Indeed, direction selective ganglion cells (DSGCs) have been discovered in the retina of a number of species, and most of the DSGCs project to the superficial SC (Dhande and Huberman, 2014). In mice, several subtypes of DSGCs preferentially terminate their axons in the upper half of the SGS, while most of the non-DSGCs tend to project to the lower half (Huberman et al., 2008; Huberman et al., 2009; Kay et al., 2011; Kim et al., 2010). Interestingly, DS collicular neurons are also organized in a depth-specific manner, where they are most concentrated in the topmost lamina of the SGS and become less prevalent with depth (Inayat et al., 2015). This correspondence between the anatomical and functional organization supports the idea that similarly tuned DSGCs could project to common targets, thereby providing SC neurons with a synaptic drive that is biased towards certain directions.

Second, direction selectivity in the SC could arise from a specific arrangement of retinal inputs that are not individually tuned. Reichardt proposed in his motion detector model that direction selectivity could be generated by non-selective inputs that have different temporal delays (Reichardt, 1961). In such a model, these inputs are arranged in such a way that stimuli moving in the preferred direction would result in synchronous arrival of synaptic inputs and consequently a

large depolarization in the postsynaptic cell onto which they converge. On the other hand, stimuli moving in the opposite direction would cause only a small depolarization because the inputs arrive asynchronously. This scenario was indeed shown to underlie direction selectivity in cat V1, as revealed by both extracellular and intracellular recordings (Priebe and Ferster, 2005; Saul and Humphrey, 1992). Whether a similar mechanism exists for direction selectivity in the SC is not known.

Finally, direction selectivity in the SC could be computed *de novo*. Under such scenario, the combined retinal input that a DS SC neuron receives would be non-selective for motion direction. Direction selectivity could then arise via dynamic interactions within the local circuits, such as tuned or spatially-offset inhibition as originally proposed by Barlow and Levick for retinal direction selectivity (Barlow and Levick, 1965).

In this study, we reduced the selectivity of DSGCs by genetically manipulating retinal circuits and then studied the impact on SGS direction selectivity using 2-photon calcium imaging. This experiment demonstrates for the first time that direction selectivity in the SGS is inherited from DSGCs in the retina; and consequently, disrupting DSGCs' tuning leads to altered feature selectivity in the SC.

Materials and Methods

Animal preparation

WT littermate controls and *Vgat* KO mice of both sexes were used in this study. For 2-photon calcium imaging in the retina and SC, *Slc32a1*$^{flox/flox}$ (i.e. *Vgat*$^{flox/flox}$) mice (Stock no. 012897*)* and *ChAT-IRES-Cre* mice (Stock no. 006410) were originally acquired from Jackson Laboratory and crossed to knock out (KO) the vesicular GABA transporter (Vgat) gene (*Slc32a1*) from choline acetyltransferase (ChAT)+ cells. These strains were backcrossed to the C57BL/6 background (Pei et al., 2015). Both KOs (n = 22) and littermate controls (n = 14) were used. All mice were kept on a 12hr light:12hr dark cycle, 1 to 5 mice per cage. All experimental procedures were approved by the Northwestern University and the University of Chicago Institutional Animal Care and Use Committees.

For *in vivo* experiments, mice between postnatal day 45 and 90 were anesthetized with urethane (1.2 g/kg in 10% saline solution, i.p.) and then sedated by chlorprothixene (10 mg/kg in water, i.m.) as described before (Inayat et al., 2015; Zhao et al., 2014). Atropine (0.3 mg/kg in 10% saline) and dexamethasone (2 mg/kg in 10% saline) were administrated subcutaneously. The animal was then transferred onto a heating pad for recording or imaging. The animal's body temperature was monitored through a rectal thermoprobe and maintained at 37 ℃ through a feedback heater control module (Frederick Haer Company, Bowdoinham, ME). Toe-pinch reflex was monitored during experiments to test for depth of anesthesia. Additional urethane (0.2–0.3 g/kg) was administered when necessary. After the mice were anesthetized, the scalp was shaved and skin removed to expose the skull. We followed our recently published procedures for 2-photon imaging of the superficial SGS neurons (Inayat et al., 2015). Briefly, a craniotomy was performed

on the left hemisphere, starting at the lambda point and extending ~3 mm both laterally and rostrally. Tissues overlaying the SC were then removed by aspiration.

Two-photon calcium imaging of SGS neurons

Once the SC was exposed, a glass pipette (inner diameter of 10-20 μm) filled with freshly-made solution containing the fluorogenic calcium-sensitive dye Cal-520AM (Tada et al., 2014) (1.13 mM, ATT Bioquest) and SR101 (100 μM) was lowered into the tissue. Twenty pulses of 2.3 nl each (46 nl total volume), at 20 s interval, were delivered to inject the Cal-520 solution at a depth of 500 μm below the surface. The same procedure was repeated after retracting the pipette to a depth of 250 μm. The pipette was left in the tissue for 1-2 min before being slowly retracted. The SC was then covered by ACSF. Imaging was performed 1-2h after loading.

Once the injection procedure was complete, a small metal plate was mounted on the mouse's head with Metabond (Parkell, Edgewood, NY), which, when clamped under the microscope, resulted in the imaged SC surface being largely flat and perpendicular to the objective. A shield was placed around the craniotomy to block light from the visual stimulus during imaging. The SC was covered by 3% agarose in ACSF for stability. Imaging was performed with a 2-photon microscope (2P-SGS, Bruker Nano Surface Division) and a Ti:sapphire laser (Coherent Chameleon Ultra II) at an excitation wavelength of 800 nm, and with a 40X/0.8NA objective (Leica). Data were acquired using PrairieView software with a spiral scan at 2X optical zoom, resulting in a circular field of view with a diameter of 135 μm. Image resolution was 256x256 pixels and the acquisition rate was 8.079 Hz.

Visual stimulation

For *in vivo* experiments, visual stimuli were generated with Matlab Psychophysics toolbox (Brainard, 1997; Niell and Stryker, 2008) on a LCD (37.5 cm × 30 cm, 60 Hz refresh rate, ~50 cd/m^2 mean luminance). The monitor was placed 25 cm away from the eye contralateral to the imaging site (the right eye), and tilted at an angle matching that of the mouse's head, given that the mouse's nose was slightly elevated to correct for the curvature of SC and allow imaging from a relatively flat surface. The screen was adjusted so that the imaged cells' receptive fields were near the center of the screen. The ipsilateral eye was covered throughout the experiments.

Two types of visual stimuli were used to determine direction selectivity of SGS neurons. First, sweeping bars, 5° wide and drifting at a speed of 30°/s, were used. The drifting directions were varied between 0° and 330° (12 steps, 30° spacing), which were presented in a pseudorandom sequence together with a "blank stimulus" (gray screen at the mean luminance). The inter-stimulus interval was 3 sec. Second, drifting sinusoidal gratings were also used, at 0.08 cpd, 2Hz, 100% contrast (Inayat et al., 2015). They were presented at 12 movement directions (0°-330°, with 30° increments) in a pseudorandom order within a circular window (32° in diameter and surrounded by a grey background) near the center of the imaged cells' receptive fields (which was determined by flashing white or black squares as described in reference (Inayat et al., 2015). The stimulus duration was 3 sec and inter-stimulus interval 5 sec. Each stimulus was repeated 4-6 times.

SC calcium imaging and data analysis

For SC 2-photon imaging and data analysis, the experimenter was blind to the genotype of the mice. Animals that had visible tissue damage to their SC after dye loading, or where the dye failed

to be incorporated into the cells were not subject to imaging. Data analysis was performed on all animals that were subject to imaging, and no data points were excluded from the resulting data sets. We followed our published procedures of analysis (Inayat et al., 2015). Briefly, regions of interest (ROIs) were drawn manually on the average images, and the intensity values for all pixels in each ROI were averaged for each frame to obtain the raw Ca^{2+} signal of each cell. From the raw signal, for each stimulus presentation, $\Delta F/F_0 = (F - F_0)/F_0$, was calculated, where F_0 was the mean of the baseline signal over a fixed interval of 1.25 sec (for gratings) or 0.75sec (for bars) before stimulus onset; and F was the fluorescence signal from 250 ms after stimulus onset to 500 ms after stimulus offset. A cell was considered responsive if its mean F (for gratings) or peak F (for bars) was more than two standard deviations above F_0 for at least one of the stimulus conditions. The mean (for gratings) or peak (for bars) value of $\Delta F/F_0$ for each of the stimulus conditions was then used to determine the direction tuning curves for every responsive cell.

To quantify the degree of direction selectivity, we calculated a global direction selectivity index (gDSI), which is the vector sum of responses normalized by the scalar sum of responses (Gale and Murphy, 2014; Inayat et al., 2015): $gDSI = \frac{\sum R_\theta e^{i\theta}}{\sum R_\theta}$, where R_θ is the response magnitude of $\Delta F/F_0$, at θ direction of bars or gratings. The preferred direction is quantified as the angle of the vector sum of responses. Previous studies of direction selectivity mostly used $DSI = \frac{R_{pref} - R_{opp}}{R_{pref} + R_{opp}}$, where R_{pref} is the cell's maximal response, and R_{opp} is the cell's response to the opposite direction. To facilitate the comparison with such studies, we plotted the relationship between gDSI and DSI of individual neurons (Fig. 3.5).

Retinal calcium imaging and data analysis

WT littermate controls and *Vgat* KO mice were injected intravitreally after eye opening at P18 with an AAV2 viral vector carrying GCaMP6s (University of Pennsylvania Vector Core). After 21 days, the injected mice were dark adapted for 1 hour and their retinas were dissected in the dark under infrared (IR) light. During dissection, the retina was cut into dorsal and ventral pieces following the procedure described by Wei et al. 2010 (Wei et al., 2010) and the nasal direction for each piece was noted. The dissected retinas were kept in darkness at room temperature in Ames' medium bubbled with 95% O_2/5% CO_2 until use (0–7 h). Cells were visualized with IR light (>900 nm) and an IR-sensitive video camera (Watec). Light responsive, GCaMP6s-positive cells were identified by a two-photon microscope (Bruker Nano Surface Division) and a Ti:sapphire laser (Coherent Chameleon Ultra II) tuned to 920 nm while presenting a flashing spot (660 um diameter) from a white organic light-emitting display (OLEDXL, eMagin; 800 × 600 pixel resolution, 60-Hz refresh rate). Imaging was performed at an excitation wavelength of 920 nm with a 60X objective while the field of view was presented with a positive contrast 990 μm x 220 μm moving bar stimulus in a dark background moving in 8 pseudorandomly chosen directions spaced at 45 degree intervals at a speed of 440 μm/sec on the retina (~15 °/sec in visual space). Data were acquired using PrairieView software in a 100 μm x 100 μm field of view. Image resolution was 256 x 256 pixels and the acquisition rate ~13 Hz.

Raw frames were uploaded onto ImageJ software in which regions of interest (ROIs) were manually drawn to enclose the soma of each GCaMP6s expressing cell and for a background region where there was no detectable GCaMP6s expression. Using the TimeSeries Analyzer plugin for ImageJ, we calculated the average intensity over time for all ROIs. In MATLAB, the

background trace was subtracted from the light responsive somatic traces to remove noise. The background subtracted traces were then truncated and sorted by direction of the moving bar stimulus and the peak of each calcium transient was used to calculate $\Delta F/F_0$ as described above. For each responsive cell, we calculated gDSI and gOSI as described above and $DSI = \frac{R_{pref} - R_{opp}}{R_{pref} + R_{opp}}$, where R_{pref} is the cell's response at the preferred direction (i.e., maximal response), and R_{opp} is the cell's response to the direction opposite to the preferred one. Cells showing responses to both the leading and trailing edge of the positive contrast moving bar and whose DSI > 0.2 and gDSI > gOSI were classified as ON-OFF DSGCs.

Statistics

All pooled data were presented as mean ± SEM. Statistical significance was calculated using non-parametric, two-sided, Mann-Whitney U test, Kolmogorov-Smirnov (K-S) test, or χ^2 test as mentioned in the text. All analyses and graph plotting were performed in MATLAB (MathWorks) or Prism (GraphPad Software Inc). No statistical methods were used to predetermine sample sizes, but our sample sizes are similar to those reported in the field. KOs and littermate controls were assigned to groups according to their genotypes.

Data and code availability

The data that support the findings of this study and the custom Matlab code are available from the corresponding author upon reasonable request.

Results

Genetic disruption of retinal direction selectivity reduces selectivity in the SGS.

Our *in vivo* whole-cell experiments support the conclusion that the direction selectivity of SGS neurons originates from converging inputs of similarly-tuned DSGCs. If this is indeed the case, a reduction of retinal direction selectivity would compromise the selectivity in the SGS. We next tested this prediction using a genetic manipulation. GABAergic inhibition provided by starburst amacrine cells is a critical factor in generating direction selectivity in the retina (Vaney et al., 2012; Wei and Feller, 2011), and it can be eliminated by knocking out (KO) the vesicular GABA transporter (Vgat) gene *Slc32a1* from these cells by crossing *Slc32a1*$^{flox/flox}$ (i.e. *Vgat*$^{flox/flox}$) with choline acetyltransferase *(ChAT)-IRES-Cre* mice (Pei et al., 2015). We then performed 2-photon calcium imaging in the ganglion cell layer of these KO mice using the genetically-encoded calcium indicator GCaMP6s (Chen et al., 2013). In particular, we focused on the On-Off DSGCs because they are the ones that primarily project to the SGS (Dhande and Huberman, 2014). In wildtype littermate controls, 9.3% of cells in the ganglion cell layer were On-Off DSGCs (Fig. 3.1a-c, n = 60/648 cells, from 9 mice), consistent with previous studies (Baden et al., 2016; Sanes and Masland, 2015). In contrast, in the KO mice, the percentage of cells that displayed On-Off DS responses was significantly reduced (Fig. 3.1c, n = 19/566 cells, 3.4%, from 14 mice. p <0.001, χ^2 test). Because cholinergic inputs (i.e., ChAT+ cells) to the SC terminate in the intermediate and deep layers and do not co-release GABA, these "ChAT-Vgat" KOs mice provide us with a unique opportunity to study the effect of altered retinal direction selectivity on the visual response properties of superficial SC neurons.

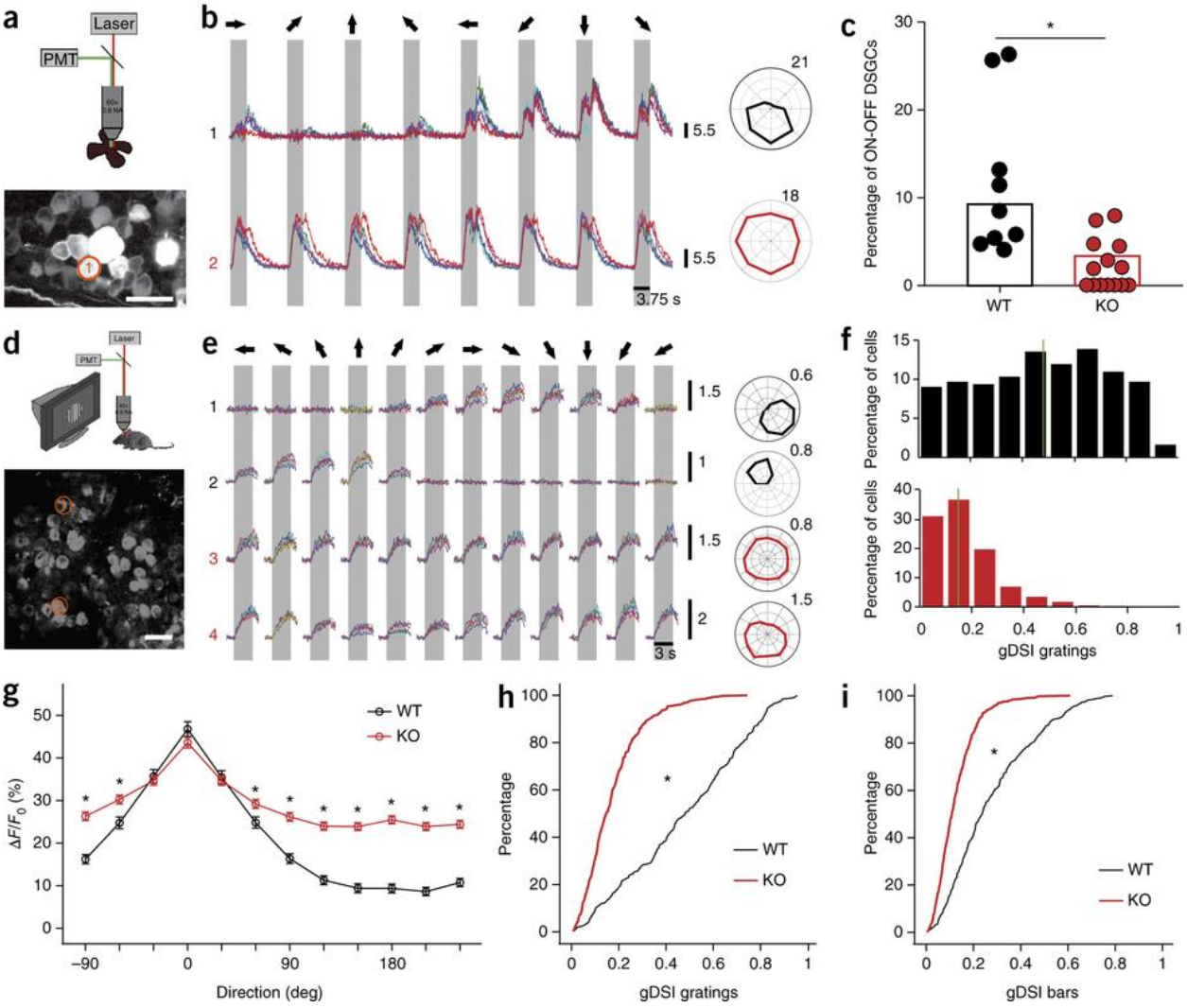

Figure 3.1. Genetic disruption of retinal direction selectivity reduces selectivity in the SGS. **a**, A schematic of two-photon calcium imaging of retina (top). The bottom panel shows a max-intensity projection of GCaMP6 fluorescence in an example field of view. Scale bar, 25 μm. **b**, Top (trace 1): Ca^{2+} signals of the RGC circled in (**a**) to the presentation of moving bars in eight directions (different colors represent separate trials). The gray shade corresponds to the time interval in which the bar stimulus sweeps across the field of view and the arrows represent the directions of movement in relation to the polar plots on the right. This cell showed DS responses to both leading and trailing edges of the moving bars, indicating that it was an ON-OFF DSGC. Bottom (trace 2): an ON-OFF cell from a *Vgat* conditional KO mouse. Corresponding polar plots are shown to the right. **c**, Summary plot showing the percentages of ON-OFF DSGCs in WT (black, $n = 60$ of 648 cells from 9 mice) and KO (red, $n = 19$ of 566 cells from 14 mice) retinas ($P < 0.001$, $\chi^2 = 17.3$, χ^2 test). Data points represent percentages of ON-OFF DSGCs in individual mice. **d**, A schematic of two-photon imaging of the SGS (top) and an example field of view from a WT (bottom). Scale bar, 20 μm. **e**, Ca^{2+} signals of the two neurons (1 and 2) circled in (**d**) and of two neurons from a *Vgat* KO (3 and 4), in response to drifting gratings. The gray boxes mark

the duration of stimulation. The movement directions of the bar are represented by arrows on top. Corresponding polar plots are shown to the right. **f**, gDSI distribution of WT (top, black) and KO (bottom, red) cells to drifting gratings. The solid green lines indicate the medians of distributions. **g**, Average WT (black, n = 310 cells from 5 mice) and KO (red, n = 407 from 8 mice) tuning curves to gratings after aligning each cell's preferred direction at 0. Data are presented as mean ± s.e.m. *P < 0.001, Mann-Whitney U-test. **h**, Cumulative distribution of the data shown in (**f**)(P < 0.001, K-S statistic = 0.61, Kolmogorov-Smirnov test). **i**, Cumulative distribution of gDSI to sweeping bars (P < 0.001, K-S statistic = 0.43, Kolmogorov-Smirnov test). Scale bars for the Ca^{2+} signals and polar plots in (**b** and **e)** represent the change in fluorescence from baseline ($\Delta F/F_0$).

We first performed intrinsic imaging and found normal SC retinotopic maps in the KOs (Fig. 3.2). Next, we performed 2-photon calcium imaging of the topmost SGS lamina, which we have previously shown to be enriched with DS neurons that have overlapping ON-OFF receptive fields (Inayat et al., 2015). The receptive field structures of the imaged cells were largely normal in the KOs, with subtle increase in subfield size and completely normal ON-OFF overlap (Fig. 3.3). The small increase in subfield size was consistent with the reduced inhibition in their retina of the KOs. Also consistent with this was that slightly more cells were responsive in the KOs.

When stimulated with drifting gratings or sweeping bars, 46.5% (310/667 cells to gratings) or 47.2% (315/667 to bars) were responsive in WT littermate controls, compared to 50.0% (407/821 cells, to gratings) or 61.5% (505/821, to bars) in the KOs. As expected, the vast majority of the responsive cells in this lamina were DS in WT (Fig. 3.1d-f, gDSI ≥ 0.25; n = 235/310 cells to gratings, 76%; and 146/315 to bars, 46%). Preferred motion directions were more widely represented than the 4 cardinal directions in the retina (Fig. 3.4), presumably due to specifically combining inputs of DSGCs that prefer neighboring cardinal directions. Remarkably, in the KOs, much fewer cells were DS in this lamina (n = 84/407 to gratings, 21%; and 35/505 to bars, 7%. Fig. 3.1f). The mean and median gDSI values in the KOs (0.17 ± 0.01 and 0.15 to gratings, 0.13 ± 0.00 and 0.11 to bars) were significantly lower than in the controls (0.48 ± 0.01 and 0.48 to

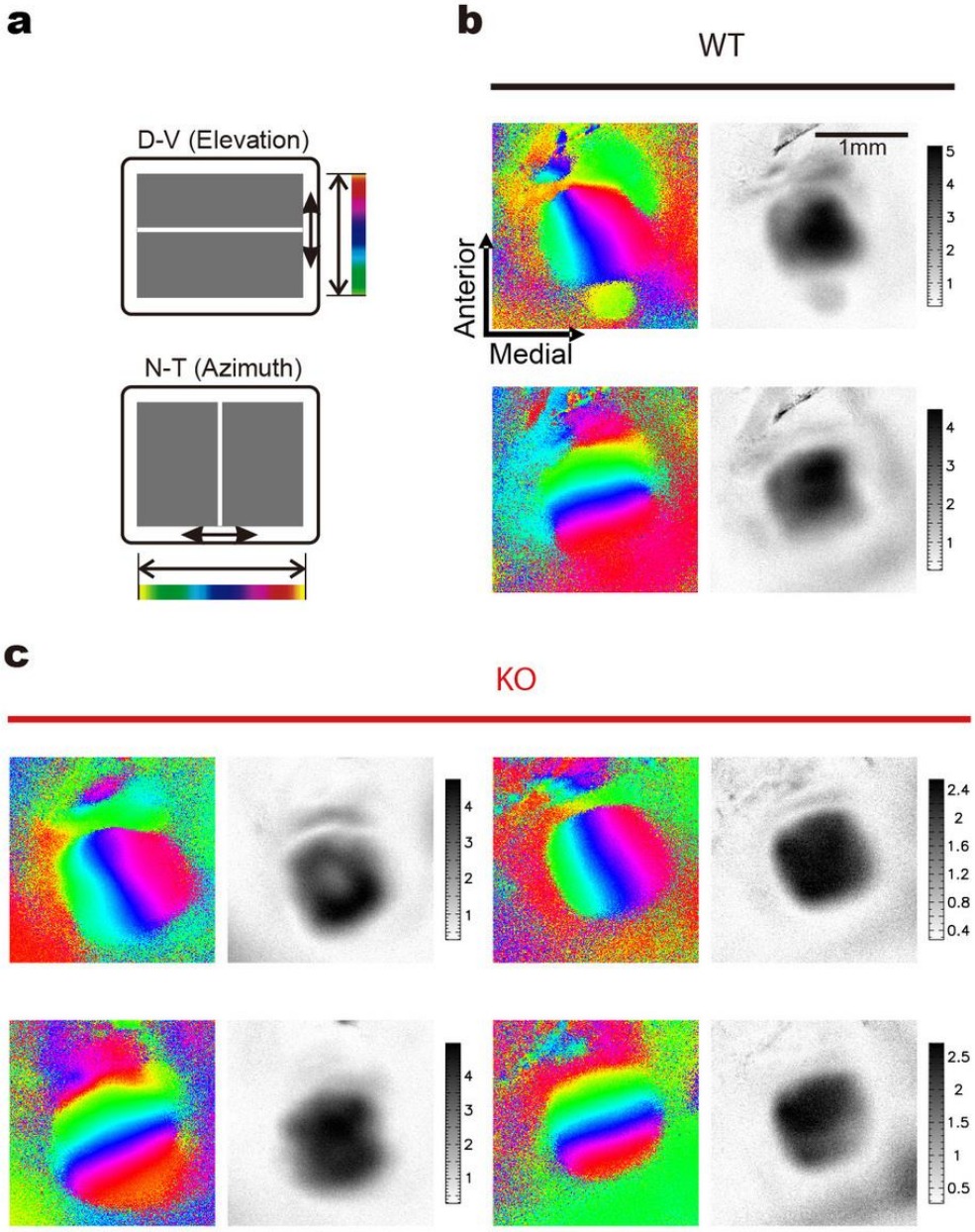

Figure 3.2. Normal retinotopic maps in ChAT-Vgat KO mice.
a, Visual stimulus protocol for generating the elevation (top) and azimuth (bottom) maps in the SC. The color scales represent the position of the moving bar on the stimulus monitor and the corresponding retinotopic locations in the SC. **b**, (top) Elevation map in a WT mouse. Both retinotopy (left) and response magnitude (right) are shown. The gray scale represents the response amplitude as a fractional change in reflection x 10^4. (bottom) Azimuth map for the same animal. **c**, Elevation and azimuth maps from two *Vgat* KO mice. The panel layout is the same as in (**b**). D, dorsal; V, ventral; N, nasal; T, temporal. See (Cang et al., 2008), for details of intrinsic imaging of retinotopic maps in the SC.

gratings, 0.28 ± 0.01 and 0.24 to bars, Fig. 3.1h and 3.1i, $p < 0.001$ for both gratings and bars, K-S test). Importantly, this reduction in direction selectivity was caused by increased responses to the non-preferred directions (Fig. 3.1g), consistent with decreased inhibitory inputs onto On-Off

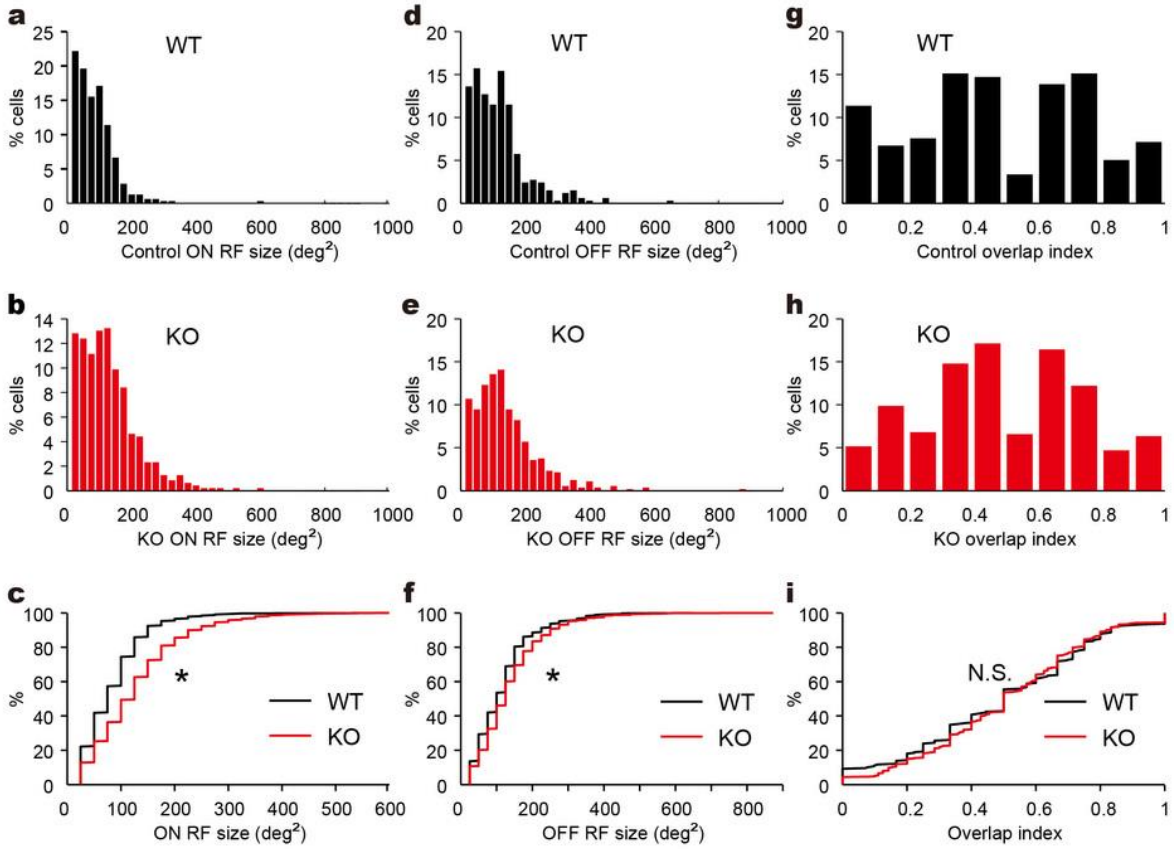

Figure 3.3. Receptive field structure of superficial SGS neurons.
a, Distribution of ON receptive field (RF) sizes (in deg^2) in WT (n = 316, 5 mice, mean ± s.e.m. = 85.84 ± 3.46, median = 75). **b**, Distribution of ON RF sizes in KO (n = 476, 8 mice, 128.31 ± 4.04, 125). **c**, Cumulative distributions of the data shown in (**a**) and (**b**) (asterisk (*) indicates $p < 0.001$, K-S statistic = 0.2500, Kolmogorov-Smirnov test). **d**, Distribution of OFF RF sizes in WT (n = 331, 5 mice, 118.20 ± 4.72, 100). **e**, Distribution of OFF RF sizes in KO (n=561, 8 mice, 138.19 ± 4.10, 125). **f**, Cumulative distributions of the data shown in (**d**) and (**e**) (asterisk (*) indicates p = 0.0137, K-S statistic = 0.1084, Kolmogorov-Smirnov test). **g**, ON-OFF overlap index in WT (n = 238, 5 mice, 0.50 ± 0.02, 0.50). **h**, ON-OFF overlap index in KO (n = 426, 8 mice, 0.51 ± 0.01, 0.50). **i**, Cumulative distribution of the data shown in (**g**) and (**h**) (p = 0.5909, K-S statistic = 0.0618, Kolmogorov-Smirnov test). See Inayat et al (*Journal of Neuroscience*, 2015, 35(20):7992-8003), for details of 2-photon imaging of SGS neurons' RFs and quantification.

DSGCs in the retina. Together, these data demonstrate that disrupting DSGCs' tuning leads to reduced selectivity in SGS neurons, thereby confirming the retinal origin of SGS direction selectivity.

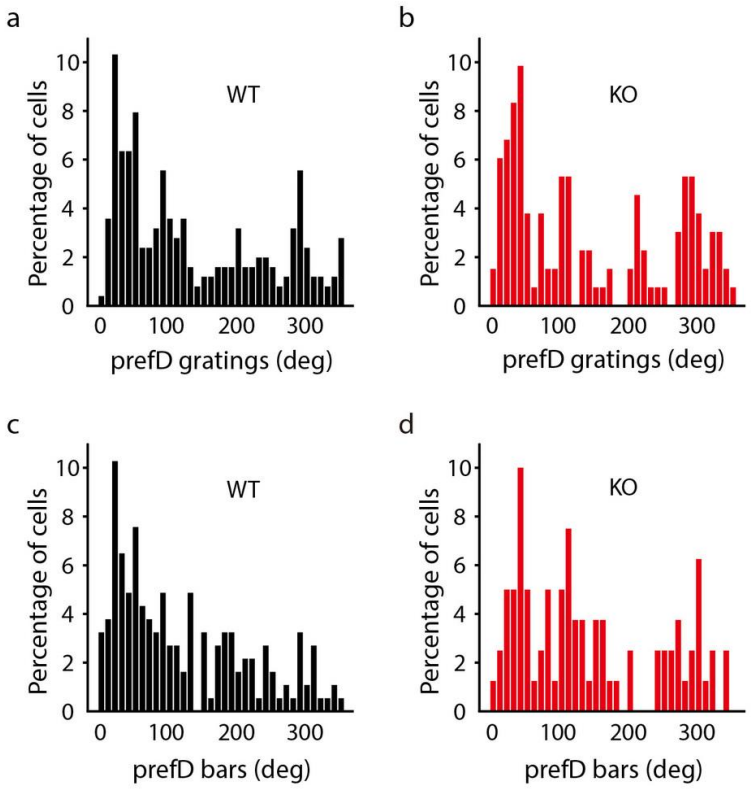

Figure 3.4. Preferred directions of superficial SGS neurons as determined by two-photon calcium imaging.
a, Histogram of the preferred direction (prefD) distribution of superficial SGS neurons in WT mice, in response to drifting gratings. Only cells that had gDSI ≥ 0.2 were included (n = 252 out of 310 total responsive cells). This cutoff was applied to all panels. **b**, Histogram of the preferred direction distribution in *Vgat* KO mice, in response to drifting gratings (n = 132/407 total responsive cells). **c-d**, Histogram of the preferred direction distribution in WT (**c**) and *Vgat* KO (**d**) mice, in response to sweeping bars (n = 185/315 in WT and 80/505 in KOs).

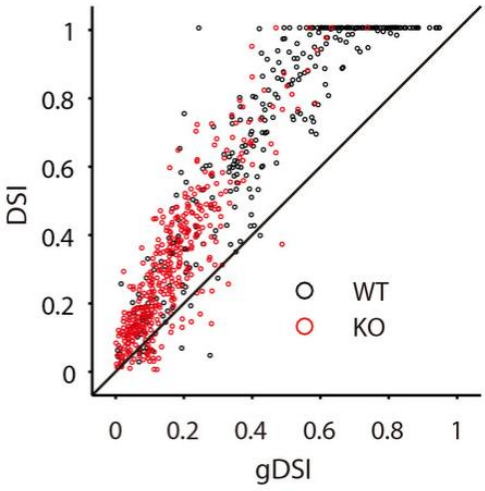

Figure 3.5. Relationship between DSI and gDSI.
Relationship between DSI and gDSI for two-photon imaging data of the SC, in response to drifting gratings (n = 310, 5 WT mice, black; n = 407, 8 KO mice, red). The solid line is the line of identity.

Discussion

In this study, we have manipulated the retinal input in order to study its role in generating SGS direction selectivity. As a result, we were able to demonstrate that SGS neurons inherit their direction selectivity from DSGCs in the retina, a finding that has important implications for understanding signal processing in the early visual system.

It is known that individual SGS neurons are innervated by several RGCs (Chandrasekaran et al., 2007). Consequently, in order to provide DS excitation to the postsynaptic neuron, the converging DSGCs must prefer similar directions. In addition, a new directional preference would emerge when the DSGCs that prefer neighboring cardinal directions precisely converge. Our findings therefore indicate that well-controlled developmental mechanisms must exist to ensure the precise and selective targeting of DSGCs in the SGS. Consistent with this idea, several subtypes of DSGCs have been found to project primarily to the upper SGS (Dhande and Huberman, 2014), which contains more DS cells than the lower SGS (Inayat et al., 2015). How such depth-specific targeting is established during development, and how even more precise patterns of connectivity are generated at the level of individual cells, have not been studied.

A non-random connectivity has been revealed for orientation selective cells in the mouse visual cortex (Ko et al., 2013; Ko et al., 2011; Lee et al., 2016), and its emergence shown to require visual experience (Ko et al., 2013). The exact wiring diagram of the SGS circuits and its development have not yet been studied. Given that the mouse retinocollicular pathway is already a productive model for studying cell types and neural development (Cang and Feldheim, 2013), future studies of this pathway will likely reveal the molecular and cellular mechanisms that

establish the precise connections from the retina to the SGS and also within the SGS, which are necessary to generate and maintain feature selectivity in the superior colliculus.

Direction selectivity is an evolutionarily-conserved property seen in many visual structures and in various species. In zebrafish, for example, RGC subtypes that prefer different directions project to segregated layers in the optic tectum, and the tectal neurons with matching preferred directions arborize their dendrites in the corresponding layers (Gabriel et al., 2012; Lowe et al., 2013; Nikolaou and Meyer, 2012; Robles et al., 2013). This suggests that the DS retinal inputs could determine the direction preference of tectal neurons, just like what we discovered here in the mouse SC. In monkeys, a very small population of DS neurons was found in the SC (Cynader and Berman, 1972; Marrocco and Li, 1977), largely consistent with the fact that DSGCs have so far remained elusive in primates. It is certainly possible that DSGCs may be discovered with new genetic and imaging techniques in the future and that they may give rise to observed SC direction selectivity. Alternatively, the weak DS responses in the primate SC could result from the excitatory input from visual cortex, which includes DS cells. This possibility has in fact been addressed in cats by lesioning or cooling the cortex, but unfortunately these studies yielded conflicting results (Hoffmann and Straschill, 1971; Ogasawara et al., 1984). On the other hand, cortical input does not appear to affect SC selectivity in rodents. For example, in ground squirrels, SC direction selectivity remain unchanged when visual cortex is removed, leading to the proposal that the DS cells receive their inputs from the retina (Michael, 1970). We have recently shown that in mice cortical inputs do not affect the magnitude or looming speed tuning of SC responses under anesthesia and only increase the response magnitude in awake condition (Zhao et al., 2014). Our current study, where the animals were anesthetized and their V1 removed, demonstrates that retinal

input is the origin of the direction selectivity in the mouse SC. Future studies will be needed to determine whether cortical input could modulate SC direction selective responses under certain behaviors in mice or even give rise to SC direction selectivity in primates.

In addition to direction selectivity, SGS neurons also display a number of other response properties, such as size preference, motion selectivity and speed tuning (Gale and Murphy, 2014; Wang et al., 2010; Zhao et al., 2014). These properties could be generated by integrating inputs from DSGCs, other RGC subtypes, local intracollicular circuits, and afferent inputs from visual cortex. In terms of local circuits, the SGS contains a large population of inhibitory neurons. Inhibition could sharpen direction selectivity if it is tuned to the opposite direction or offset spatiotemporally, as shown for DS neurons in zebrafish tectum (Gabriel et al., 2012) and mouse visual cortex (Li et al., 2015). Inhibitory neurons in the topmost SGS lamina are known to be DS (Inayat et al., 2015). It is thus conceivable that these inhibitory neurons may provide direction-specific interactions between stimulus center and surround in response to complicated visual scenes. Future studies will be needed to determine the spatial and direction tuning of inhibition in SGS neurons in order to reveal its functions in visual processing.

In conclusion, we've shown that DSGCs are the source of direction selectivity in the SGS. Questions thus arise about the role of local SGS circuits, and especially local inhibition, in transforming this retinal input. Given the fundamental importance of the SC in visually-guided behaviors, our discovery will motivate exciting future studies of visual system organization, function and development.

Notes on CHAPTER 3

In this chapter, I presented only my personal contribution to a collaborative effort with Dr. Xuefeng Shi, which resulted in the following publication:

Shi, X.*, Barchini, J.*, Ledesma, H.A., Koren, D., Jin, Y., Liu, X., Wei, W., and Cang, J. (2017). Retinal origin of direction selectivity in the superior colliculus. Nat Neurosci *20*, 550-558.

* These authors contributed equally to this work.

In the published paper, Dr. Shi performed voltage-clamp recordings from direction selective neurons in the SGS while optogenetically silencing local excitation (ChR2 in $GAD2^{+}$ neurons), in order to isolate retinal inputs to these cells. He showed that EPSCs in SGS neurons were already directionally tuned, and could account for the measured membrane potential in these cells. Local SGS excitation served only to amplify the input, with no influence on tuning. Additionally, by comparing the integrated retinal input at the preferred and null directions, Dr. Shi found it to be coming from already tuned ganglion cells (DSGCs), and not from a delayed integration of unturned retinal inputs that gives rise to postsynaptic direction selectivity.

I included in this chapter retinal imaging data from the KO mouse performed by Hector Acaron Ledesma and David Koren, in the laboratory of Dr. Wei Wei at the University of Chicago. Their results are tightly linked to my findings, and warranted to be presented in conjunction. I did not, however, discuss Dr. Shi's findings beyond the provided summary above. I thank Dr. Hui Chen for his help in analyzing the data that went into this chapter.

CHAPTER 4

Bidirectional Encoding of Motion Contrast in the Mouse Superior Colliculus

Summary

Detecting salient objects in the visual field is important for an animal's interactions with the environment. Here, we show that neurons in the mouse superior colliculus (SC) encode visual saliency by detecting motion contrast between stimulus center and surround. Excitatory neurons in the most superficial lamina of the SC are contextually modulated, monotonically increasing their response from suppression by the same-direction surround to maximal potentiation by an oppositely-moving surround. The degree of this potentiation declines with depth in the SC. Inhibitory neurons, on the other hand, are suppressed by any surround at all depths. These findings establish the mouse SC as a locus of motion saliency computation, and provide hypotheses for mechanistic studies to explore this phenomenon at the circuit level.

Introduction

The detection of salient objects in the environment is crucial for an animal's ability to efficiently and safely navigate the world. In the visual system, objects are processed by neurons that respond to specific features in their receptive fields (RFs), such as orientation, movement direction, luminance, and color. Being spatially restricted, RFs provide a "pixel-like" representation of the visual scene. At the perceptual level, however, the same stimulus presented within an RF could appear drastically different depending on its context. For example, a vertical bar would "pop out" perceptually when it is surrounded by horizontal bars, but not among other identical vertical bars. At the neuronal level, such saliency computation requires a comparison of features inside and outside of the RF.

Most studies on feature-specific saliency computation have been conducted in primate and cat primary visual cortex (V1), predominantly in the context of orientation selectivity. It was shown that V1 neurons are suppressed by stimuli of the same orientation in regions surrounding the RF (Jones et al., 2002; Knierim and van Essen, 1992; Sengpiel et al., 1997), consistent with the classical surround suppression seen at the level of the retina and lateral geniculate nucleus (Sachdev et al., 2012). Importantly, V1 neurons displayed lower levels of suppression when static gratings of orthogonal orientations were shown in the surround (Kastner et al., 1999; Knierim and van Essen, 1992; Nothdurft et al., 1999). In response to moving gratings, orthogonal surrounds were even able to induce a certain level of response facilitation in primate V1 (Jones et al., 2001; Jones et al., 2002; Sillito et al., 1995). In other words, depending on the relationship between the properties of the center and surround stimuli, differential levels of suppression or facilitation can occur, thus providing a neural basis for the perceptual "pop-out" phenomenon.

It is theorized that feature-specific saliency computations are combined into a map to represent the total saliency value of each point in space (Veale et al., 2017; Zhaoping and Zhe, 2015). Although the exact location of where the saliency map is first generated is still a matter of debate, there is a general agreement that the superior colliculus (SC) in the midbrain contains such a map (Veale et al., 2017; Zhaoping, 2016). In primates, SC neurons are not tuned to specific visual properties, consistent with the notion of feature-agnostic saliency representation (White et al., 2017). In contrast, in lower vertebrates such as birds and fish where neocortex has not evolved, neurons in the optic tectum, the homologue of mammalian SC, can perform certain feature-specific saliency computations (Ben-Tov et al., 2015; Frost et al., 1981; Sun et al., 2002; Zahar et al., 2012). This has led to the idea that the locus of saliency computation has migrated evolutionarily, among many other visual system functions, from the tectum to the visual cortex (Zhaoping, 2016).

These considerations thus raise an intriguing question about saliency computation in mice. Although mouse V1 neurons show similar selectivity compared to those in higher mammals (Niell and Stryker, 2008), the SC is still the most prominent retinal target in mice and mediates visually-guided behaviors (Ellis et al., 2016; Liang et al., 2015; Shang et al., 2015; Wei et al., 2015; Zhao et al., 2014). Unlike in primates, most visual neurons in the mouse SC are tuned to features such as motion direction or stimulus orientation (Gale and Murphy, 2014; Wang et al., 2010). Whether and how these feature-selective SC neurons encode visual saliency in mice has not been investigated.

Here, we study how neurons in the *stratum griseum superficiale* (SGS) of the mouse SC respond to motion contrast in the form of differential movement directions between RF center and surround. We use 2-photon calcium imaging to study this property in large populations of SGS

neurons, demonstrating a depth-specific response profile. More importantly, by imaging in transgenic mice with labeled GABAergic neurons, we reveal striking differences in the responses of excitatory and inhibitory neurons to motion contrast. Our findings are not only valuable for a circuit-level understanding of mouse vision, but also provide useful information for studying the evolution and conserved principles of visual saliency computation.

Materials and Methods

Animal preparation

Adult C57BL/6 mice of both sexes were used in this study (n = 21, postnatal days 75-131). *Gad2*-IRES-cre mice (from the Jackson Laboratory, Stock no. 010802) were either crossed with an Ai9 line (*RCL-tdT*, Stock no. 007909), or injected with AAV1.CAG.Flex.tdTomato.WPRE.bGH (University of Pennsylvania Vector Core, Allen Institute 864) in their SC, to express the red fluorescent protein tdTomato in glutamate decarboxylase 2 positive ($GAD2^+$, GABAergic) neurons. All mice were kept on a 12-h light/dark cycle, with one to five animals housed per cage. All experimental procedures were approved by the Northwestern University Institutional Animal Care and Use Committee.

Mice were anesthetized with urethane (1.2 g/kg in 0.9% saline solution, i.p.) and then sedated with chlorprothixene (10 mg/kg in water, i.p.). Atropine (0.3 mg/kg in 0.9% saline) and dexamethasone (2 mg/kg in 0.9% saline) were subsequently administrated subcutaneously to minimize respiratory secretions and brain inflammation, respectively. The animals were then transferred onto a heating pad, and their body temperature was monitored via a rectal thermoprobe and maintained at 37 °C through a feedback heater control module (Frederick Haer Company, Bowdoinham, Maine). Artificial tears (Henry Schein) were applied to the eyes for protection during surgery. The scalp was then shaved, and the skin removed to expose the skull. A craniotomy was performed on the left hemisphere along the midline and posterior sutures, covering an area of ~3.0 x 3.0 mm^2. The overlaying cortical tissues (including V1 and hippocampus) were removed by aspiration to expose the left SC. A head bar was finally mounted on the skull using Metabond (Parkell, Edgewood, NY) mixed with black ink. Animals previously injected with H2B-GCaMP6s

would be ready for imaging. Animals to undergo imaging using the calcium-sensitive dye Cal-520 would have the dye loaded into their SC as described below.

Preparation and administration of the calcium-sensitive dye Cal-520

A fresh solution of the fluorogenic calcium-sensitive dye Cal-520 AM (AAT Bioquest; (Tada et al., 2014)) was prepared for every experiment. A solution of 20% Pluronic F-127 in DMSO was initially prepared and sonicated for 10-15 min. Four microliters of this solution were used to reconstitute 50 μg of powdered Cal-520. The resulting solution was sonicated for another 12–15 min and then brought to a total volume of 40 μl by adding 36 μl of a calcium-free solution (in mM: 150 NaCl, 2.5 KCl, and 10 HEPES, pH 7.4), for a final concentration of 1.13 mM Cal-520. After 5 more min of sonication, the solution was ready to be bolus loaded using a Nanoject II (Drummond) fitted with a glass pipette with a beveled tip and an inner diameter of 10–20 μm.

Once the SC was exposed, the pipette was filled with the previously prepared solution and lowered into the tissue. Twenty pulses of 2.3 nL each (46 nL total volume), at 20-s intervals, were administered to deliver the solution first at a depth of 450 μm below the surface, then at 200 μm after retracting the pipette to that depth. The pipette was left in the tissue for 1–2 min before being slowly retracted. The SC was then covered with ACSF (in mM: 125 NaCl, 5 KCl, 10 glucose, 10 HEPES, 2 $CaCl_2$, pH 7.4, 300 mOsm). Imaging was performed 1–2 h after dye loading.

Injection of H2B-GCaMP6s

Mice were anesthetized with isoflurane (5% for induction, 1.5% for maintenance, in O_2) then transferred onto a heating pad. Their body temperature was monitored via a rectal thermoprobe

and maintained at 37 °C through a feedback heater control module (Frederick Haer Company, Bowdoinham, Maine). Artificial tears (Henry Schein) were applied to the eyes for protection during surgery. The scalp was then shaved, and a small cut was made to expose the skull near the lambda point. A burr hole was drilled on the left hemisphere using a dental drill, 0.75 mm lateral and 0.5 mm anterior of the lambda point.

A Nanoject II (Drummond) fitted with a glass pipette with a beveled tip and an inner diameter of 10–20 μm, was used for viral injection. Viral particles were loaded into the pipette, which was then lowered into the brain through the burr hole, first to a depth of 1.4 mm below the pial surface, and then retracted to a depth of 1.2 mm. At each depth a total volume of roughly 50 nL was delivered, in 2.3 nL pulses, 15 seconds apart. AAV-syn-H2B-GCaMP6s (generously provided by Dr. Loren Looger, Janelia Research Campus) was injected into the SC of GAD2-Cre x AI9 (*RCL*-tdT) animals (1:1 in PBS). Alternatively AAV-syn-H2B-GCaMP6s was mixed with AAV1.CAG.Flex.tdTomato.WPRE.bGH ($5.1x10^{12}$ GC/mL, University of Pennsylvania Vector Core, Allen Institute 864) (1:1:2 in PBS) and the same volumes were injected in the SC of GAD2-Cre mice at the aforementioned depths. The pipette was left in the tissue for 1–2 min before being slowly retracted. The skin was subsequently sutured back. Mice were given a dose of buprenex during surgery (0.05 mg/Kg, Sub-Q), and a dose of carprofen after (5 mg/Kg, Sub-Q), and were monitored daily for pain and wound health. Imaging was performed 10 to 21 days after injection.

Two-photon calcium imaging

After the mice were prepared for imaging as described in the previous sections, they were moved onto a heating pad under a two-photon scanning microscope (2P-SGS, Bruker Nano Surface

Division). The head bar was clamped at an angle so that the imaged SC surface was largely flat and perpendicular to the optical axis of the objective. A thin film of silicone oil was applied to the eyes for protection. A shield was placed around the craniotomy to block light from the visual stimulus during imaging. The SC was covered with 3% agarose in ACSF for stability. Imaging was performed with a Ti:sapphire laser (Coherent Chameleon Ultra II) at excitation wavelengths of 800 nm for Cal-520, 920 nm for H2B-GCaMP6s, and 720 or 1020 nm for tdTomato, using a 40X, 0.8-NA objective (Leica) immersed in ACSF. Emitted signals from the Ca^{2+} indicators and tdTomato were filtered into separate photomultiplier tubes (PMTs, green and red channels). Laser excitation power after the objective was around 10 mW for Cal-520 imaging, and varied between roughly 10 and 120 mW (depending on the depth) for H2B-GCaMP6s imaging. Data were acquired using PrairieView software (Versions 5.0 and 5.3) in spiral scan mode at 2X optical zoom, resulting in a circular field of view with a diameter of 135 μm. Image resolution was 256 × 256 pixels and the acquisition rate was 8.079 Hz. Imaging with Cal-520 was performed in the superficial SGS (sSGS, no deeper than 50 μm from the SC surface), while imaging with H2B-GCaMP6s was performed across different depths of the SGS, ranging from the sSGS down to 205 μm below the surface.

Visual stimulus

Visual stimuli were generated with Matlab Psychophysics toolbox (Brainard, 1997; Niell and Stryker, 2008) on an LCD monitor (37.5 cm × 30 cm, 60 Hz refresh rate, ~50 cd/m^2 mean luminance, gamma corrected). The screen was placed 25 cm away from the eye contralateral to the imaging site (the right eye), and slightly tilted at an angle matching that of the mouse's head,

given that the mouse's nose was slightly elevated to correct for the curvature of SC and allow imaging from a relatively flat surface. The monitor was moved for every imaged field of view so that the cells' receptive fields were near the center of the screen. The placement of the monitor center in visual space varied between 20° and -25° in elevation (0° representing eye-level) and between 30° and 90° across the azimuth (0° representing the center of the binocular field) in all imaging experiments reported in this study. The ipsilateral eye was covered throughout the experiment.

Two types of visual stimuli were used for imaging. First, a flashing black square (5°x5° in visual angle) on a gray background was used to map the receptive fields of the imaged neurons. The square was flashed in a 6x6 grid (30°x30° in visual angle), for a duration of 1 sec, followed by the presentation of a gray screen for 3 seconds. This stimulus set was shown to the mouse at least 4 times in a pseudo-random fashion for every imaged field of view.

The second visual stimulus was “center-surround” square wave drifting gratings (100% contrast, 0.08 cpd, 2 Hz), presented on a gray background at the center of the screen so that the center component (20° across) covered the receptive fields of the imaged neurons. The surround was an annulus that started at the very edge of the center stimulus and extended 60° across. Eight different directions of motion were used for both center and surround, ranging from 0° to 315° and tiling all of direction space in 45° increments. 0° represented forward motion from the animal’s perspective; positive values followed in a clockwise fashion, and negative values in a counterclockwise fashion. A blank (gray) condition was added to the 8 directions for both center and surround for a total of 81 (9x9) unique center-surround combinations (including center alone conditions, surround alone conditions, and a gray screen condition). Each stimulus condition was

presented for 2 s, followed by a gray screen for 5 s. This stimulus set was shown to the mouse at least 4 times in a pseudo-random fashion for every imaged field of view.

Data analysis

Animals that had visible tissue damage to their SC after dye loading, where the dye failed to be incorporated into the cells, or where there was poor expression of H2B-GCaMP6s, were not subject to imaging. Data analysis was performed on all animals that were subject to imaging, and no data points were excluded from the resulting datasets.

Time-series frames were averaged to produce an average image of the field of view. In the cases where the imaging field shifted in the x-y plane over the course of the series, a semi-automated procedure was used to realign the frames. Specifically, a subset of the frames along the recording were manually realigned to match the first frame of the recording, and the corrected positions of all the intermediate frames were automatically extrapolated, leading to a sharper corrected average image, and spatially stable regions of interest (ROIs).

To determine whether each selected ROI is an inhibitory ($GAD2^+$) or excitatory neuron ($GAD2^-$), the experimenter referred to the red channel image of each field of view where $GAD2^+$ cells were labeled with tdTomato. This selection process relied exclusively on the expression of tdTomato and was performed blindly to the functional properties of the cells, which were determined at a later stage of the process.

For the analysis of Cal-520 imaging data, we followed our published procedures (Inayat et al., 2015). Briefly, ROIs were manually drawn on the average image of the collected time-series, and the intensity values of all pixels in each ROI were averaged for each frame to obtain the raw

Ca^{2+} signal for each cell. From the raw trace, and for each stimulus presentation, $\Delta F/F_0 = (F - F_0)/F_0$, was calculated, where F_0 was the mean of the baseline signal over a fixed interval (1.25 s for gratings; 0.75 s for flashing squares) before stimulus onset, and F was the average fluorescence signal over a 2.5 s duration starting at 250 ms after stimulus onset and ending at 750 ms after stimulus offset for gratings (1.1 s duration, 250 ms after onset and 350 ms after offset, for flashing squares). A cell was considered responsive if its mean $\Delta F/F_0$ was more than two standard derivations above its F_0 for at least one of the stimulus conditions. The mean value of $\Delta F/F_0$ for each of the stimulus conditions was then used to determine the direction tuning curve for every responsive cell, and to calculate a direction selectivity index and a response modulation index by the surround.

A similar procedure was used to analyze the H2B-GCaMP6s imaging data, with the exception that the 2.5 s integration time window of $\Delta F/F_0$ was shifted forward in time by 375 ms in order to account for the slower dynamics of H2B-GCaMP6s, compared to Cal-520. We analyzed this dataset with time windows of different latencies and duration, and our conclusions were not affected (Fig. 4.1 and 4.9, and See "Simultaneous two-photon imaging and cell-attached recording" below).

To quantify the degree of direction selectivity, we calculated a global direction selectivity index (gDSI), which is the vector sum of $\Delta F/F_0$ responses normalized by their scalar sum (Gale and Murphy, 2014; Inayat et al., 2015):

$$\text{gDSI} = \frac{\sum R_\theta e^{i\theta}}{\sum R_\theta}$$

Where Rθ is the response magnitude in $\Delta F/F_0$ at direction θ of the center stimulus.

To calculate the modulation index, we first determined each neuron's preferred direction as the center-stimulus direction that elicited the peak average $\Delta F/F_0$. In the case of neurons that were non-response to the center stimulus alone (center-silent neurons), the preferred direction was chosen as the center direction of the center-surround stimulus combination that elicited the peak average $\Delta F/F_0$. The modulation index was then calculated as follows:

$$\text{Modulation Index} = \frac{R_{\text{pref. C } with\ S} - R_{\text{pref. C}}}{R_{\text{pref. C } with\ S} + R_{\text{pref. C}}}$$

Where $R_{\text{pref. C with S}}$ is the neuron's response (in $\Delta F/F_0$) to coupling its preferred direction at the center with whichever surround we were assessing, and $R_{\text{pref. C}}$ is the neuron's response to the presentation of its preferred direction at the center alone. Negative numbers indicate a suppression by the surround of the response to the center alone, while positive numbers indicate potentiation. Values that were below -1 or above 1 due to negative $\Delta F/F_0$ values were adjusted to -1 and 1, respectively.

A small population of center-silent inhibitory neurons were silent to the presentation of the center and surround separately, but responded to particular C-S combinations (n = 85, Fig. 4.7F). Only a few of these neurons increased their "preferred center" response when stimulated together with the opposite surround (n = 31/85, Fig. 4.7F). Those neurons were not included in the modulation index calculations of Fig. 4.6D. In contrast a much larger population of excitatory neurons exhibited this type of response (n = 154/191, Fig. 4.2F), and were included in the modulation index calculations of Fig. 4.2G.

Simultaneous two-photon imaging and cell-attached recording

We performed imaging-guided cell-attached recordings to characterize H2B-GCaMP6s and assess its capacity to report spiking activity. We used glass micropipettes (1.8-2.5 μm tip diameter, 2.2-6.5 MΩ tip resistance) filled with ACSF (in mM: 125 NaCl, 5 KCl, 10 glucose, 10 HEPES, and 2 $CaCl_2$, pH 7.4) and containing a mixture of 20 μM Alexa Fluor 488 and 594, for visualization under the microscope. Positive pressure was applied to the pipette, and the tip was brought to a position on top of a target neuron. The tip was subsequently lowered onto the cell, until a change in resistance was detected. Light suction was then applied to generate a seal and detect spiking activity. A MultiClamp 700B amplifier (Molecular Devices) in current-clamp mode and a System 3 workstation (Tucker-Davis Technologies) were used to record extracellular spiking. A minimal version of the Center-Surround stimulus (4 directions and a blank in both center and surround) was used to elicit visual responses, and both image acquisition and the electrophysiological recording were synchronized to the visual stimulus.

The imaging and spiking data were then analyzed to compare their response magnitude to each stimulus condition (Fig. 4.1A-B). Spike rate was averaged over the 2 second period of visual stimulus presentation (firing rate to the blank stimulus was subtracted). Due to its slow dynamics, the H2B-GCaMP6s calcium signal was averaged between 625 ms after stimulus onset and 1125 ms after offset for a duration of 2.5 seconds. This particular delay was longer than that used for Cal-520 (250 ms and 750ms respectively). It was chosen so that for either reporter the start time coincided with a 20% response increase from baseline to the preferred C-S combination (Fig. 4.1C, blue and red curves). Note that because of the slow dynamics of H2B-GCaMP6s, and particularly the slow fluorescence decay time following a stimulus offset, a stable baseline was not always

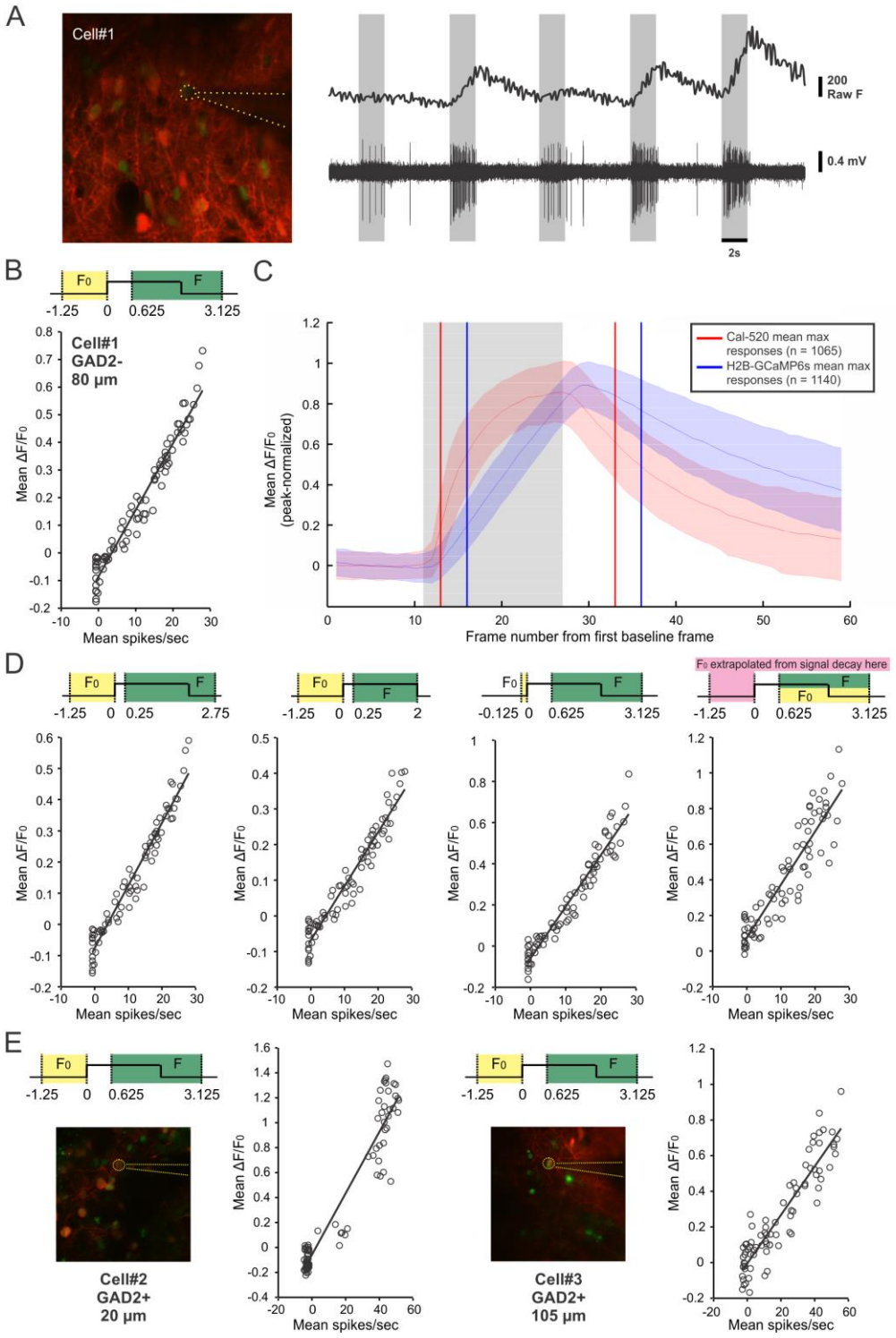

Figure 4.1. Characterization of H2B-GCaMP6s activity with cell-attached recording.
(**A**) Example GAD2$^-$ neuron patched at a depth of 80 µm (left) and the corresponding raw calcium trace and spiking activity of the same neuron (Cell#1) to the presentation of 5 randomized

conditions of the C-S visual stimulus (right). (**B**) Linear relationship between the $\Delta F/F_0$ signal and the corresponding spiking activity for Cell#1. Each data point represents a single trial. (**C**) Comparison between the response dynamics of Cal-520 and H2B-GCaMP6s by averaging the maximum responses of all cells (i.e. each cell's response to its preferred C-S combination), after normalization to the peak of each trace (Red, mean and SD of the Cal-520 responses, n = 1065; Blue, mean and SD of the H2B-GCaMP6s responses, n = 1140). The gray shaded region represents the 2 s period of visual stimulus presentation. The red vertical lines delimit the $\Delta F/F_0$ window for analyzing Cal-520; the blue vertical lines delimit the $\Delta F/F_0$ window for H2B-GCaMP6s. (**D**) Relationship between $\Delta F/F_0$ and spike rate for Cell#1 using four different methods for calculating $\Delta F/F_0$. For panels **B**, **D**, and **E**, diagrams on top of each panel represent the different methods for $\Delta F/F_0$ calculation. The onset and offset of the stimulus is depicted as a square wave. Time stamps are in seconds, and the yellow and green shaded regions represent the respective time windows for F_0 and F that were considered for the calculation of $\Delta F/F_0$. For the last panel in **D**, F_0 for every point in F was extrapolated from the signal decay before stimulus onset (pink shaded region). Note that regardless of the method, the relationship between $\Delta F/F_0$ and spiking is maintained; the only major difference being the magnitude of $\Delta F/F_0$. (**E**) Relationship between $\Delta F/F_0$ and spike rate for two more example cells (Cell#2, left; Cell#3, right), using the adopted $\Delta F/F_0$ calculation method in this study.

reached before the onset of the following stimulus. This resulted in negative $\Delta F/F_0$ values at some non-responsive conditions (Fig. 4.1B). This could lead to an overestimation of the selectivity of cells, a foreseeable problem with calcium indicators that are slow or do not have single-spike resolution. Nevertheless, given the reasonably linear relationship between H2B-GCaMP6s and spike responses (n = 3, 2 mice; Fig. 4.1B, E), relative comparisons of responses within a single tuning curve and between cells are still valid.

Some neurons exhibited uncharacteristic activity when patched (n = 2, 2 mice), which resulted in the immediate saturation of their calcium signal; a phenomenon very rarely observed during regular imaging sessions, and clearly induced by the recording procedure. Those cells were excluded from further analysis (data not shown).

Statistics

All pooled data were presented as mean ± s.e.m, unless stated otherwise. Significance was calculated using two-sided statistical tests, including Mann-Whitney *U*-tests and Kolmogorov-Smirnov (K-S) tests. Correlation coefficients and their corresponding p-values were calculated, in addition to first degree polynomial fits and their corresponding R^2 values and y-intercepts, as mentioned in the text.

To determine a significant difference between a neuron's responses to any given pair of center-surround conditions (e.g. preferred-direction center vs. preferred center + oppositely-moving surround), we performed a bootstrapping test. The four $\Delta F/F_0$ values (4 trials) for each of the two compared stimulus conditions were pooled for a set of 8 values. Eight values were then sampled from that set 10,000 times, with replacement. Each of the generated sets was subsequently split into two subsets of 4 values randomly and the means of the two subsets subtracted to generate a distribution of the difference. The difference between the mean $\Delta F/F_0$ of the observed data was calculated, and depending on where that value fell with respect to the 95% confidence interval of the distribution, the response was considered significantly potentiated, suppressed, or unaltered. This measure gave us a more statistically tractable measure of modulation compared to the calculation of the modulation index, where a hard cutoff value of 0 separated between potentiated and suppressed neurons.

Note that when using this bootstrapping analysis we observe a significant response suppression in center-silent neurons by a surround moving in the same direction, compared to their "response" to the center alone (Fig. 4.4F). This indicates that our method for assigning response significance is rather conservative, and that some of these neurons might actually have some low-

magnitude response to the center stimulus alone.

All analyses and graph plotting were performed in Matlab (MathWorks). No statistical methods were used to predetermine sample sizes, but our sample sizes are similar to those reported in the field. We did not randomly assign animals to groups because it is not applicable to the experimental design of this study.

Results

Responses of sSGS excitatory neurons are modulated by motion contrast

We performed 2-photon calcium imaging of SGS neurons in anesthetized mice (Fig. 4.2A), where the visual cortex was removed to allow optical access and eliminate any potential cortical influence on SC responses. We first focused on the neurons in the most superficial lamina of the SGS (sSGS, < 50 μm from the surface) using the synthetic calcium dye Cal-520. We recently used the same imaging method to discover that the sSGS is enriched with neurons that are highly selective for movement direction (Inayat et al., 2015). Here, we uncoupled the movement direction between the stimulus center and surround, and determined how sSGS responses were modulated by this form of motion contrast (Fig. 4.2C). These experiments were done in mice where $GAD2^+$ neurons were fluorescently labeled with tdTomato, allowing us to compare the response properties of inhibitory ($GAD2^+$, GABAergic) and excitatory ($GAD2^-$) neurons (Fig. 4.2B).

In each imaging session, we first mapped the RFs of the imaged cells using a flashing black square on a gray background. A small circular patch of gratings (10° radius) was then placed at the center of the RFs and drifted in different directions. Consistent with our previous finding, about half of sSGS neurons were responsive to the drifting gratings (n = 355/811 $GAD2^-$ and n = 379/652 $GAD2^+$, from 9 mice, see Methods for details of determining responsiveness), and most of them were direction selective (DS), showing much higher increases in fluorescence to their preferred directions than to the opposite (Fig. 4.2C, 283/355, 79.7% $GAD2^-$, and 264/379, 69.7% $GAD2^+$ neurons had gDSI > 0.2).

For most responsive excitatory neurons (n = 294/355, 82.8%), the small grating covered their entire RFs (Fig. 4.3A), such that gratings in the surround (an annulus from 10° to 30° radius)

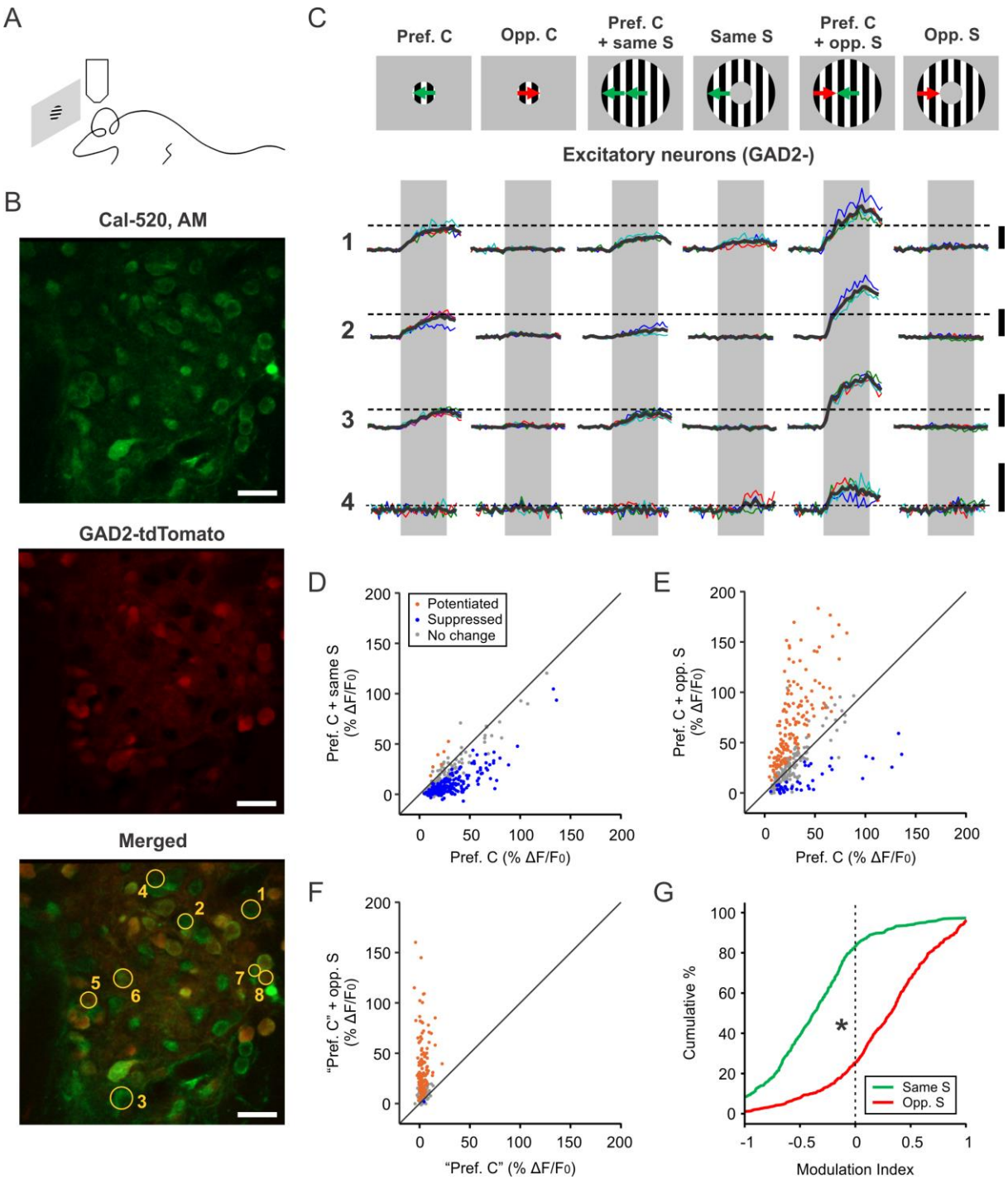

Figure 4.2. Excitatory neurons in the sSGS are bidirectionally modulated by motion direction in the receptive field surround.

(**A**) Two-photon calcium imaging in the mouse sSGS. (**B**) Field of view containing sSGS neurons (at 20 μm below the surface) loaded with Cal-520 (**top**), GAD2^{+} neurons (expressing tdTomato) and GAD2^{-} neurons (**middle**), and a merged image of both channels (**bottom**). Scale bars are 20

μm. (**C**) Calcium signal of 4 GAD2$^-$ neurons in response to six chosen conditions of the center-surround (C-S) stimulus. C, center; S, surround; Pref, preferred; Opp, opposite. The diagrams on top are for illustration purpose only, while the actual preferred directions vary from cell to cell. The numbers on the left represent the neurons circled in **B, bottom**. Neurons 5, 6, 7, and 8 are GAD2$^+$, and their responses are shown in Fig. 4.6A. Thin multicolored traces are individual trials, and thick black traces are the average. All scale bars represent 100% $\Delta F/F_0$. The dotted horizontal lines are aligned to the peak of the black trace in response to the preferred direction at the center. The gray boxes delimit the 2 s period of stimulus presentation. (**D**-**E**) Response comparison for individual center-responsive GAD2$^-$ neurons at the preferred center direction and when the preferred center was coupled with the same-direction surround (**D**), or when coupled with opposite-direction surround (**E**, n = 355 cells, 9 mice). (**F**) Same plot as **E**, but for center-silent neurons. See Results and Methods for the determination of the "preferred center direction" for these neurons (n = 191 cells, 9 mice). (**G**) Modulation index distribution under same-surround (green) and opposite-surround (red) conditions (n = 355+191 = 546, 9 mice). The color scheme used in panels **D**-**F** illustrates the results of a bootstrapping test to determine the significance of the C-S modulation for individual neurons (orange indicates potentiation; blue, suppression; gray, no statistically significant change; See Methods for details).

did not cause any response when presented alone (e.g., Fig. 4.2C). However, when the surround gratings were presented simultaneously with the center stimulus, the response magnitude of sSGS neurons was dramatically altered. First, when both center and surround gratings moved along the preferred direction of a given excitatory neuron, we saw a classical surround-suppression of the center response (Fig. 4.2C-D). In striking contrast, when the preferred direction in the center was coupled with a surround stimulus of opposite direction, most excitatory sSGS neurons increased their responses (Fig. 4.2C-E). In other words, to the same stimulus in their RF center, excitatory sSGS neurons could increase or decrease their response, depending on what is shown in the background.

Interestingly, a substantial population of excitatory sSGS neurons did not respond to the center or the surround gratings when presented separately but became responsive to particular Center-Surround (C-S) combinations (n = 191/811, 23.6%). This was despite the fact that the majority of these cells (154/191, 80.6%) had mappable RFs that were covered by the center patch

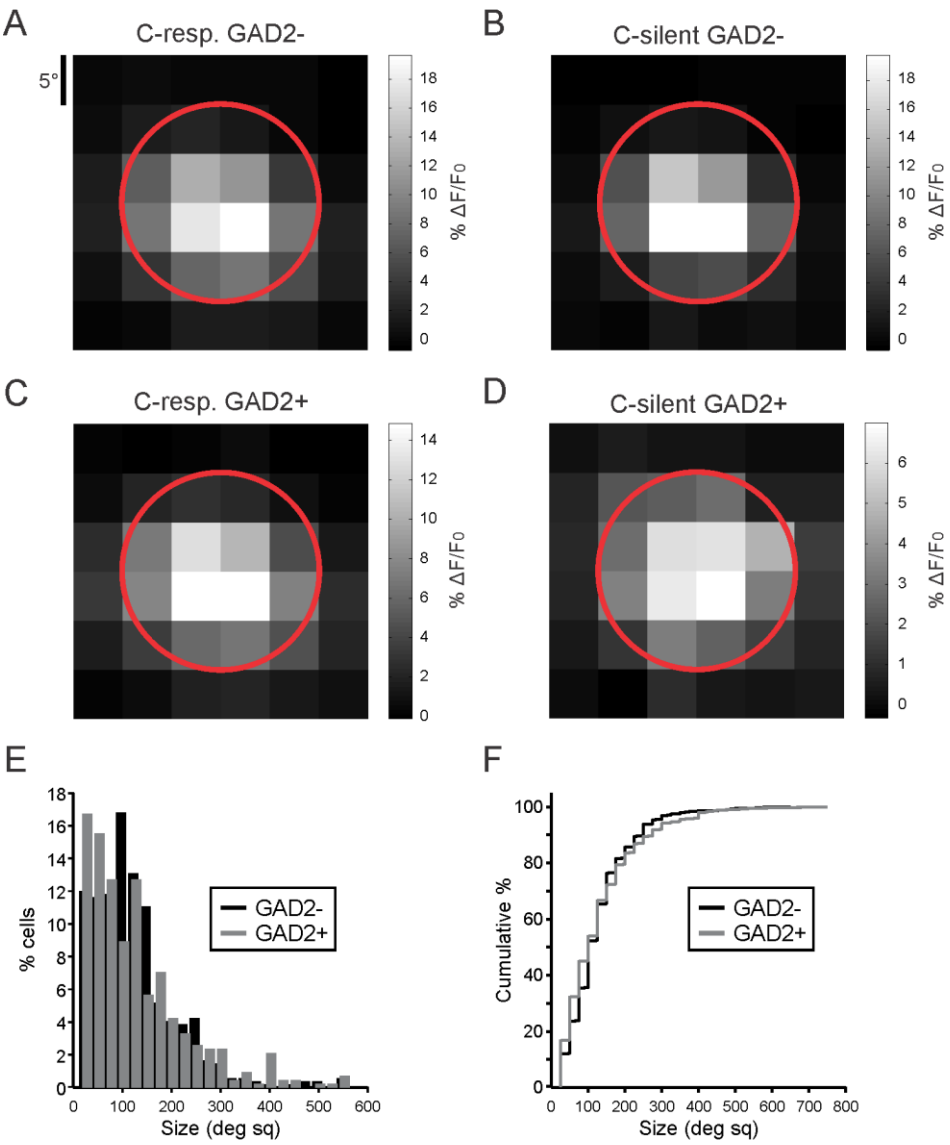

Figure 4.3. Receptive field size of GAD2$^-$ and GAD2$^+$ neurons in the sSGS. (**A**) Average responses evoked by flashing black squares of GAD2$^-$ neurons that were responsive to the center drifting gratings stimulus ("C-resp.", n = 355, 9 mice). The red circle represents the extent of spatial coverage by the center gratings stimulus, which also applies to panels **B**-**D**. (**B**) Average responses of GAD2$^-$ neurons that were silent to the separate presentations of center and surround but responded to a C-S combination ("C-silent", n = 191, 9 mice). (**C**) Average responses of GAD2$^+$ neurons that were responsive to the center drifting gratings stimulus (n = 379, 9 mice). (**D**) Average responses of GAD2$^-$ neurons that were silent to the separate presentations of center and surround but responded to a C-S combination (n = 85, 9 mice). (**E**) Histogram of the receptive field size of GAD2$^-$ (black) and GAD2$^+$ (gray) cells that were responsive to the flashing square stimulus (n = 542 GAD2$^-$; n = 425 GAD2$^+$). (**F**) Cumulative distributions of the same data in **E** (p = 0.19, Mann-Whitney *U*-test).

(Fig. 4.3B). We assigned the "preferred direction" for these "center-silent" neurons as the center direction of their preferred center-surround (C-S) stimulus. When this "preferred direction" in the center was coupled with the opposite direction surround, an emergent response was observed in

those cells (e.g., cell 4 in Fig. 4.2C, and Fig. 4.2F).

To quantify the effect of the modulating surround, we calculated a "modulation index" for each neuron to compare its response to center stimulus alone at the preferred direction with that to the same center coupled with a particular surround. The index ranged between -1 and 1 where negative values represented decreases in response and positive values represented increases. Over the entire population of these excitatory sSGS cells (n = 355 "center responsive" + 191 "center silent" = 546), the response to the center stimulus became smaller with the introduction of the same direction surround in 83.3% of cells (n = 455/546), and larger in 74.7% of cells (n = 408/546) when the surround was moving in the opposite direction (Fig. 4.2G, Kolmogorov Smirnov [KS] test, p = 3.96e-83, KS stat = 0.5861).

sSGS excitatory neurons encode motion contrast

The above results demonstrate that excitatory neurons in the sSGS detect motion saliency by virtue of their sensitivity to the difference in direction between the RF center and surround. To study how sSGS neurons are tuned to this form of motion contrast, we systematically and independently varied the direction of the center and surround of the C-S gratings. Specifically, our stimulus set consisted of 81 C-S combinations (Fig. 4.4A; 8 directions and 1 blank for both center and surround).

We shifted the 81 condition response matrix of all excitatory cells that responded to center gratings (n = 355) in order to align their preferred directions. These shifted responses were then averaged and illustrated in a heat map (Fig. 4.4A). As expected, these neurons were DS in response to the center grating alone, showing greater responses to the preferred directions than to the

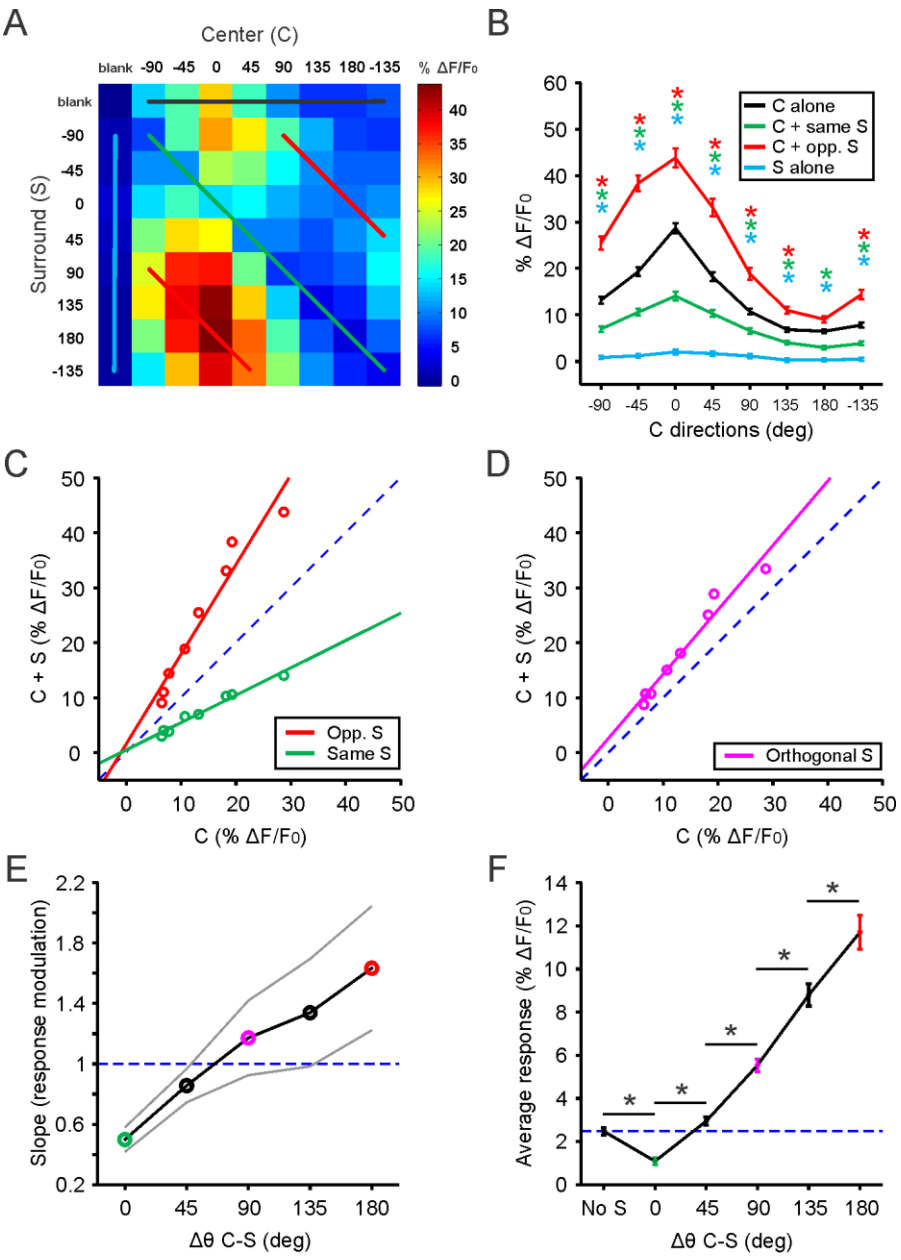

Figure 4.4. GAD2$^-$ neurons in the sSGS encode motion contrast. (**A**) Aligned and averaged response matrix of center-responsive GAD2$^-$ neurons to all 81 combinations of the C-S stimulus (n = 355 cells, 9 mice). The color scale to the right represents the response magnitude in % $\Delta F/F_0$. (**B**) Aligned and averaged population tuning curves for these neurons under particular C-S combinations. The x-axis represents the direction of the center stimulus relative to the preferred direction at 0 deg. The different colored curves represent the relationship of the surround to the center, corresponding to the same colored lines in **A**. All data points are compared statistically to their corresponding points in the black tuning curve. (**C**) Geometric modulation of the center tuning curve by the 2 different surrounds in **B**; same surround induced divisive suppression (green, slope = 0.50, y-intercept = 0.48, $R^2 = 0.97$), and opposite surround induced multiplicative potentiation (red, slope = 1.63, y-intercept=1.55, $R^2 = 0.94$). (**D**) Multiplicative potentiation of the center tuning curve by orthogonal-direction surrounds (slope = 1.17, y-intercept = 2.54, $R^2 = 0.96$). The dashed blued lines in **C** and **D** are lines of identity. (**E**) The slopes of modulation illustrated in (**C-D**, corresponding colors) as well as the intermediate conditions vs. C-S direction difference (gray lines delimit the 95% confidence interval). The dashed blued line indicates a slope of 1, i.e., no modulation. (**F**) Mean averaged responses ($\Delta F/F_0$) of center-silent GAD2- neurons vs. C-S direction difference (n = 191 cells, 9 mice). The dashed blue line is averaged "response" to center alone. Data in **B** and **F** are presented as mean ± s.e.m. *: $p < 0.05$, Mann-Whitney *U*-test.

opposite direction (the top row in Fig. 4.4A and the black trace in Fig. 4.4B). Furthermore, surround suppression was seen for all directions of the center stimulus when the surround gratings were moving in the same direction as the center (green traces in Fig. 4.4A-B). Similarly, the potentiation by opposite surround was also seen for all directions of the center stimulus (red traces in Fig. 4.4A-B).

Interestingly, this modulation was geometric in nature, ranging from a divisive suppression by the same surround to a multiplicative potentiation by the opposite surround (Fig. 4.4C). In fact, a linear modulation of the center responses was also seen with intermediate differences between C-S directions (e.g., Fig. 4.4D). We thus calculated the slope of these linear relationships (i.e., fold changes of center responses by the surround), and found that it gradually increased with the C-S direction difference (Fig. 4.4E). In other words, excitatory sSGS neurons are monotonically tuned to motion contrast, showing maximal responses to the most salient stimulus with oppositely-moving center and surround. While these slopes were calculated for the population response, the same principle held true when they were calculated for individual neurons before being averaged (Fig. 4.5A), despite some variability in the goodness of fit (Fig. 4.5B-C).

We performed a similar analysis for the center-silent neurons (n = 191), by averaging their fluorescent changes to individual C-S direction differences. An emergent, and again monotonically increasing, response was seen as the C-S direction difference increased (Fig. 4.4F). These cells thus display similar tuning to direction contrast as their center-responsive neighbors.

We noted that although excitatory sSGS neurons as a population were maximally active when the center and surround drifted in opposite directions, this was not always the case for individual neurons. Nonetheless, for the vast majority of cells, the center direction of the most

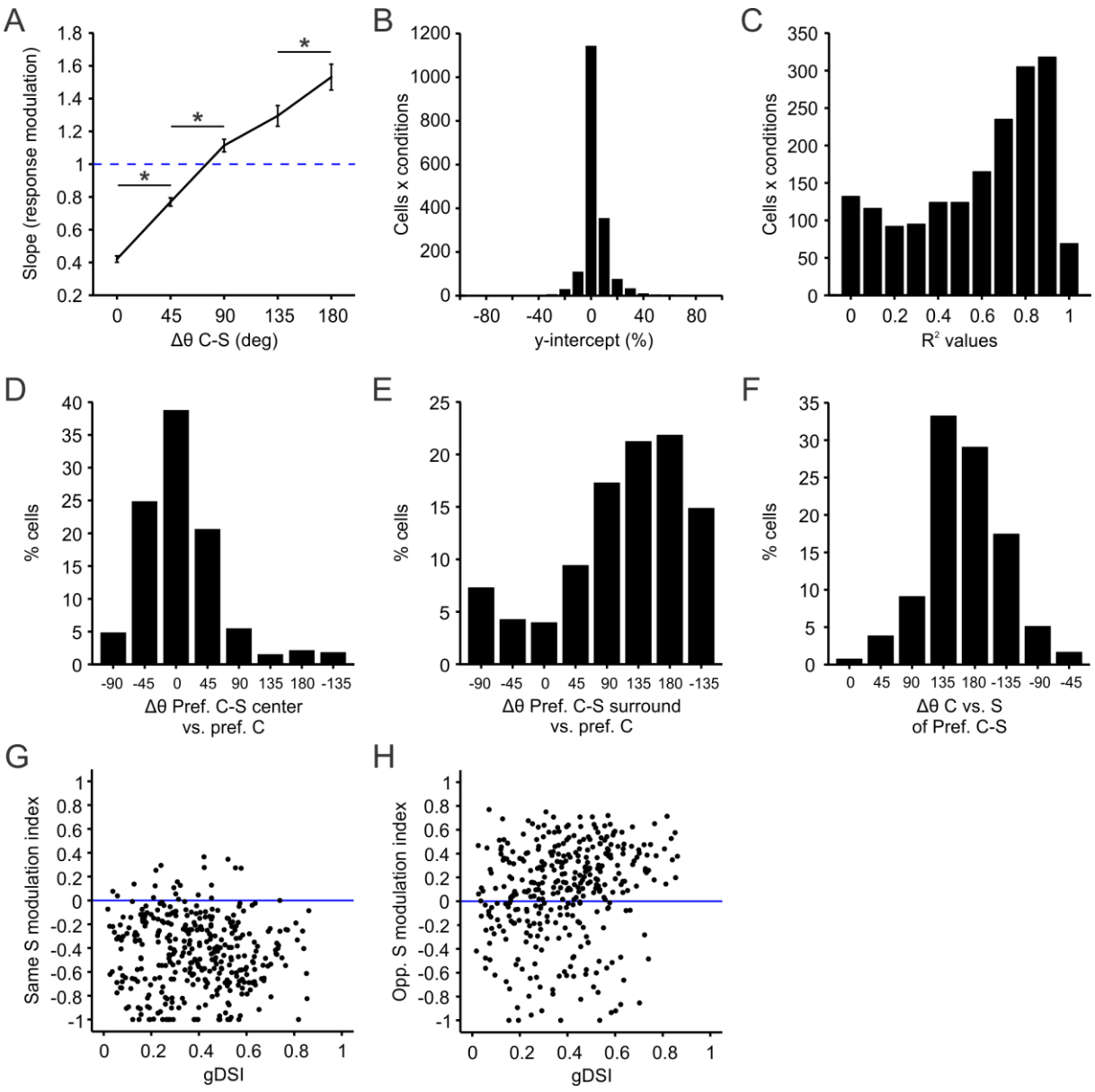

Figure 4.5. Center-surround ("C-S") interactions in GAD2$^-$ neurons.
(**A-C**) Analysis of motion contrast encoding for individual center-responsive GAD2- cells (n = 355, 9 mice). For each cell, its response to a particular C-S difference was fitted to a first degree polynomial against its response to the corresponding center gratings alone. The fitted slope was averaged over all cells and plotted against the C-S difference in **A** (mean ± s.e.m, *: $p < 0.01$, Mann-Whitney U-test). The dashed blue line indicates a slope of 1, i.e., no modulation. (**B**) Distribution of the y-intercept of the fit for all cells, at all C-S combinations. (**C**) Distribution of the R^2 value. (**D-F**) Analysis involving the C-S combination that evoked the maximum responses in individual GAD2$^-$ cells ("Pref. C-S"). The difference between the center direction of the Pref. C-S and the preferred direction of each cell was determined and plotted in a distribution in **D**; and the difference between the surround direction of the Pref. C-S and the cell's preferred direction

was plotted in **E**. Only center-responsive GAD2$^-$ neurons were included (n = 355, 9 mice), and cells were excluded from this analysis if their peak response occurred to center alone or surround alone stimuli (n = 25). The distribution of the angle difference between the center and surround directions of the Pref. C-S is plotted in **F**. This included all responsive GAD2$^-$ cells unless their maximum response was to center or surround alone (n = 551 cells). (**G-H**) Relationship between the modulation index and gDSI for center-responsive GAD2$^-$ neurons under same-direction surround (**G**, r = -0.05, p = 0.33) and opposite-direction surround (**H**, r = 0.20 p = 1.03e-04).

effective C-S stimulus either matched the cell's preferred direction or was within 45°of it (Fig. 4.5D), the smallest tested difference in stimulus direction. Moreover, the surround of this C-S combination was usually clustered around the cell's null direction, and away from its preferred one (Fig. 4.5E), consistent with the monotonic tuning at the population level. Finally, when we simply calculated the C-S angle difference of their most effective C-S stimulus, we found that this difference clustered around 180° for the majority of cells (Fig. 4.5F), cementing their role as motion contrast encoders.

Inhibitory neurons in the sSGS are suppressed by motion contrast

Next, we analyzed how inhibitory sSGS neurons (GAD2$^+$) responded to C-S direction contrast. Just like excitatory neurons, inhibitory neurons also experienced surround suppression when the surround direction matched the direction in the RF center (Fig. 4.6A-B). They were, however, significantly less suppressed than their excitatory counterparts (Fig. 4.7C, KS test, p = 1.73e-19, KS stat = 0.3106). Furthermore, when the surround grating was moving in the opposite direction, the inhibitory neurons' response to the preferred center stimulus was quite strongly suppressed (Fig. 4.6A and C). This is in stark contrast with the potentiation seen in excitatory sSGS neurons under the same conditions (Fig. 4.7D, KS test, p = 6.09e-77, KS stat = 0.6222). In fact, the suppression by the opposite surround was even greater than that by the same-direction surround

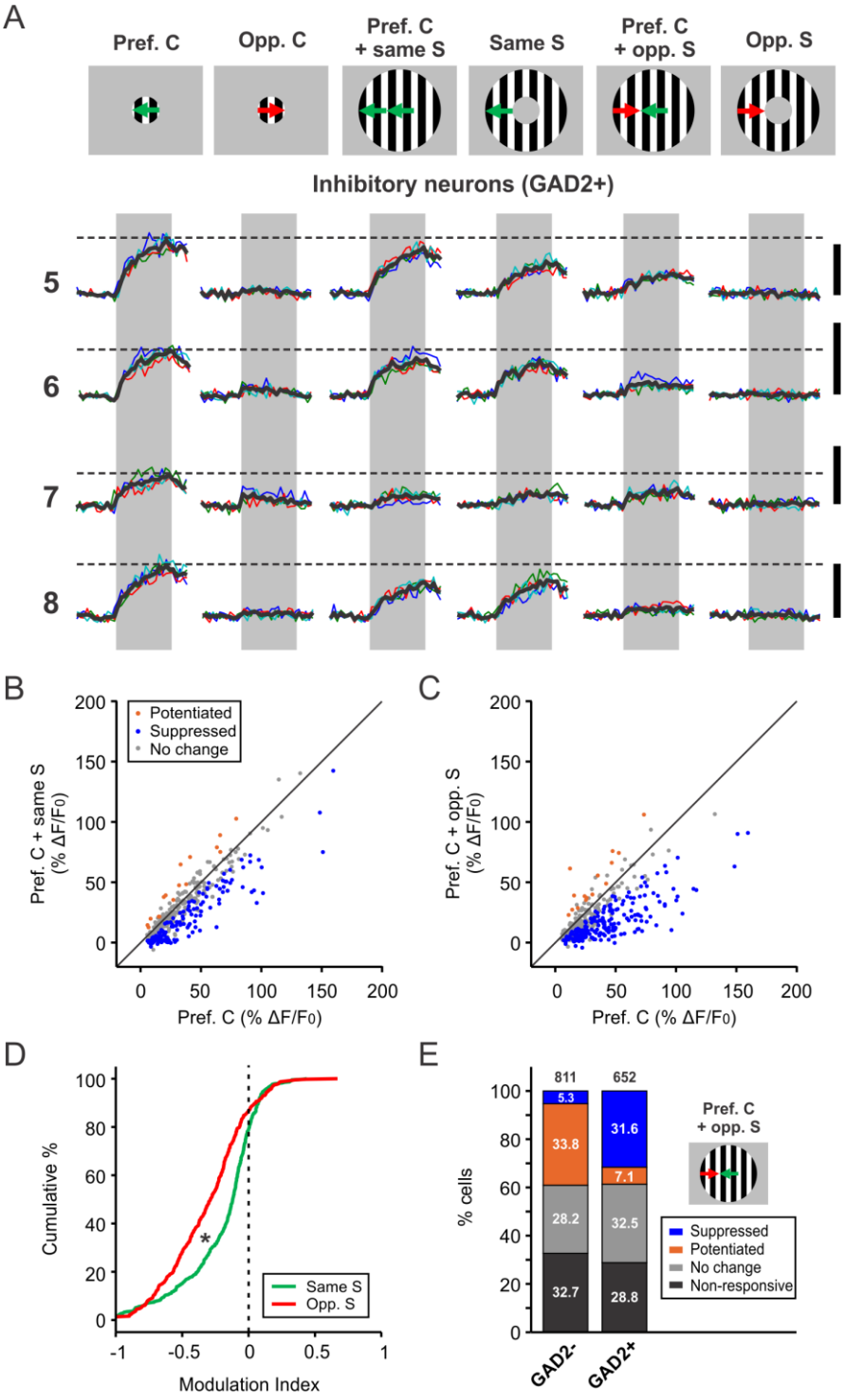

Figure 4.6. Inhibitory neurons in the sSGS are suppressed by motion contrast.
(**A**) Same as in Fig. 4.2C, for 4 inhibitory neurons, with numbers on the left representing the neurons circled in Fig. 4.2B, bottom. (**B-C**) Response comparison for individual center-responsive GAD2$^+$ neurons to the preferred center direction and when the preferred center was coupled with same-direction surround (**B**), or opposite-direction surround (**C**, n = 379, 9 mice). The color scheme follows that in Fig. 4.2D-F. (**D**) Modulation index distribution for the neurons in panels **B-C** under same-surround (green) and opposite-surround (red) conditions. (**E**) Percentages of GAD2$^-$ and GAD2$^+$ neurons in 4 response categories (determined by a bootstrapping test) to the presentation of the preferred center + opposite surround combination: non-responsive, non-modulated, potentiated, and suppressed. Values in the boxes represent the percentages of neurons in each category; numbers at the top represent the total numbers of neurons in the study. The "non-responsive" category included neurons that did not respond to any of the C-S conditions and a small population of neurons that responded to the surround alone, but not the center stimulus.

for most inhibitory cells (Fig. 4.7E and Fig. 4.6D, KS test, p = 1.53e-13, KS stat = 0.2797), as well as at the population level (compare green and red curves in Fig. 4.7A-B).

In addition to calculating a modulation index, we also used a bootstrapping test to determine statistical significance for individual neurons when comparing their response to C-S combinations with that to the center stimulus alone (see Methods for details). Consistently, using this method, we found that a much larger proportion of excitatory sSGS neurons was significantly potentiated by the opposite-direction surround (n = 274 out of 546 responsive cells, 50.2%), compared to inhibitory neurons (n = 46 out of 464, 9.9%; Fig. 4.6E).

Finally, and quite surprisingly, many center-responsive inhibitory neurons (204/379, 53.8%) could still be activated by a surround-alone stimulus moving in their preferred direction (Fig. 4.6A and Fig. 4.7B, blue curve), something we rarely observed in excitatory neurons. This was despite the fact that excitatory and inhibitory neurons had similar RF sizes when mapped with flashing squares (Fig. 4.3, p = 0.19, Mann-Whitney *U*-test, n = 542 $GAD2^-$ and 425 $GAD2^+$ neurons responsive to flashing squares). It is possible that flashing squares might not provide enough drive to activate inhibitory neurons away from the center, leading to an underestimation of their effective RF size. Drifting gratings, on the other hand, could provide that drive, thereby revealing a potential difference between the RF properties of excitatory and inhibitory neurons in the sSGS. This is consistent with the observation that inhibitory neurons are less susceptible to surround suppression than their excitatory counterparts.

Together, these results demonstrate that sSGS excitatory and inhibitory neurons have different RF properties and are differentially modulated by motion contrast. The striking difference between the polarities of their modulations by the opposite-direction surround suggests a possible

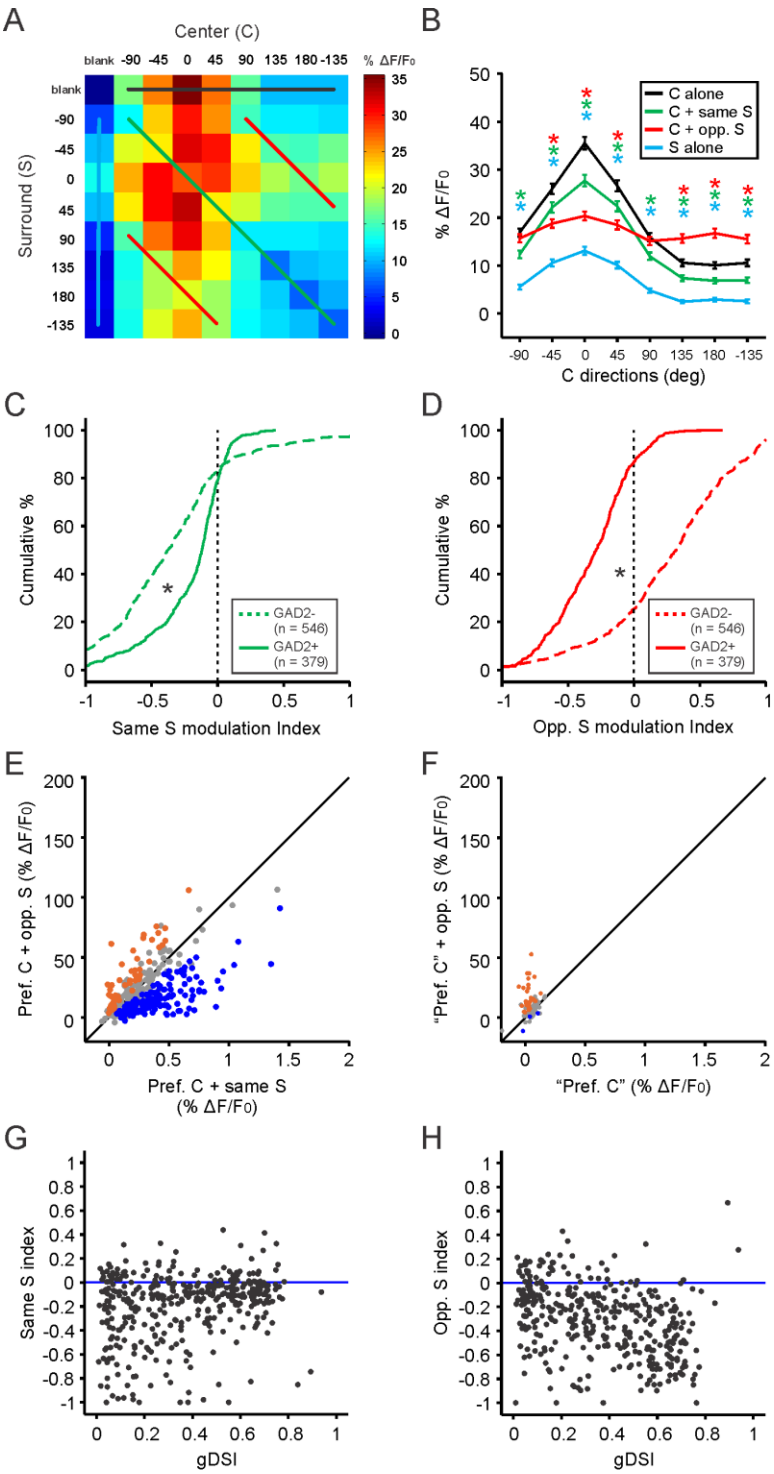

Figure 4.7. Center-surround interactions in GAD2$^+$ neurons. (**A**) Aligned and averaged response matrix of center-responsive GAD2$^+$ neurons to all 81 combinations of C-S stimulus (n = 379 cells, 9 mice). The color scale to the right represents the response magnitude in % $\Delta F/F_0$. (**B**) Aligned and averaged population tuning curves for these neurons under particular C-S combinations. The x-axis represents the direction of the center stimulus relative to the preferred direction at 0 deg. The different colored curves represent the relationship of the surround to the center, corresponding to the same colored lines in **A**. (**C-D**) The cumulative distributions from Fig. 4.2G and Fig. 4.6D, grouped in order to highlight the differences in modulation between GAD2$^-$ and GAD2$^+$ neurons by the same-direction surround (**C**), and by the opposite-direction surround (**D**). (**E**) Comparing center + opposite surround and center + same surround responses of center-responsive GAD2$^+$ neurons (n = 379 cells, 9 mice, y-axis of fig. 4.6C vs. y-axis of fig. 4.6B). (**F**) Response comparison for GAD2$^+$ neurons that were silent to the separate presentations of center and surround but responded to a C-S combination, at the "preferred center" and when coupled with the opposite-direction surround. See Methods for the determination of the "preferred center" for those neurons (n = 85 cells, 9 mice). Color scheme in **E** and **F** is the same as in Fig. 4.6B. (**G-H**) Relationship between the modulation index and gDSI for center-responsive GAD2$^+$ neurons (n = 379 cells, 9 mice) under same-direction surround (**G**, r = 0.24, p = 1.45e-06), and under opposite-direction surround (**H**, r = -0.35 p = 1.99e-12).

role of the local inhibitory circuit in mediating the potentiation of excitatory neurons (see Discussion).

Depth-dependent motion contrast coding in the SGS

Studies in a number of species have shown that the visual layers of the SC or optic tectum can be further divided into sub-laminae (May, 2006). Indeed, based on a small number of single unit recordings, we recently found that direction selectivity in the mouse SGS declines with depth (Inayat et al., 2015). We thus assessed the depth profile of motion contrast response and its relationship with direction selectivity. We were limited in our imaging depth when using calcium indicators that disperse throughout the cell body and processes, due to the strong neuropil signal in the deeper SGS. To overcome this limitation, we used a genetically-encoded calcium indicator (AAV-H2B-GCaMP6s) that was largely restricted to the cell nucleus (Fig. 4.8A). This led to a substantial reduction of the neuropil signal in the deeper layers of the SGS, and allowed us to confidently image down to depths of around 200 μm. We characterized the performance of this indicator by performing simultaneous two-photon imaging and cell-attached recording in order to correlate the fluorescent signal with spiking activity. Although the "nuclear" GCaMP6s was significantly slower than Cal-520 and could not resolve single spike activity (Fig. 4.1A-C), it was able to reliably report the tuning of SGS neurons to the C-S stimuli (Fig. 4.1D-E and Fig. 4.9).

We first quantified SGS neurons' direction selectivity in response to the center gratings. Largely consistent with the results using Cal-520, the very superficial SGS lamina was enriched with highly DS cells, including both excitatory and inhibitory neurons (black curves in Fig. 4.8B and D, respectively; 110/125, 88.0% of $GAD2^-$ and 115/146, 78.8% of $GAD2^+$ neurons had

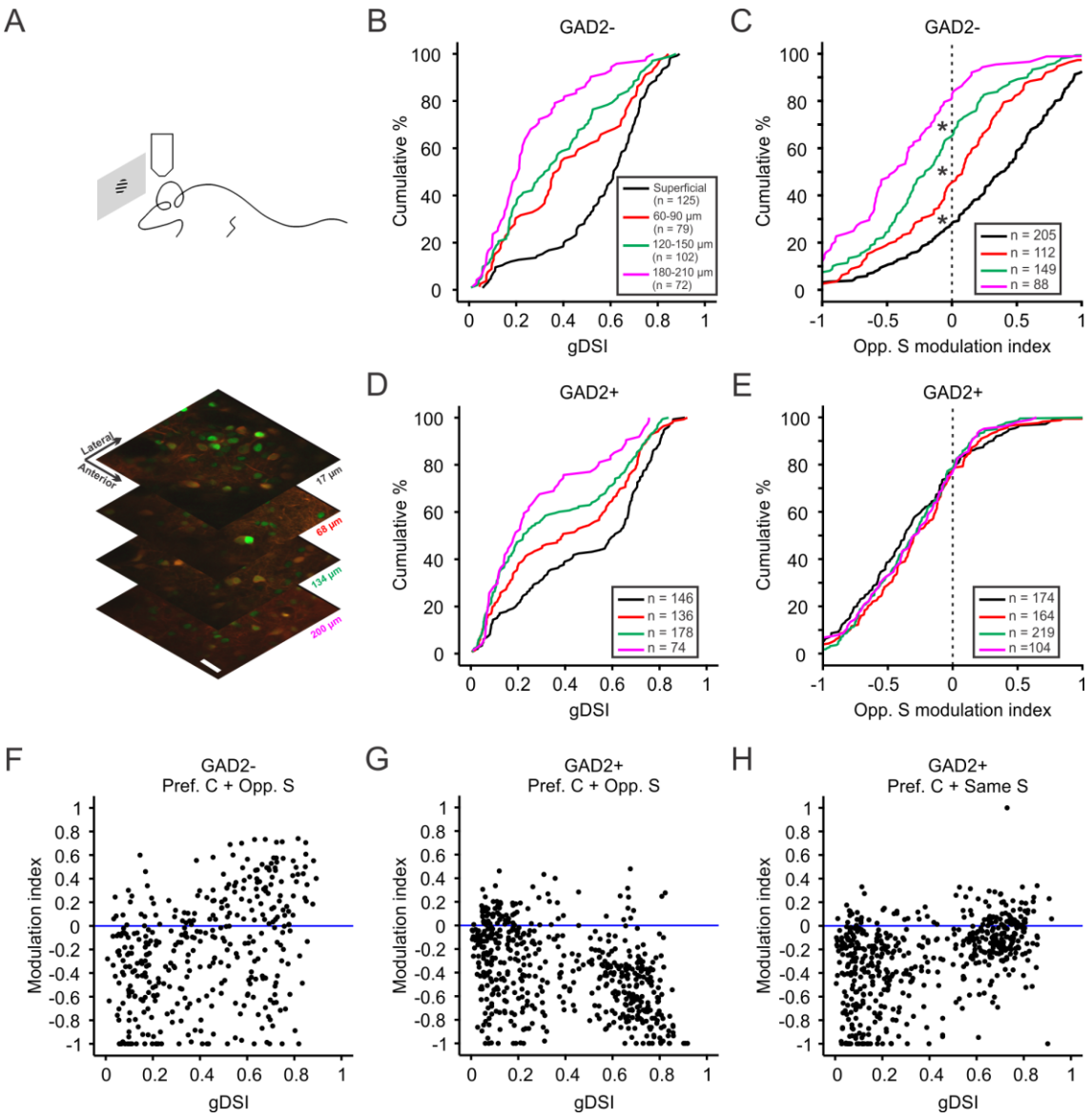

Figure 4.8. Motion contrast sensitivity declines with depth in the SGS.
(**A**) Two-photon calcium imaging at different depths of the SGS, using AAV-H2B-GCaMP6s. Shown are neurons expressing H2B-GCaMP6s at 4 different depths in the SGS of a GAD2^{-} tdTomato mouse. Scale bar is 20 µm. (**B**) Cumulative distribution of gDSI divided into four depth categories for center-responsive GAD2^{-} neurons (n = 378, 10 mice). The same depth color code applies to panels **B-E**. (**C**) Cumulative distribution of the opposite-surround modulation index for center-responsive and center-silent GAD2^{-} neurons (n = 378+176 = 554, 10 mice). (**D-E**) Same as in (**B-C**), but for GAD2^{+} neurons (n = 534 in **D**; and n = 534+127 = 661 in **E**, 10 mice). (**F-G**) Relationship between the opposite-surround modulation index and gDSI for center-responsive GAD2^{-} neurons (**F**, n = 378, 10 mice) and GAD2^{+} neurons (**G**, n = 534, 10 mice) at all depths combined. (**H**) Relationship between the same-surround modulation index and gDSI for the same cells in **G**.

gDSI>0.2). The degree of direction selectivity declined with depth in the SGS, confirming our previous single unit results. Importantly, the decline was observed for both excitatory (Fig. 4.8B, KS test, p = 1.72e-16, KS stat = 0.6237, between the most superficial (black) and deepest (magenta) cell populations) and inhibitory neurons (Fig. 4.8D, KS test, p = 4.63e-07, KS stat = 0.3869).

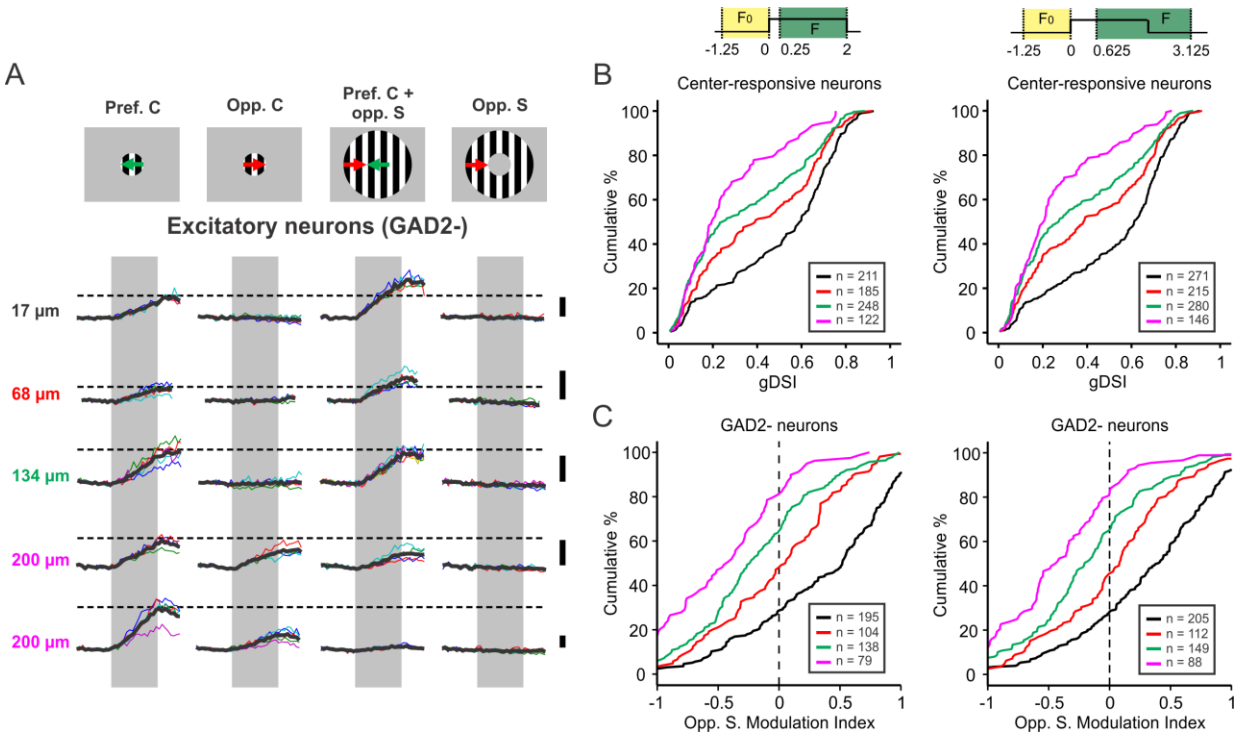

Figure 4.9. Varying the time window of H2B-GCaMP6s signal analysis does not impact the main findings.
(**A**) Calcium signal of 5 GAD2$^-$ neurons in response to 4 chosen conditions of C-S stimulus. The depth of each neuron in the SGS is specified to the left. Figure conventions are the same as in Fig. 4.2C and 4.6A. (**B**) Comparison in the distribution of the gDSI using two different $\Delta F/F_0$ calculation methods, showing very similar trends. The $\Delta F/F_0$ calculation methods are described at the top and apply to the corresponding panels in both **B** and **C** below. (**C**) The distribution of the modulation index of GAD2$^-$ cells by the opposite surround is also preserved under those two $\Delta F/F_0$ calculation methods. The depth color code in panels **B** and **C** is the same as in Fig. 4.8B-E.

We then examined the depth profile of the modulation by the oppositely-moving surround. The potentiation of response in excitatory neurons that we observed in the sSGS using Cal-520 was replicated with nuclear GCaMP6s. Interestingly, this potentiation gradually turned into suppression with depth (Fig. 4.8C, KS test, $p < 0.01$ between the 4 depths). In the case of inhibitory neurons, no significant change was seen in the modulation index with depth, as the cells remained equally suppressed by the opposite surround (Fig. 4.8E, KS test, $p > 0.05$ between the 4 depths). The concurrent decline in excitatory cells' gDSI and modulation index with depth suggested a potential correlation between these properties. Indeed, a significant, albeit noisy, correlation was seen between the two variables for excitatory neurons (Fig. 4.8F, $r = 0.38$, $p = 1.34e-14$), where highly DS neurons tend to be potentiated by the opposite surround, while the non-selective ones tend to be suppressed. In contrast, we observed a negative correlation for inhibitory neurons between the modulation index and gDSI (Fig. 4.8G, $r = -0.42$, $p = 4.20e-24$), where the highly DS cells were much more suppressed by the opposite surround. Interestingly, a positive correlation was seen between the modulation index and gDSI for inhibitory neurons when the same surround was presented (Fig. 4.8H, $r = 0.43$, $p = 8.08e-26$). Correlations of the same polarities were also observed for the sSGS excitatory and inhibitory neurons that were imaged with Cal-520 (Fig. 4.5G-H and Fig. 4.7G-H). The difference between excitatory and inhibitory cells in these correlations is again suggestive of a possible role for inhibition in motion contrast encoding.

Discussion

In this study, we determined how neurons in the mouse SGS encode motion contrast between their RF center and surround. The responses of superficial excitatory neurons are bidirectionally modulated, increasing monotonically as a function of the direction difference between the center and surround, from suppression by the same-direction surround to maximal potentiation by an oppositely-moving surround. Such response profiles are likely important for the animal to detect object motion in the environment and distinguish it from self-induced full-field motion in the background. Interestingly, the degree of potentiation declined with depth in the SGS, along with direction selectivity, suggesting a likely specialization of the most superficial lamina of the SGS in motion processing. Inhibitory neurons, on the other hand, are always suppressed by the surround stimuli, although different levels of suppression were observed. This striking difference in the response profile of excitatory and inhibitory neurons suggests the involvement of local inhibitory circuits in the SGS in the emergence of bidirectional motion contrast coding.

Saliency computation and representation

Current theories postulate that visual saliency is analyzed separately by feature-specific channels, which are then combined into a feature-agnostic saliency map (Veale et al., 2017). A classic example of feature-specific saliency computation takes place in V1. Being orientation selective, V1 neurons modulate their responses depending on the orientation difference between the RF and its surround. In primate and cat V1, lower levels of suppression, or even facilitation, could occur when cross-oriented stimuli were shown in the surround (Jones et al., 2001; Jones et al., 2002; Kastner et al., 1999; Knierim and van Essen, 1992; Nothdurft et al., 1999; Sengpiel et al., 1997;

Sillito et al., 1995). More recent studies have shown similar findings in mouse V1, where responses were suppressed by an iso-oriented surround, but experienced an attenuation of suppression to a cross-oriented surround (Self et al., 2014). This type of differential neuronal activity might help the animal distinguish between self-induced motion in the visual scene, manifested as full-field motion, and actual object motion in the RF. Indeed, a similar role has been proposed for a population of neurons in mouse V1, under awake and running conditions (Keller et al., 2012; Zmarz and Keller, 2016). Importantly, mouse studies have allowed researchers to explore the circuit mechanisms underlying surround suppression in more detail. With the available genetic toolkit in this species, the specific contributions of different types of cortical inhibitory neurons to surround-suppression are now being elucidated (Adesnik et al., 2012; Nienborg et al., 2013).

In lower vertebrate where neocortex has not evolved, the SC homologue optic tectum is the main visual center for signal processing, including saliency analysis. Tectal neurons in these species are usually motion sensitive and selective for movement direction. In barn owls, tectal neurons are differentially suppressed depending on the motion direction in the surround (Zahar et al., 2012). In the pigeon tectum, a potentiating effect could be elicited under conditions of center-surround motion-opponency (Frost et al., 1981; Sun et al., 2002). Additionally, studies in the archer fish showed that their tectal neurons exhibited contextual modulation which might underlie pop out in a visual search paradigm (Ben-Tov et al., 2015).

In the primate SC, very few visual neurons are tuned to specific features such as direction or orientation. The SC is therefore thought to be the locus of integration of feature-specific cortical inputs into a feature-agnostic saliency map (Veale et al., 2017), where neurons would respond indiscriminately to any feature contrast between the RF center and the surround. In contrast,

neurons in the mouse SGS are mostly tuned to particular visual features such as motion direction. We demonstrate here that these neurons in fact perform feature-specific saliency computations by encoding direction contrast in a monotonic and bidirectional fashion. Interestingly, this computation is cell-type specific and more prominent in the very superficial SGS. Direction selectivity is lost in the deeper laminae of the SGS, and the intermediate layers of the mouse SC are multisensory integrators (Cang and Feldheim, 2013; Inayat et al., 2015). It is therefore possible that the transformation from feature-specific saliency analysis to feature–agnostic saliency map, or even more generally to a modality–agnostic saliency map, takes place between the deep SGS and the intermediate layers of the SC. Our results thus significantly expand on past findings of contextual modulation in the tectum as well as the SC in cats and rats (Girman and Lund, 2007; Sterling and Wickelgren, 1969). Importantly, the comparison of SC response properties across vertebrate species, including our current findings, supports the idea of a gradual evolutionary migration of saliency computation from a single locus in the SC/OT to a multi-structural process that involves cortical inputs (Zhaoping, 2016).

Mechanisms for motion contrast computation in the mouse SGS

One of the main reasons for studying saliency computation in mice is that we can monitor the activity of specific cell types using modern genetic and imaging techniques. Here we show that SGS excitatory and inhibitory neurons respond differently to the same motion contrast stimuli, an important finding that has not been shown in any other species. The inhibitory circuits in the rodent SGS have only been studied in the context of classical surround suppression, using stimulus size tuning as a measure of modulation, while avoiding stimuli with feature contrast between center

and surround (Binns and Salt, 1997; Kasai and Isa, 2016). These studies are also hindered by the lack of cell-type specific driver lines that allow a functional dissection of inhibitory neuron subtypes, as had been routinely done in the cortex. Presently, all inhibitory neurons in the SGS are lumped under one category without distinction between locally connecting neurons and long range projecting ones (Endo et al., 2003; Mize, 1992). A recent two-photon imaging study in the mouse SGS using a two-point visual stimulus to probe surround-suppression showed that the activity of local inhibitory and excitatory neurons is equally suppressed by the surround. This implicates long range inhibitory inputs in mediating the phenomenon (Kasai and Isa, 2016). In our current study, however, we observe interesting differences in the responses of excitatory and inhibitory neurons to the presentation of different sizes of drifting gratings. Inhibitory neurons are less susceptible to surround suppression, especially when they are direction selective (Fig. 4.8H). These neurons can nonetheless be much more suppressed by a surround moving in the opposite direction (Fig. 4.8G), potentially contributing to the increased responses in excitatory neurons.

In addition, input from other brain areas could also contribute to the direction-contrast dependent modulation of SGS activity. The SGS receives direct inputs from both retina and visual cortex, in addition to a few other structures (May, 2006). Visual cortex was removed in our experiments, ruling out its involvement. Retinal inputs, on the other hand, were shown to be the source of direction selectivity in the SGS (Shi et al., 2017) and could provide contextually-modulated input. Surround-modulated suppression was observed under several motion-contrast regimes (spatial phase, spatial frequency, and velocity) in direction-selective retinal ganglion cells in rabbits (Chiao and Masland, 2003). Importantly, no potentiation was observed under those conditions (but see (Girman and Lund, 2010), for orientation-dependent response potentiation in

rat retina). This makes it unlikely that this phenomenon is completely inherited from the retina. Additionally, the fact that excitatory and inhibitory neurons in the sSGS, both of which receive direct retinal input, exhibit strikingly different responses to center-surround stimuli argues for a role of intracollicular circuit mechanisms. Nonetheless, the differentially-suppressed retinal inputs could still be a critical component for saliency computation through the primed SGS circuit described above. In other words, an interplay between a differential withdrawal of feedforward retinal excitation and a differential capacity of intracollicular circuits for inhibition would lead to an altered excitation/inhibition balance under different surround conditions, which accounts for the bidirectional motion contrast encoding in the SGS.

In conclusion, our study identifies response correlates of motion saliency in the mouse SGS. The striking distinction between the responses of excitatory and inhibitory neurons to motion contrast in this structure makes it a strong candidate to be a locus of saliency computation. This opens the door for future mechanistic studies that, under awake behaving conditions, manipulate local inhibitory circuits in the SGS and examine the cellular and behavioral consequences. Our findings thus offer a unique opportunity to describe a circuit-level mechanism of saliency in the brain.

Notes on CHAPTER 4

I thank Dr. Loren Looger and Dr. Na Ji from the Janelia Research Campus for providing H2B-GCaMP6s. I also thank Dr. Xuefeng Shi for helping with the cell-attached recordings, and Dr. Hui Chen for his help with data analysis.

A version of this chapter is currently under review at a scientific journal.

CHAPTER 5

Discussion

In this thesis, I explored standing questions about the organization and function of the superficial layers of the mouse superior colliculus (SC). Specifically, I addressed questions related to functional organization (chapter 2), origin of response properties (chapter 3), and the potential role of local circuits in transforming sensory inputs in that brain structure (chapter 4). In this section, I discuss my contributions to those topics, and attempt to situate my findings within a broader context provided by the available literature. Additionally, I raise some new questions and challenges brought about by those findings that would hopefully inspire further exploration.

Functional Architectures: Dedicated Local and Global Circuits

In chapter 2 of this thesis, I showed that neurons in the *stratum griseum superficiale* (SGS) of the mouse SC can be organized in a depth-specific manner according to the degree of their direction selectivity (DS). Using two-photon calcium imaging, I identified a previously poorly characterized lamina of the mouse SGS, the superficial SGS (sSGS), where both excitatory and inhibitory

neurons are highly DS. I've also shown, using single unit extracellular recordings, that the degree of DS in the SGS gradually declines with depth.

This proposed cytoarchitecture is in agreement with anatomical data showing a preferential projection of direction selective ganglion cells (DSGCs) to the upper SGS (uSGS), in contrast with the more deeply projecting non-DSGCs (Huberman et al., 2008; Huberman et al., 2009). This projection pattern, however, is more nuanced, as some non-DSGCs can still project to the superficial layers, like the untuned but motion-sensitive W3 retinal ganglion cells (RGCs) (Kim et al., 2010). Moreover, the extensive vertical dendritic arborization of the different cells types in the SGS well beyond the location of their cell body meant that they could receive different types of retinal inputs. Any potential functional architecture in the SGS therefore warranted to be directly demonstrated, rather than indirectly inferred from retinal projections.

The concentration of DS neurons in the sSGS draws an interesting comparison with the relative distribution of orientation and direction selective neurons in the mouse dorsal lateral geniculate nucleus (dLGN) of the thalamus. Although less prevalent in the dLGN than in the SC, tuned neurons can predominantly be found in the dorsal ("shell") and posterior regions of the dLGN (Marshel et al., 2012; Piscopo et al., 2013). Interestingly, those are the regions that DSGCs tend to innervate. Indeed, using viral trans-synaptic tracing, a dedicated circuit has been described in mice which connects DSGCs in the retina to layer 1 of V1 through the shell region of the dLGN (Cruz-Martin et al., 2014). This circuit relays direction selective responses to the cortex, in parallel to the more canonical retino-geniculo-cortical pathway, which connects non-DSGCs to layer 4 of V1 through the deeper core region of the dLGN. It is unclear whether or not orientation selective (OS) RGCs are part of this dedicated circuit, but a theoretical model foregoes the need for these

cells in establishing OS responses in the dLGN, and attributes these responses to random connectivity that occasionally combines inputs from DSGCs preferring opposite directions of motion (Marshel et al., 2012). However, the subsequent demonstration of OS responses in the mouse retina (Zhao et al., 2013), and the genetic isolation of different types of OS RGCs (Nath and Schwartz, 2016) now challenge that model.

It's been recently demonstrated that the SGS projects to the shell of the dLGN to "plug into" this specialized circuit that relays retinal feature selectivity to V1 (Bickford et al., 2015). This strengthens the argument for specialized and dedicated parallel pathways, which evolved for different purposes, and ended up forming the broader visual system. How the wealth and diversity of information that is carried by these pathways contributes to different types of behaviors, and to what extent these pathways interact, remains to be explored in depth.

Our findings in chapter 2 coincided with the description of a different types of functional organization in the mouse SGS (Ahmadlou and Heimel, 2015; Feinberg and Meister, 2015). Using two-photon calcium imaging and intrinsic signal imaging, Feinberg and Meister (2015) demonstrated the existence of orientation columns spanning the depth of the mouse SGS. These columns were much coarser than the retinotopic map, in such a way that neurons representing a particular region of space preferred only one particular stimulus orientation.

It is worth mentioning that Feinberg and Meister (2015) did not image the sSGS, but reported their findings from deeper laminae in the SGS. We found no orientation-specific clusters in the sSGS. In fact, neurons in that lamina had very weak orientation selectivity. Moreover, neurons in the sSGS didn't seem to cluster according to their preferred direction either; we observed no relationship between the difference in preferred direction of a given pair of cells and

the physical distance separating them in the sSGS (Inayat et al., 2015).

This difference in the imaged depth between our two studies, coupled with other methodological differences, such as the imaged region along the rosto-caudal axis and the state of the animal (awake vs. anesthetized), put our findings less at odds, although they remain not entirely complementary.

In another study, which looked at multiunit activity and GCaMP epifluorescence signal, a similar but differently organized columnar architecture was described (Ahmadlou and Heimel, 2015). A large pinwheel columnar structure spanned the entire SGS retinotopy, in such a way that neurons responded best to stimuli moving along the axes of optic flow. This suggests a function for the SC that has less to do with fine feature discrimination and more to do with global motion detection.

In light of these recent findings, and some of the discrepancies between them, a more comprehensive and unified view of the functional organization of the mouse SC remains to be attained.

The Development of Response Properties

In chapter 3 of this thesis, I used a genetic mouse model to show that DSGCs are the source of direction selectivity in SGS neurons. These mice had the vesicular GABA transporter (VGAT) gene knocked out of cholinergic neurons. In the retina, these neurons are the starburst amacrine cells; the cells responsible for establishing direction selectivity in DSGCs, through asymmetric GABAergic inputs (Wei and Feller, 2011). This leads to a reduction in DS in the retina, and an

equivalent reduction of tuning in the sSGS; a lamina where neurons in the wild type animals are highly DS.

This discovery was also supported by whole cell recording experiments performed by Dr. Xuefeng Shi in the lab. He isolated retinal excitation onto DS neurons in the SGS by optogenetically silencing local circuits. He showed that the retinal input was already tuned, and that it was conveyed by DSGCs. Local SGS circuits served only to amplify that input, without altering its tuning (Shi et al., 2017).

These findings raise two important questions. One concerns the role of local inhibition in the SGS in further transforming this already tuned retinal input, which I will discuss in the following section. In this section I will discuss the second question raised by these findings, about the developmental process that leads to this functionally specific targeting of SGS neurons by similarly tuned DSGCs. This targeting must superimpose a more precise mechanism on top of retinotopic connectivity.

The development of direction selective responses in the mouse retina had been shown to take place during the second postnatal week, before eye opening. RGCs acquire their DS as a result of a developmental process that does not require spontaneous retinal activity. Specifically, initially unbiased GABAergic inputs from SACs onto DSGCs are asymmetrically reorganized and strengthened on the null side during this period in development; leading to the recognized adult phenotype (Wei et al., 2011; Yonehara et al., 2011). The molecular players in this developmental process are only now becoming known. The FRMD7 gene was found to be required for establishing motion direction preferences along the horizontal, but not vertical, axis (Yonehara et

al., 2016). The gene product is expressed throughout the processes of SACs, and so its specific role in generating direction selectivity in DSGCs is not known, nor is it easily inferred.

While the DS of DSGCs is not dependent on spontaneous activity or visual experience after eye opening, a less biased distribution of preferred directions begins to emerge in the adult (Elstrott et al., 2008). This normalization might be dependent on visual experience, or could simply be the result of a continued maturation process of specific retinal synapses that merely coincides with the onset of visual experience.

The development of DS in the mouse SC has also been shown to be independent of visual experience, by dark rearing the animals from birth to P60 (Wang et al., 2010). Either molecular cues or spontaneous retinal waves might therefore play a role in the development of this property in the SGS.

Support for the molecular cues hypothesis comes from the recent identification of receptor/ligand molecules that guide the projection of different types of On-DSGCs to their specific target nuclei in the accessory optic system (AOS) (Osterhout et al., 2015; Sun et al., 2015). On-DSGCs prefer three different motion directions, and each type projects to a particular nucleus or faction of a nucleus in the AOS, providing the first example of molecular cues that guide functionally specific retinal outputs to their respective targets in the brain. However, the SC is known to receive inputs from all major types of identified DSGCs so far (Dhande et al., 2015). Even more precise molecular cues must therefore be at play to guide these different types of inputs to their individual neuronal targets within the same structure. While different functional types of RGCs have been shown to terminate at different depths of the SGS (Dhande and Huberman, 2014), the molecular cues for this targeting are not yet known.

Since we've shown that SGS neurons inherit their direction selectivity from DSGCs (Shi et al., 2017), and knowing that individual SGS neurons receive inputs from multiple RGCs (Chandrasekaran et al., 2007), an even greater level of precision might be required to connect DSGCs with particular preferred directions to their postsynaptic partners in the SGS. Many DSGCs in the mouse retina have now been shown to have rather specific molecular identifiers depending on their preferred direction and the luminance polarity of the stimuli they respond to (Dhande et al., 2015). However, these identifiers do not necessarily play a role in determining the functional properties of these cells, or in setting up their projection affinity to specific targets in the SGS. It therefore remains to be demonstrated that the specific targeting of SGS neurons by functionally similar DSGCs actually follows a developmental molecular program.

Spontaneous retinal waves before eye opening might be the other important player in the convergence of inputs from similar DSGCs onto individual SGS neurons. This convergence of inputs might be achieved through Hebbian mechanisms (Constantine-Paton et al., 1990). While disrupting the normal pattern of spontaneous retinal waves during the first postnatal week does little to interfere with the normal emergence of DS in DSGCs during the second week, it results in a specific reduction of DS in SGS neurons along the naso-temporal axis (Wang et al., 2009). However, since the disruption of retinal waves in the beta-2 KOs takes place before the emergence of DS in the mouse retina, the initial establishment of abnormally refined RFs in SGS neurons might be the determinant of the subsequent emergence of abnormal DS there. Normally developed DSGCs will therefore have ended up connected to the "wrong" postsynaptic target in the SGS.

Despite the speculations, the mechanisms that relay retinal direction selectivity and preferred directions to individual SGS neurons remain a mystery today.

Local Circuit Computations

Our findings in chapter 3 demonstrate that local neurons in the SGS are not involved in the emergence of DS, but instead inherit that feature from DSGCs in the retina. Given the morphological diversity of neurons in the SGS, and the almost equal proportions of excitatory and inhibitory neurons in that lamina (Inayat et al., 2015), local SGS circuits seem primed to transform this incoming tuned input. Our findings in chapter 4 constitute the first line of evidence towards that claim. In addition to direction selective responses, we show motion contrast tuning in excitatory cells, revealing their capacity to monotonically track differences in motion direction between their RF and the surround. Importantly, we show a striking difference between the response properties of excitatory and inhibitory neurons to motion contrast. While excitatory neurons are potentiated by opposite motion between center and surround, inhibitory neurons are suppressed by it. It is therefore possible that local SGS inhibition might play a role in mediating the monotonic increase in the activity of excitatory neurons in response to motion contrast.

However, the involvement of SGS inhibitory circuits in the emergence of this phenomenon is yet to be directly demonstrated. It is conceivable that the effects we observe are computed elsewhere and simply relayed to the SGS, just like DS is. Possible sources of this input are the retina and V1. It is plausible that these effects might be relayed by V1, especially in primates where SC neurons are not particularly tuned to specific features (Veale et al., 2017). This is however less likely in mice whose SGS neurons are tuned to simple features like DS (Wang et al., 2010). Additionally, in order to the expose the SC in our experiments, we resorted to removing V1 entirely, and so the phenomenon we describe does not depend on visual cortex in mice.

While differential levels of suppression that depend of feature-contrast have been reported in RGCs, a potentiating effect by the surround is seldom observed (Chiao and Masland, 2003). This makes it unlikely that the motion-contrast induced bidirectional modulation of excitatory cell activity in the SGS is directly inherited from the retina without some transformation by local or extrinsic circuits. We therefore proposed an interplay between a differential withdrawal of retinal excitation and tuned inhibition from the surround in the SGS, which under different center-surround direction contrasts could lead to differential changes in the excitation/inhibition balance, and explain this bidirectional modulation of activity in local excitatory neurons.

There have been some reports of response potentiation in the retina that might nonetheless challenge that (Girman and Lund, 2010). Motion-contrast responses could thus arise in RGCs and be simply relayed to the SGS. However, this still raises questions about the observed differences in the way excitatory and inhibitory SGS neurons encode motion-opponency between the center and surround. We've previously shown that both excitatory and inhibitory DS neurons in the SGS receive direct retinal inputs from DSGCs (Shi et al., 2017), and so unless they share inputs from segregated and functionally distinct populations of DSGCs it is difficult to account for their different response properties under those conditions.

Another possibility is the involvement of an extrinsic source of inhibition to the SGS in mediating this effect. The pretectum is a major source of GABAergic input to the SGS in a retinotopic fashion. While it had been suggested that the pretectum provides direct inhibitory input to local GABAergic neurons (Boller and Schmidt, 2003; Schmidt et al., 2001), more recent studies have shown that these inputs are to excitatory projection neurons (Born and Schmidt, 2004, 2007).

The exact role of pretectal inhibition, if any, in mediating response modulation to motion contrast in the SGS remains to be demonstrated.

Ethological Implications

Given its layered sensory-motor organization, as well as its extensive projections to numerous brain areas, the SC is studied within the context of sensory-motor integration and visually-guided orienting behaviors. Initial studies in primates found eye movement maps in the dSC, cementing its function as a saccade generator and gaze control center (Schiller and Stryker, 1972). These findings fit within the framework of topographically aligned sensory and motor maps in the different layers of the SC, where sensory input directly guides reflexive orienting behaviors. Indeed, extensive work on the development and function of the barn owl tectum promotes its role in sensory-motor integration and orienting behaviors (du Lac and Knudsen, 1990, 1991; Knudsen and Brainard, 1995). In mice, it has been shown that stimulation of the dSC elicits directed eye movements, demonstrating the presence of a motor map in the deep layers. The development and refinement of this map has also been shown to require visual experience (Wang et al., 2015). This suggests the importance of feedback sensory inputs in the developmental alignment of sensory and motor maps. However, the interlaminar pathways and mechanisms that transform sensory inputs into premotor outputs in the adult animal are yet to be elucidated in detail.

In addition to its role in orienting behaviors, the SC has also been implicated in mediating escape and defensive behaviors. These behaviors can be elicited by electrical stimulation of the SC; and the type of response that is produced seems to depend not only on the dorsoventral site of the simulation, but also on its mediolateral location (Northmore et al., 1988; Sahibzada et al.,

1986). Indeed, interesting mediolateral differences have been proposed in the rodent SC that could have important behavioral implications. A histological study in rats found that the intermediate and deep layers of the SC receive different sources and types of inputs based on their medio-lateral position. This arrangement can have an ethological function related to the predator-prey relationships of the rat; whereby predators and preys are expected in the upper (represented by the medial SC) and lower (lateral SC) visual fields, respectively (Comoli et al., 2012). Moreover, a study in parasagittal SC slices in rats demonstrated a $GABA_A$-mediated, rostrally-directed, bias in inhibition in the visual layers. This allows an electrical stimulus to propagate preferentially in the caudal direction. Activation of the caudal SC might therefore help the animal pay attention to stimuli entering its peripheral vision (Bayguinov et al., 2015).

In contrast with internally generated premotor activity in the SC that might serve as the basis for orienting behaviors, visually responsive neurons of the SGS can lead to defensive behaviors by virtue of their projections to different brain regions. Both the PBg and LP connect to the amygdala, a major "fear" center in the brain, and both these structures receive direct input from the SGS. These pathways have been shown to mediate visually-evoked fear responses in mice, and a particular SGS cell type (PV+ neurons) relaying the necessary visual information has been identified in at least one of the pathways (Shang et al., 2015; Wei et al., 2015).

A better understanding of the functional architecture, the response properties, and connectivity of the SC, internally and with other brain structures, will generate insight about its role in behavior. Better experimental tools, that allow the finer manipulation of different circuit components, will finally allow us to link specific circuit-level processes with ethologically relevant behaviors.

Whether the animal orients towards or escapes a particular object, the visual representation of that object to the animal needs to report its saliency. Given our findings in chapter 4, from a behaviorally relevant perspective, excitatory neurons in the SGS might be acting as reporters of incongruence between the predicted response in their RF center (based on background motion) and the actual response. This type of neuronal activity can help the animal distinguish between self-induced motion in the visual scene, manifested as a dismissible congruent shift of objects, and actual object motion that might require appropriate action. A similar type of response has been shown in a population of neurons in mouse V1, under awake and running conditions (Keller et al., 2012; Zmarz and Keller, 2016). If indeed SGS neurons are integrating self-induced motion, they might not be obtaining this information as a motor efference copy, given our imaging conditions under anesthesia. These neurons might therefore be substantially relying on full-field visual input as a proxy for locomotion. That is not to say that locomotion and different modulatory systems couldn't further influence SGS neurons, or even drastically change some of their response properties under different behavioral states (Ayaz et al., 2013; Niell and Stryker, 2010; Stubblefield et al., 2015). Additionally, even under stationary conditions, a center-surround feature contrast detection capacity can help segment a visual scene into its separate objects.

Conclusions

In this thesis, I discussed my contributions towards a better understanding of the structure and function of the superior colliculus (SC), using the mouse as an animal model. First, I used two-photon calcium imaging and single unit extracellular recordings to show that neurons in the SGS are organized according to the degree of their direction selectivity, whereby DS decreases with

depth. Next, I used a KO mouse model with reduced DS in the retina to show the DSGCs are the source of selective responses in the SGS. Finally, I described a fundamental difference in the response of excitatory and inhibitory SGS neurons to motion contrast, with implications for local computations of motion saliency.

Studying the mouse visual system presents us with a unique opportunity to understand visual signal processing at the microcircuit level in a mammalian species. This is due to the ever-expanding genetic toolkit now at our disposal, and to the possibility of performing functional imaging in these animals at single cell resolution or even higher (Holtmaat et al., 2005). Indeed, taking advantage of these advances, much has been uncovered about the development and function of the visual system than had been possible in the past.

However, two different but complementary departures from this approach might become necessary to further our understanding of the visual system. The first is an expansion of our genetic toolkit and imaging capabilities to study the organization and computational principles in the visual system of higher mammals. The second is to study the mouse visual system within a mouse-centered behavioral context that better reflects their use for vision, and helps us extract overarching principles about how vision instructs behavior in natural settings.

We study mice given that the visual response properties of their V1 neurons are similar to those in higher mammals (Niell and Stryker, 2008). However, there exist some differences in the principles of function and organization of the visual system between mice and higher mammals. Mice, for instance, have poorer acuity compared to carnivores and primates. Their visual cortex also does not exhibit a columnar organization of orientation preference akin to what is observed in those species, but rather has a “salt and pepper” scattering of neurons in a non-structured

organization (Bonin et al., 2011). We must therefore be careful when interpreting certain findings in mouse V1, like the non-specific pooling of excitation by the major class of inhibitory neurons (PV+) in that structure, which results in their characteristic poor tuning. For example, ferret V1 exhibits a columnar organization, and inhibitory neurons in that structure have recently been shown to be orientation selective, even in regions of high response heterogeneity (Wilson et al., 2017). This challenges the notion of "non-specific pooling", and brings about the possibility that different principles might govern computations in V1 of different species. Thus, in addition to a reductionist approach to understanding vision, these types of findings also call for a comparative approach between species.

Current approaches study mouse vision largely independently from behavior, or within unnatural behavioral settings, in order to answer specific questions about its mechanisms. While this approach is invaluable to understanding how the visual system functions at a fundamental circuit level, it might not be recruiting it within the range and context of its natural capacity (Krakauer et al., 2017). Why the visual system evolved plays a major role in dictating its functional properties and organization, which might differ between species. Studying mouse vision in a natural behavioral setting, such as vision-guided prey capture (Hoy et al., 2016), will therefore illuminate the types of problems that vision evolved to solve in the natural world.

References

Adesnik, H., Bruns, W., Taniguchi, H., Huang, Z.J., and Scanziani, M. (2012). A neural circuit for spatial summation in visual cortex. Nature *490*, 226-231.

Ahmadlou, M., and Heimel, J.A. (2015). Preference for concentric orientations in the mouse superior colliculus. Nat Commun *6*, 6773.

Albano, J.E., Humphrey, A.L., and Norton, T.T. (1978). Laminar organization of receptive-field properties in tree shrew superior colliculus. J Neurophysiol *41*, 1140-1164.

Andermann, M.L., Kerlin, A.M., Roumis, D.K., Glickfeld, L.L., and Reid, R.C. (2011). Functional specialization of mouse higher visual cortical areas. Neuron *72*, 1025-1039.

Atallah, B.V., Bruns, W., Carandini, M., and Scanziani, M. (2012). Parvalbumin-expressing interneurons linearly transform cortical responses to visual stimuli. Neuron *73*, 159-170.

Ayaz, A., Saleem, A.B., Scholvinck, M.L., and Carandini, M. (2013). Locomotion controls spatial integration in mouse visual cortex. Curr Biol *23*, 890-894.

Baden, T., Berens, P., Franke, K., Roman Roson, M., Bethge, M., and Euler, T. (2016). The functional diversity of retinal ganglion cells in the mouse. Nature *529*, 345-350.

Barlow, H.B., and Hill, R.M. (1963). Selective sensitivity to direction of movement in ganglion cells of the rabbit retina. Science *139*, 412-414.

Barlow, H.B., and Levick, W.R. (1965). The mechanism of directionally selective units in rabbit's retina. J Physiol *178*, 477-504.

Bayguinov, P.O., Ghitani, N., Jackson, M.B., and Basso, M.A. (2015). A Hard-Wired Priority Map in the Superior Colliculus Shaped by Asymmetric Inhibitory Circuitry. J Neurophysiol, jn 00144 02015.

Behan, M., Steinhacker, K., Jeffrey-Borger, S., and Meredith, M.A. (2002). Chemoarchitecture of GABAergic neurons in the ferret superior colliculus. J Comp Neurol *452*, 334-359.

Ben-Tov, M., Donchin, O., Ben-Shahar, O., and Segev, R. (2015). Pop-out in visual search of moving targets in the archer fish. Nat Commun *6*, 6476.

Berson, D.M., Dunn, F.A., and Takao, M. (2002). Phototransduction by retinal ganglion cells that set the circadian clock. Science *295*, 1070-1073.

Bickford, M.E., Zhou, N., Krahe, T.E., Govindaiah, G., and Guido, W. (2015). Retinal and Tectal "Driver-Like" Inputs Converge in the Shell of the Mouse Dorsal Lateral Geniculate Nucleus. J Neurosci *35*, 10523-10534.

Binns, K.E., and Salt, T.E. (1997). Different roles for GABAA and GABAB receptors in visual processing in the rat superior colliculus. J Physiol *504 (Pt 3)*, 629-639.

Bock, D.D., Lee, W.C., Kerlin, A.M., Andermann, M.L., Hood, G., Wetzel, A.W., Yurgenson, S., Soucy, E.R., Kim, H.S., and Reid, R.C. (2011). Network anatomy and in vivo physiology of visual cortical neurons. Nature *471*, 177-182.

Boller, M., and Schmidt, M. (2003). GABAC receptors in the rat superior colliculus and pretectum participate in synaptic neurotransmission. J Neurophysiol *89*, 2035-2045.

Bonhoeffer, T., and Grinvald, A. (1991). Iso-orientation domains in cat visual cortex are arranged in pinwheel-like patterns. Nature *353*, 429-431.

Bonin, V., Histed, M.H., Yurgenson, S., and Reid, R.C. (2011). Local diversity and fine-scale organization of receptive fields in mouse visual cortex. J Neurosci *31*, 18506-18521.

Born, G., and Schmidt, M. (2004). Inhibition of superior colliculus neurons by a GABAergic input from the pretectal nuclear complex in the rat. Eur J Neurosci *20*, 3404-3412.

Born, G., and Schmidt, M. (2007). GABAergic pathways in the rat subcortical visual system: a comparative study in vivo and in vitro. Eur J Neurosci *26*, 1183-1192.

Bosking, W.H., Crowley, J.C., and Fitzpatrick, D. (2002). Spatial coding of position and orientation in primary visual cortex. Nat Neurosci *5*, 874-882.

Brainard, D.H. (1997). The Psychophysics Toolbox. Spat Vis *10*, 433-436.

Byun, H., Kwon, S., Ahn, H.J., Liu, H., Forrest, D., Demb, J.B., and Kim, I.J. (2016). Molecular features distinguish ten neuronal types in the mouse superficial superior colliculus. J Comp Neurol *524*, 2300-2321.

Cang, J., and Feldheim, D.A. (2013). Developmental mechanisms of topographic map formation and alignment. Annu Rev Neurosci *36*, 51-77.

Cang, J., Wang, L., Stryker, M.P., and Feldheim, D.A. (2008). Roles of ephrin-as and structured activity in the development of functional maps in the superior colliculus. The Journal of neuroscience : the official journal of the Society for Neuroscience *28*, 11015-11023.

Chandrasekaran, A.R., Shah, R.D., and Crair, M.C. (2007). Developmental homeostasis of mouse retinocollicular synapses. J Neurosci *27*, 1746-1755.

Chen, B., Hu, X.J., and Pourcho, R.G. (1996). Morphological diversity in terminals of W-type retinal ganglion cells at projection sites in cat brain. Vis Neurosci *13*, 449-460.

Chen, H., Zhao, Y., Liu, M., Feng, L., Puyang, Z., Yi, J., Liang, P., Zhang, H.F., Cang, J., Troy, J.B., *et al.* (2015). Progressive degeneration of retinal and superior collicular functions in mice with sustained ocular hypertension. Invest Ophthalmol Vis Sci *56*, 1971-1984.

Chen, T.W., Wardill, T.J., Sun, Y., Pulver, S.R., Renninger, S.L., Baohan, A., Schreiter, E.R., Kerr, R.A., Orger, M.B., Jayaraman, V., *et al.* (2013). Ultrasensitive fluorescent proteins for imaging neuronal activity. Nature *499*, 295-300.

Cheong, S.K., Tailby, C., Solomon, S.G., and Martin, P.R. (2013). Cortical-Like Receptive Fields in the Lateral Geniculate Nucleus of Marmoset Monkeys. J Neurosci *33*, 6864-6876.

Chiao, C.C., and Masland, R.H. (2003). Contextual tuning of direction-selective retinal ganglion cells. Nat Neurosci *6*, 1251-1252.

Chklovskii, D.B., and Koulakov, A.A. (2004). Maps in the brain: what can we learn from them? Annu Rev Neurosci *27*, 369-392.

Comoli, E., Das Neves Favaro, P., Vautrelle, N., Leriche, M., Overton, P.G., and Redgrave, P. (2012). Segregated anatomical input to sub-regions of the rodent superior colliculus associated with approach and defense. Front Neuroanat *6*, 9.

Constantine-Paton, M., Cline, H.T., and Debski, E. (1990). Patterned activity, synaptic convergence, and the NMDA receptor in developing visual pathways. Annu Rev Neurosci *13*, 129-154.

Cruz-Martin, A., El-Danaf, R.N., Osakada, F., Sriram, B., Dhande, O.S., Nguyen, P.L., Callaway, E.M., Ghosh, A., and Huberman, A.D. (2014). A dedicated circuit links direction-selective retinal ganglion cells to the primary visual cortex. Nature *507*, 358-361.

Cynader, M., and Berman, N. (1972). Receptive-field organization of monkey superior colliculus. J Neurophysiol *35*, 187-201.

Daniels, J.D., Norman, J.L., and Pettigrew, J.D. (1977). Biases for oriented moving bars in lateral geniculate nucleus neurons of normal and stripe-reared cats. Exp Brain Res *29*, 155-172.

Demb, J.B., and Singer, J.H. (2015). Functional Circuitry of the Retina. Annual review of vision science *1*, 263-289.

Dhande, O.S., Estevez, M.E., Quattrochi, L.E., El-Danaf, R.N., Nguyen, P.L., Berson, D.M., and Huberman, A.D. (2013). Genetic dissection of retinal inputs to brainstem nuclei controlling image stabilization. J Neurosci *33*, 17797-17813.

Dhande, O.S., and Huberman, A.D. (2014). Retinal ganglion cell maps in the brain: implications for visual processing. Curr Opin Neurobiol *24*, 133-142.

Dhande, O.S., Stafford, B.K., Lim, J.A., and Huberman, A.D. (2015). Contributions of Retinal Ganglion Cells to Subcortical Visual Processing and Behaviors. Annual review of vision science *1*, 291-328.

Diamond, I.T., Conley, M., Fitzpatrick, D., and Raczkowski, D. (1991). Evidence for separate pathways within the tecto-geniculate projection in the tree shrew. Proc Natl Acad Sci U S A *88*, 1315-1319.

Douglas, R.J., and Martin, K.A. (2004). Neuronal circuits of the neocortex. Annu Rev Neurosci *27*, 419-451.

Drager, U.C., and Hubel, D.H. (1975). Responses to visual stimulation and relationship between visual, auditory, and somatosensory inputs in mouse superior colliculus. J Neurophysiol *38*, 690-713.

du Lac, S., and Knudsen, E.I. (1990). Neural maps of head movement vector and speed in the optic tectum of the barn owl. Journal of neurophysiology *63*, 131-146.

du Lac, S., and Knudsen, E.I. (1991). Early visual deprivation results in a degraded motor map in the optic tectum of barn owls. Proc Natl Acad Sci U S A *88*, 3426-3430.

Ellis, E.M., Gauvain, G., Sivyer, B., and Murphy, G.J. (2016). Shared and distinct retinal input to the mouse superior colliculus and dorsal lateral geniculate nucleus. Journal of neurophysiology *116*, 602-610.

Elstrott, J., Anishchenko, A., Greschner, M., Sher, A., Litke, A.M., Chichilnisky, E.J., and Feller, M.B. (2008). Direction selectivity in the retina is established independent of visual experience and cholinergic retinal waves. Neuron *58*, 499-506.

Endo, T., Yanagawa, Y., Obata, K., and Isa, T. (2003). Characteristics of GABAergic neurons in the superficial superior colliculus in mice. Neurosci Lett *346*, 81-84.

Feinberg, E.H., and Meister, M. (2015). Orientation columns in the mouse superior colliculus. Nature *519*, 229-232.

Fortin, S., Chabli, A., Dumont, I., Shumikhina, S., Itaya, S.K., and Molotchnikoff, S. (1999). Maturation of visual receptive field properties in the rat superior colliculus. Brain Res Dev Brain Res *112*, 55-64.

Frost, B.J., Scilley, P.L., and Wong, S.C. (1981). Moving background patterns reveal double-opponency of directionally specific pigeon tectal neurons. Exp Brain Res *43*, 173-185.

Gabriel, J.P., Trivedi, C.A., Maurer, C.M., Ryu, S., and Bollmann, J.H. (2012). Layer-specific targeting of direction-selective neurons in the zebrafish optic tectum. Neuron *76*, 1147-1160.

Gale, S.D., and Murphy, G.J. (2014). Distinct representation and distribution of visual information by specific cell types in mouse superficial superior colliculus. The Journal of neuroscience : the official journal of the Society for Neuroscience *34*, 13458-13471.

Gandhi, N.J., and Katnani, H.A. (2011). Motor functions of the superior colliculus. Annu Rev Neurosci *34*, 205-231.

Girman, S., and Lund, R. (2010). Orientation-specific modulation of rat retinal ganglion cell responses and its dependence on relative orientations of the center and surround gratings. J Neurophysiol *104*, 2951-2962.

Girman, S.V., and Lund, R.D. (2007). Most superficial sublamina of rat superior colliculus: neuronal response properties and correlates with perceptual figure-ground segregation. J Neurophysiol *98*, 161-177.

Goldberg, M.E., and Wurtz, R.H. (1972). Activity of superior colliculus in behaving monkey. I. Visual receptive fields of single neurons. J Neurophysiol *35*, 542-559.

Goodale, M.A., and Milner, A.D. (1992). Separate visual pathways for perception and action. Trends Neurosci *15*, 20-25.

Graham, J. (1977). An autoradiographic study of the efferent connections of the superior colliculus in the cat. J Comp Neurol *173*, 629-654.

Grama, A., and Engert, F. (2012). Direction selectivity in the larval zebrafish tectum is mediated by asymmetric inhibition. Frontiers in neural circuits *6*, 59.

Harting, J.K., Casagrande, V.A., and Weber, J.T. (1978). The projection of the primate superior colliculus upon the dorsal lateral geniculate nucleus: autoradiographic demonstration of interlaminar distribution of tectogeniculate axons. Brain Res *150*, 593-599.

Hoffmann, K.P., and Straschill, M. (1971). Influences of cortico-tectal and intertectal connections on visual responses in the cat's superior colliculus. Exp Brain Res *12*, 120-131.

Holtmaat, A.J., Trachtenberg, J.T., Wilbrecht, L., Shepherd, G.M., Zhang, X., Knott, G.W., and Svoboda, K. (2005). Transient and persistent dendritic spines in the neocortex in vivo. Neuron *45*, 279-291.

Hoy, J.L., Yavorska, I., Wehr, M., and Niell, C.M. (2016). Vision Drives Accurate Approach Behavior during Prey Capture in Laboratory Mice. Curr Biol *26*, 3046-3052.

Hubel, D.H., and Wiesel, T.N. (1961). Integrative action in the cat's lateral geniculate body. J Physiol *155*, 385-398.

Hubel, D.H., and Wiesel, T.N. (1962). Receptive fields, binocular interaction and functional architecture in the cat's visual cortex. The Journal of physiology *160*, 106-154.

Hubel, D.H., and Wiesel, T.N. (1968). Receptive fields and functional architecture of monkey striate cortex. The Journal of physiology *195*, 215-243.

Hubel, D.H., and Wiesel, T.N. (1974). Sequence regularity and geometry of orientation columns in the monkey striate cortex. J Comp Neurol *158*, 267-293.

Huberman, A.D., Clandinin, T.R., and Baier, H. (2010). Molecular and cellular mechanisms of lamina-specific axon targeting. Cold Spring Harb Perspect Biol *2*, a001743.

Huberman, A.D., Manu, M., Koch, S.M., Susman, M.W., Lutz, A.B., Ullian, E.M., Baccus, S.A., and Barres, B.A. (2008). Architecture and activity-mediated refinement of axonal projections from a mosaic of genetically identified retinal ganglion cells. Neuron *59*, 425-438.

Huberman, A.D., and Niell, C.M. (2011). What can mice tell us about how vision works? Trends Neurosci *34*, 464-473.

Huberman, A.D., Wei, W., Elstrott, J., Stafford, B.K., Feller, M.B., and Barres, B.A. (2009). Genetic identification of an On-Off direction-selective retinal ganglion cell subtype reveals a layer-specific subcortical map of posterior motion. Neuron *62*, 327-334.

Hunter, P.R., Lowe, A.S., Thompson, I.D., and Meyer, M.P. (2013). Emergent properties of the optic tectum revealed by population analysis of direction and orientation selectivity. J Neurosci *33*, 13940-13945.

Inayat, S., Barchini, J., Chen, H., Feng, L., Liu, X., and Cang, J. (2015). Neurons in the most superficial lamina of the mouse superior colliculus are highly selective for stimulus direction. J Neurosci *35*, 7992-8003.

Joly, T.J., and Bender, D.B. (1997). Loss of relative-motion sensitivity in the monkey superior colliculus after lesions of cortical area MT. Exp Brain Res *117*, 43-58.

Jones, H.E., Grieve, K.L., Wang, W., and Sillito, A.M. (2001). Surround suppression in primate V1. J Neurophysiol *86*, 2011-2028.

Jones, H.E., Wang, W., and Sillito, A.M. (2002). Spatial organization and magnitude of orientation contrast interactions in primate V1. J Neurophysiol *88*, 2796-2808.

Kasai, M., and Isa, T. (2016). Imaging population dynamics of surround suppression in the superior colliculus. Eur J Neurosci *44*, 2543-2556.

Kastner, S., Nothdurft, H.C., and Pigarev, I.N. (1999). Neuronal responses to orientation and motion contrast in cat striate cortex. Vis Neurosci *16*, 587-600.

Kay, J.N., De la Huerta, I., Kim, I.J., Zhang, Y., Yamagata, M., Chu, M.W., Meister, M., and Sanes, J.R. (2011). Retinal ganglion cells with distinct directional preferences differ in molecular identity, structure, and central projections. J Neurosci *31*, 7753-7762.

Keller, G.B., Bonhoeffer, T., and Hubener, M. (2012). Sensorimotor mismatch signals in primary visual cortex of the behaving mouse. Neuron *74*, 809-815.

Kerlin, A.M., Andermann, M.L., Berezovskii, V.K., and Reid, R.C. (2010). Broadly tuned response properties of diverse inhibitory neuron subtypes in mouse visual cortex. Neuron *67*, 858-871.

Kim, E.J., Juavinett, A.L., Kyubwa, E.M., Jacobs, M.W., and Callaway, E.M. (2015). Three Types of Cortical Layer 5 Neurons That Differ in Brain-wide Connectivity and Function. Neuron *88*, 1253-1267.

Kim, I.J., Zhang, Y., Meister, M., and Sanes, J.R. (2010). Laminar restriction of retinal ganglion cell dendrites and axons: subtype-specific developmental patterns revealed with transgenic markers. J Neurosci *30*, 1452-1462.

Knierim, J.J., and van Essen, D.C. (1992). Neuronal responses to static texture patterns in area V1 of the alert macaque monkey. J Neurophysiol *67*, 961-980.

Knudsen, E.I., and Brainard, M.S. (1995). Creating a unified representation of visual and auditory space in the brain. Annu Rev Neurosci *18*, 19-43.

Ko, H., Cossell, L., Baragli, C., Antolik, J., Clopath, C., Hofer, S.B., and Mrsic-Flogel, T.D. (2013). The emergence of functional microcircuits in visual cortex. Nature *496*, 96-100.

Ko, H., Hofer, S.B., Pichler, B., Buchanan, K.A., Sjostrom, P.J., and Mrsic-Flogel, T.D. (2011). Functional specificity of local synaptic connections in neocortical networks. Nature *473*, 87-91.

Krakauer, J.W., Ghazanfar, A.A., Gomez-Marin, A., MacIver, M.A., and Poeppel, D. (2017). Neuroscience Needs Behavior: Correcting a Reductionist Bias. Neuron *93*, 480-490.

Kuffler, S.W. (1953). Discharge patterns and functional organization of mammalian retina. J Neurophysiol *16*, 37-68.

Langer, T.P., and Lund, R.D. (1974). The upper layers of the superior colliculus of the rat: a Golgi study. J Comp Neurol *158*, 418-435.

Lee, P.H., Schmidt, M., and Hall, W.C. (2001). Excitatory and inhibitory circuitry in the superficial gray layer of the superior colliculus. J Neurosci *21*, 8145-8153.

Lee, S.H., Kwan, A.C., Zhang, S., Phoumthipphavong, V., Flannery, J.G., Masmanidis, S.C., Taniguchi, H., Huang, Z.J., Zhang, F., Boyden, E.S., *et al.* (2012). Activation of specific interneurons improves V1 feature selectivity and visual perception. Nature *488*, 379-383.

Lee, W.C., Bonin, V., Reed, M., Graham, B.J., Hood, G., Glattfelder, K., and Reid, R.C. (2016). Anatomy and function of an excitatory network in the visual cortex. Nature *532*, 370-374.

Li, Y.T., Liu, B.H., Chou, X.L., Zhang, L.I., and Tao, H.W. (2015). Strengthening of Direction Selectivity by Broadly Tuned and Spatiotemporally Slightly Offset Inhibition in Mouse Visual Cortex. Cereb Cortex *25*, 2466-2477.

Liang, F., Xiong, X.R., Zingg, B., Ji, X.Y., Zhang, L.I., and Tao, H.W. (2015). Sensory Cortical Control of a Visually Induced Arrest Behavior via Corticotectal Projections. Neuron *86*, 755-767.

Lien, A.D., and Scanziani, M. (2013). Tuned thalamic excitation is amplified by visual cortical circuits. Nat Neurosci *16*, 1315-1323.

Liu, B.H., Li, P., Li, Y.T., Sun, Y.J., Yanagawa, Y., Obata, K., Zhang, L.I., and Tao, H.W. (2009). Visual receptive field structure of cortical inhibitory neurons revealed by two-photon imaging guided recording. J Neurosci *29*, 10520-10532.

Liu, M., Wang, L., and Cang, J. (2014). Different roles of axon guidance cues and patterned spontaneous activity in establishing receptive fields in the mouse superior colliculus. Frontiers in neural circuits *8*, 23.

Lowe, A.S., Nikolaou, N., Hunter, P.R., Thompson, I.D., and Meyer, M.P. (2013). A systems-based dissection of retinal inputs to the zebrafish tectum reveals different rules for different functional classes during development. J Neurosci *33*, 13946-13956.

Madisen, L., Zwingman, T.A., Sunkin, S.M., Oh, S.W., Zariwala, H.A., Gu, H., Ng, L.L., Palmiter, R.D., Hawrylycz, M.J., Jones, A.R., *et al.* (2010). A robust and high-throughput Cre reporting and characterization system for the whole mouse brain. Nat Neurosci *13*, 133-140.

Marrocco, R.T., and Li, R.H. (1977). Monkey superior colliculus: properties of single cells and their afferent inputs. J Neurophysiol *40*, 844-860.

Marshel, J.H., Garrett, M.E., Nauhaus, I., and Callaway, E.M. (2011). Functional specialization of seven mouse visual cortical areas. Neuron *72*, 1040-1054.

Marshel, J.H., Kaye, A.P., Nauhaus, I., and Callaway, E.M. (2012). Anterior-posterior direction opponency in the superficial mouse lateral geniculate nucleus. Neuron *76*, 713-720.

Masland, R.H. (2012). The neuronal organization of the retina. Neuron *76*, 266-280.

Masland, R.H., Chow, K.L., and Stewart, D.L. (1971). Receptive-field characteristics of superior colliculus neurons in the rabbit. J Neurophysiol *34*, 148-156.

May, P.J. (2006). The mammalian superior colliculus: laminar structure and connections. Prog Brain Res *151*, 321-378.

Mazurek, M., Kager, M., and Van Hooser, S.D. (2014). Robust quantification of orientation selectivity and direction selectivity. Frontiers in neural circuits *8*, 92.

McIlwain, J.T., and Buser, P. (1968). Receptive fields of single cells in the cat's superior colliculus. Exp Brain Res *5*, 314-325.

Meyer, H.S., Schwarz, D., Wimmer, V.C., Schmitt, A.C., Kerr, J.N., Sakmann, B., and Helmstaedter, M. (2011). Inhibitory interneurons in a cortical column form hot zones of inhibition in layers 2 and 5A. Proc Natl Acad Sci U S A *108*, 16807-16812.

Michael, C.R. (1970). Integration of retinal and cortical information in the superior colliculus of the ground squirrel. Brain Behav Evol *3*, 205-209.

Michael, C.R. (1972). Functional organization of cells in superior colliculus of the ground squirrel. J Neurophysiol *35*, 833-846.

Mize, R.R. (1992). The organization of GABAergic neurons in the mammalian superior colliculus. Prog Brain Res *90*, 219-248.

Mooney, R.D., Klein, B.G., and Rhoades, R.W. (1985). Correlations between the structural and functional characteristics of neurons in the superficial laminae and the hamster's superior colliculus. J Neurosci *5*, 2989-3009.

Mooney, R.D., Nikoletseas, M.M., Ruiz, S.A., and Rhoades, R.W. (1988). Receptive-field properties and morphological characteristics of the superior collicular neurons that project

to the lateral posterior and dorsal lateral geniculate nuclei in the hamster. J Neurophysiol *59*, 1333-1351.

Mufson, E.J., Martin, T.L., Mash, D.C., Wainer, B.H., and Mesulam, M.M. (1986). Cholinergic projections from the parabigeminal nucleus (Ch8) to the superior colliculus in the mouse: a combined analysis of horseradish peroxidase transport and choline acetyltransferase immunohistochemistry. Brain Res *370*, 144-148.

Nath, A., and Schwartz, G.W. (2016). Cardinal Orientation Selectivity Is Represented by Two Distinct Ganglion Cell Types in Mouse Retina. The Journal of neuroscience : the official journal of the Society for Neuroscience *36*, 3208-3221.

Nauhaus, I., Nielsen, K.J., Disney, A.A., and Callaway, E.M. (2012). Orthogonal micro-organization of orientation and spatial frequency in primate primary visual cortex. Nat Neurosci *15*, 1683-1690.

Niell, C.M., and Smith, S.J. (2005). Functional imaging reveals rapid development of visual response properties in the zebrafish tectum. Neuron *45*, 941-951.

Niell, C.M., and Stryker, M.P. (2008). Highly selective receptive fields in mouse visual cortex. J Neurosci *28*, 7520-7536.

Niell, C.M., and Stryker, M.P. (2010). Modulation of visual responses by behavioral state in mouse visual cortex. Neuron *65*, 472-479.

Nienborg, H., Hasenstaub, A., Nauhaus, I., Taniguchi, H., Huang, Z.J., and Callaway, E.M. (2013). Contrast dependence and differential contributions from somatostatin- and parvalbumin-expressing neurons to spatial integration in mouse V1. J Neurosci *33*, 11145-11154.

Nikolaou, N., and Meyer, M.P. (2012). Imaging circuit formation in zebrafish. Dev Neurobiol *72*, 346-357.

Northmore, D.P., Levine, E.S., and Schneider, G.E. (1988). Behavior evoked by electrical stimulation of the hamster superior colliculus. Exp Brain Res *73*, 595-605.

Nothdurft, H.C., Gallant, J.L., and Van Essen, D.C. (1999). Response modulation by texture surround in primate area V1: correlates of "popout" under anesthesia. Vis Neurosci *16*, 15-34.

Oesch, N., Euler, T., and Taylor, W.R. (2005). Direction-selective dendritic action potentials in rabbit retina. Neuron *47*, 739-750.

Ogasawara, K., McHaffie, J.G., and Stein, B.E. (1984). Two visual corticotectal systems in cat. J Neurophysiol *52*, 1226-1245.

Osterhout, J.A., Stafford, B.K., Nguyen, P.L., Yoshihara, Y., and Huberman, A.D. (2015). Contactin-4 mediates axon-target specificity and functional development of the accessory optic system. Neuron *86*, 985-999.

Pei, Z., Chen, Q., Koren, D., Giammarinaro, B., Acaron Ledesma, H., and Wei, W. (2015). Conditional Knock-Out of Vesicular GABA Transporter Gene from Starburst Amacrine Cells Reveals the Contributions of Multiple Synaptic Mechanisms Underlying Direction Selectivity in the Retina. J Neurosci *35*, 13219-13232.

Pfeffer, C.K., Xue, M., He, M., Huang, Z.J., and Scanziani, M. (2013). Inhibition of inhibition in visual cortex: the logic of connections between molecularly distinct interneurons. Nat Neurosci *16*, 1068-1076.

Phillips, M.A., Colonnese, M.T., Goldberg, J., Lewis, L.D., Brown, E.N., and Constantine-Paton, M. (2011). A synaptic strategy for consolidation of convergent visuotopic maps. Neuron *71*, 710-724.

Phongphanphanee, P., Marino, R.A., Kaneda, K., Yanagawa, Y., Munoz, D.P., and Isa, T. (2014). Distinct local circuit properties of the superficial and intermediate layers of the rodent superior colliculus. Eur J Neurosci *40*, 2329-2343.

Piscopo, D.M., El-Danaf, R.N., Huberman, A.D., and Niell, C.M. (2013). Diverse visual features encoded in mouse lateral geniculate nucleus. J Neurosci *33*, 4642-4656.

Priebe, N.J., and Ferster, D. (2005). Direction selectivity of excitation and inhibition in simple cells of the cat primary visual cortex. Neuron *45*, 133-145.

Priebe, N.J., and Ferster, D. (2006). Mechanisms underlying cross-orientation suppression in cat visual cortex. Nat Neurosci *9*, 552-561.

Priebe, N.J., and Ferster, D. (2012). Mechanisms of neuronal computation in mammalian visual cortex. Neuron *75*, 194-208.

Ramdya, P., and Engert, F. (2008). Emergence of binocular functional properties in a monocular neural circuit. Nat Neurosci *11*, 1083-1090.

Reichardt, W. (1961). Autocorrelation, a principle for the evaluation of sensory information by the central nervous system. In Sensory Communication, R. W, ed. (Wiley), pp. 303-317.

Reid, R.C., and Alonso, J.M. (1995). Specificity of monosynaptic connections from thalamus to visual cortex. Nature *378*, 281-284.

Rhoades, R.W., and Chalupa, L.M. (1976). Directional selectivity in the superior colliculus of the golden hamster. Brain Res *118*, 334-338.

Ringach, D.L., Mineault, P.J., Tring, E., Olivas, N.D., Garcia-Junco-Clemente, P., and Trachtenberg, J.T. (2016). Spatial clustering of tuning in mouse primary visual cortex. Nat Commun *7*, 12270.

Robles, E., Filosa, A., and Baier, H. (2013). Precise lamination of retinal axons generates multiple parallel input pathways in the tectum. J Neurosci *33*, 5027-5039.

Sachdev, R.N., Krause, M.R., and Mazer, J.A. (2012). Surround suppression and sparse coding in visual and barrel cortices. Frontiers in neural circuits *6*, 43.

Sahibzada, N., Dean, P., and Redgrave, P. (1986). Movements resembling orientation or avoidance elicited by electrical stimulation of the superior colliculus in rats. J Neurosci *6*, 723-733.

Sanes, J.R., and Masland, R.H. (2015). The types of retinal ganglion cells: current status and implications for neuronal classification. Annu Rev Neurosci *38*, 221-246.

Sarnaik, R., Chen, H., Liu, X., and Cang, J. (2014). Genetic disruption of the On visual pathway affects cortical orientation selectivity and contrast sensitivity in mice. J Neurophysiol *111*, 2276-2286.

Saul, A.B., and Humphrey, A.L. (1992). Temporal-frequency tuning of direction selectivity in cat visual cortex. Vis Neurosci *8*, 365-372.

Schiller, P.H., and Stryker, M. (1972). Single-unit recording and stimulation in superior colliculus of the alert rhesus monkey. Journal of neurophysiology *35*, 915-924.

Schmidt, J.T. (1979). The laminar organization of optic nerve fibres in the tectum of goldfish. Proc R Soc Lond B Biol Sci *205*, 287-306.

Schmidt, M., Boller, M., Ozen, G., and Hall, W.C. (2001). Disinhibition in rat superior colliculus mediated by GABAc receptors. J Neurosci *21*, 691-699.

Scholl, B., Tan, A.Y., Corey, J., and Priebe, N.J. (2013). Emergence of orientation selectivity in the Mammalian visual pathway. J Neurosci *33*, 10616-10624.

Scott, B.B., Brody, C.D., and Tank, D.W. (2013). Cellular resolution functional imaging in behaving rats using voluntary head restraint. Neuron *80*, 371-384.

Self, M.W., Lorteije, J.A., Vangeneugden, J., van Beest, E.H., Grigore, M.E., Levelt, C.N., Heimel, J.A., and Roelfsema, P.R. (2014). Orientation-tuned surround suppression in mouse visual cortex. J Neurosci *34*, 9290-9304.

Sengpiel, F., Sen, A., and Blakemore, C. (1997). Characteristics of surround inhibition in cat area 17. Exp Brain Res *116*, 216-228.

Shang, C., Liu, Z., Chen, Z., Shi, Y., Wang, Q., Liu, S., Li, D., and Cao, P. (2015). BRAIN CIRCUITS. A parvalbumin-positive excitatory visual pathway to trigger fear responses in mice. Science *348*, 1472-1477.

Shi, X., Barchini, J., Ledesma, H.A., Koren, D., Jin, Y., Liu, X., Wei, W., and Cang, J. (2017). Retinal origin of direction selectivity in the superior colliculus. Nat Neurosci *20*, 550-558.

Sillito, A.M., Grieve, K.L., Jones, H.E., Cudeiro, J., and Davis, J. (1995). Visual cortical mechanisms detecting focal orientation discontinuities. Nature *378*, 492-496.

Smith, E.L., 3rd, Chino, Y.M., Ridder, W.H., 3rd, Kitagawa, K., and Langston, A. (1990). Orientation bias of neurons in the lateral geniculate nucleus of macaque monkeys. Vis Neurosci *5*, 525-545.

Soodak, R.E., Shapley, R.M., and Kaplan, E. (1987). Linear mechanism of orientation tuning in the retina and lateral geniculate nucleus of the cat. J Neurophysiol *58*, 267-275.

Sterling, P., and Wickelgren, B.G. (1969). Visual receptive fields in the superior colliculus of the cat. J Neurophysiol *32*, 1-15.

Stubblefield, E.A., Thompson, J.A., and Felsen, G. (2015). Optogenetic cholinergic modulation of the mouse superior colliculus in vivo. J Neurophysiol *114*, 978-988.

Sun, H.J., Zhao, J., Southall, T.L., and Xu, B. (2002). Contextual influences on the directional responses of tectal cells in pigeons. Vis Neurosci *19*, 133-144.

Sun, L.O., Brady, C.M., Cahill, H., Al-Khindi, T., Sakuta, H., Dhande, O.S., Noda, M., Huberman, A.D., Nathans, J., and Kolodkin, A.L. (2015). Functional assembly of accessory optic system circuitry critical for compensatory eye movements. Neuron *86*, 971-984.

Sun, W., Tan, Z., Mensh, B.D., and Ji, N. (2016). Thalamus provides layer 4 of primary visual cortex with orientation- and direction-tuned inputs. Nat Neurosci *19*, 308-315.

Swindale, N.V., Shoham, D., Grinvald, A., Bonhoeffer, T., and Hubener, M. (2000). Visual cortex maps are optimized for uniform coverage. Nat Neurosci *3*, 822-826.

Tada, M., Takeuchi, A., Hashizume, M., Kitamura, K., and Kano, M. (2014). A highly sensitive fluorescent indicator dye for calcium imaging of neural activity in vitro and in vivo. Eur J Neurosci *39*, 1720-1728.

Taniguchi, H., He, M., Wu, P., Kim, S., Paik, R., Sugino, K., Kvitsiani, D., Fu, Y., Lu, J., Lin, Y., *et al.* (2011). A resource of Cre driver lines for genetic targeting of GABAergic neurons in cerebral cortex. Neuron *71*, 995-1013.

Thoreson, W.B., and Mangel, S.C. (2012). Lateral interactions in the outer retina. Progress in retinal and eye research *31*, 407-441.

Van Hooser, S.D., Heimel, J.A., Chung, S., Nelson, S.B., and Toth, L.J. (2005). Orientation selectivity without orientation maps in visual cortex of a highly visual mammal. J Neurosci *25*, 19-28.

Vaney, D.I., Sivyer, B., and Taylor, W.R. (2012). Direction selectivity in the retina: symmetry and asymmetry in structure and function. Nat Rev Neurosci *13*, 194-208.

Veale, R., Hafed, Z.M., and Yoshida, M. (2017). How is visual salience computed in the brain? Insights from behaviour, neurobiology and modelling. Philos Trans R Soc Lond B Biol Sci *372*.

Vidyasagar, T.R., and Urbas, J.V. (1982). Orientation sensitivity of cat LGN neurones with and without inputs from visual cortical areas 17 and 18. Exp Brain Res *46*, 157-169.

Wang, L., Liu, M., Segraves, M.A., and Cang, J. (2015). Visual Experience Is Required for the Development of Eye Movement Maps in the Mouse Superior Colliculus. J Neurosci *35*, 12281-12286.

Wang, L., Rangarajan, K.V., Lawhn-Heath, C.A., Sarnaik, R., Wang, B.S., Liu, X., and Cang, J. (2009). Direction-specific disruption of subcortical visual behavior and receptive fields in mice lacking the beta2 subunit of nicotinic acetylcholine receptor. J Neurosci *29*, 12909-12918.

Wang, L., Sarnaik, R., Rangarajan, K., Liu, X., and Cang, J. (2010). Visual receptive field properties of neurons in the superficial superior colliculus of the mouse. J Neurosci *30*, 16573-16584.

Wang, Q., and Burkhalter, A. (2013). Stream-related preferences of inputs to the superior colliculus from areas of dorsal and ventral streams of mouse visual cortex. The Journal of neuroscience : the official journal of the Society for Neuroscience *33*, 1696-1705.

Wartzok, D., and Marks, W.B. (1973). Directionally selective visual units recorded in optic tectum of the goldfish. J Neurophysiol *36*, 588-604.

Wei, P., Liu, N., Zhang, Z., Liu, X., Tang, Y., He, X., Wu, B., Zhou, Z., Liu, Y., Li, J., *et al.* (2015). Processing of visually evoked innate fear by a non-canonical thalamic pathway. Nat Commun *6*, 6756.

Wei, W., Elstrott, J., and Feller, M.B. (2010). Two-photon targeted recording of GFP-expressing neurons for light responses and live-cell imaging in the mouse retina. Nat Protoc *5*, 1347-1352.

Wei, W., and Feller, M.B. (2011). Organization and development of direction-selective circuits in the retina. Trends Neurosci *34*, 638-645.

Wei, W., Hamby, A.M., Zhou, K., and Feller, M.B. (2011). Development of asymmetric inhibition underlying direction selectivity in the retina. Nature *469*, 402-406.

Weng, S., Sun, W., and He, S. (2005). Identification of ON-OFF direction-selective ganglion cells in the mouse retina. J Physiol *562*, 915-923.

White, A.J., Wilder, H.D., Goodchild, A.K., Sefton, A.J., and Martin, P.R. (1998). Segregation of receptive field properties in the lateral geniculate nucleus of a New-World monkey, the marmoset Callithrix jacchus. J Neurophysiol *80*, 2063-2076.

White, B.J., Berg, D.J., Kan, J.Y., Marino, R.A., Itti, L., and Munoz, D.P. (2017). Superior colliculus neurons encode a visual saliency map during free viewing of natural dynamic video. Nat Commun *8*, 14263.

Wiesel, T.N., and Hubel, D.H. (1963). Single-Cell Responses in Striate Cortex of Kittens Deprived of Vision in One Eye. Journal of neurophysiology *26*, 1003-1017.

Wilson, D.E., Smith, G.B., Jacob, A.L., Walker, T., Dimidschstein, J., Fishell, G., and Fitzpatrick, D. (2017). GABAergic Neurons in Ferret Visual Cortex Participate in Functionally Specific Networks. Neuron *93*, 1058-1065 e1054.

Wilson, N.R., Runyan, C.A., Wang, F.L., and Sur, M. (2012). Division and subtraction by distinct cortical inhibitory networks in vivo. Nature *488*, 343-348.

Xu, X., Ichida, J., Shostak, Y., Bonds, A.B., and Casagrande, V.A. (2002). Are primate lateral geniculate nucleus (LGN) cells really sensitive to orientation or direction? Vis Neurosci *19*, 97-108.

Yilmaz, M., and Meister, M. (2013). Rapid innate defensive responses of mice to looming visual stimuli. Curr Biol *23*, 2011-2015.

Yonehara, K., Balint, K., Noda, M., Nagel, G., Bamberg, E., and Roska, B. (2011). Spatially asymmetric reorganization of inhibition establishes a motion-sensitive circuit. Nature *469*, 407-410.

Yonehara, K., Fiscella, M., Drinnenberg, A., Esposti, F., Trenholm, S., Krol, J., Franke, F., Scherf, B.G., Kusnyerik, A., Muller, J., *et al.* (2016). Congenital Nystagmus Gene FRMD7 Is Necessary for Establishing a Neuronal Circuit Asymmetry for Direction Selectivity. Neuron *89*, 177-193.

Yu, H., Farley, B.J., Jin, D.Z., and Sur, M. (2005). The coordinated mapping of visual space and response features in visual cortex. Neuron *47*, 267-280.

Zahar, Y., Wagner, H., and Gutfreund, Y. (2012). Responses of tectal neurons to contrasting stimuli: an electrophysiological study in the barn owl. PLoS One *7*, e39559.

Zhang, Y., Kim, I.J., Sanes, J.R., and Meister, M. (2012). The most numerous ganglion cell type of the mouse retina is a selective feature detector. Proc Natl Acad Sci U S A *109*, E2391-2398.

Zhao, X., Chen, H., Liu, X., and Cang, J. (2013). Orientation-selective responses in the mouse lateral geniculate nucleus. J Neurosci *33*, 12751-12763.

Zhao, X., Liu, M., and Cang, J. (2014). Visual cortex modulates the magnitude but not the selectivity of looming-evoked responses in the superior colliculus of awake mice. Neuron *84*, 202-213.

Zhaoping, L. (2016). From the optic tectum to the primary visual cortex: migration through evolution of the saliency map for exogenous attentional guidance. Curr Opin Neurobiol *40*, 94-102.

Zhaoping, L., and Zhe, L. (2015). Primary Visual Cortex as a Saliency Map: A Parameter-Free Prediction and Its Test by Behavioral Data. PLoS Comput Biol *11*, e1004375.

Zmarz, P., and Keller, G.B. (2016). Mismatch Receptive Fields in Mouse Visual Cortex. Neuron *92*, 766-772.